U.PORTO

FEUP FACULDADE DE ENGENHARIA UNIVERSIDADE DO PORTO

EARTHQUAKE DAMAGE AND LOSS ASSESSMENT OF REINFORCED CONCRETE BUILDINGS

LUÍS CARLOS RIBEIRO MARTINS

Dissertation submitted in partial fulfilment of the requirements for the degree of:

DOCTOR OF PHILOSOPHY

Supervisor: Prof. Raimundo Moreno Delgado

Co-supervisors: Dr. Mário António Lage Alves Marques & Dr. Vítor Emanuel Marta da Silva

MAY 2018

Financially supported by FCT through the grant
SFRH/BD/87322/2012

REVIEW PANEL

President

Prof. Dr. Rui Artur Bártolo Calçada
Full Professor at the Faculty of Engineering of the University of Porto, Portugal

Prof. Dr. Carmine Galasso
Senior Lecturer at the University College of London, United Kingdom.

Prof. Dr. Ricardo Nuno Carvalho Monteiro
Professor at the Istituto Universitario di Studi Superiori di Pavia, Italy

Prof. Dr. Carlos Sousa Oliveira
Full Professor at the Instituto Superior Técnico, Portugal

Dr. Alfredo Campos Costa
Senior Researcher at LNEC-Laboratório Nacional de Engenharia Civil, Portugal

Prof. Dr. Humberto Salazar Amorim Varum
Full Professor at the Faculty of Engineering of the University of Porto, Portugal

Dr. Mário António Lage Alves Marques
Postdoctoral Researcher at the Faculty of Engineering of the University of Porto, Portugal

ACKNOWLEDGEMENTS

This first paragraph in this section is dedicated to my advisors Prof. Raimundo Delgado, Dr. Mário Marques and Dr. Vítor Silva. To Prof. Raimundo Delgado, who I first met during my undergrad years, I would like to thank for the permanent motivation and for all the knowledge he has shared with me over the years. To Dr. Mário Marques I would like to thank all the patience and friendship he has shown since the beginning of my graduate studies. To Dr. Vítor Silva, I want to express my extreme gratitude for the all nights spent in front of the laptop working together and the all the fruitful discussions. I am also extremely grateful for the personal relationship we developed over the years and for being able to call him now one of my best friends.

To Dr. Helen Crowley and Prof. Paolo Bazzurro, I would like to express my most profound gratitude. The opportunity to work with some of the top researchers in the field of seismic risk was one of the best experiences I had during my academic career.

My sincere appreciation goes also to everyone at the Global Earthquake Model foundation and all my friends in Pavia, namely Anirudh Rao, Catalina Yepes, Cecilia Nievas, Christopher Burton, Cigdem Yilmaz, Luís Sousa, Michael Musori and Venetia Despotaki I would like to thank them for making me feel at home in a foreign country.

To all of my friends from the great H301 office, namely Alejandro de Miguel Tejada, João Barbosa, Miguel Araújo, Nuno Pereira and Rui Barros, my most honest thank you.

A very special mention to my closest and most loyal friend Alexandra Almeida. She is one of the very few people I could always rely and has proven her value multiple times.

A huge word of appreciation goes also to my parents. Without their unconditional support and encouragement none of this would have been possible.

Finally, the financial support provided by FCT through the grant SFRH/BD/87322/2012 is also acknowledged.

SUMMARY

Seismic risk is the result of the convolution of three different quantities (i) seismic hazard, (ii) exposure and (iii) vulnerability. Considering that both seismic hazard and exposure cannot be changed, vulnerability assumes a special role in reducing the expected seismic risk level. By properly intervening on a structure's performance (e.g. by retrofitting solutions) the respective seismic risk level can be minimized. Improvements on the field of analytical performance, damage and loss assessment of reinforced concrete moment resisting frames are presented in this study.

From the study of tridimentional finite element models of structures designed for increasing levels of ground shaking intensity ranging from close to zero (i.e. buildings with very low seismic design) up to 0.4g (i.e. moderate to high seismic hazard), new simplified relationships for estimating the period of vibration the height and the seismic design level are provided. In addition, suitable fragility functions parameters for European R.C. buildings have been developed within a risk-targeted hazard assessment framework. Statistical analyses to estimate appropriate boundaries for the collapse probability of buildings experiencing the design ground motion and for its dispersion are presented. A comprehensive study on the influence of these parameters on the final risk metrics (e.g. average annual loss) is also included

Through a comprehensive analysis on the expected damage and the correspondent repair techniques, the expected losses of real Portuguese reinforced concrete buildings have been computed using real up-to-date construction costs. From the analytical results a new damage-to-loss model developed for Portuguese construction has been presented. A methodology for computing vulnerability directly from the distribution of losses per seismic intensity is also provided.

Finally, following an event based approach a new seismic risk map for mainland Portugal is presented.

Keywords: Reinforced concrete buildings; Analytical vulnerability assessment; Seismic risk

SUMÁRIO

Risco sismico é geralmente calculado através da convulução de três quantidades (i) perigosidade, (ii) exposição e (iii) vulnerabilidade. Considerando o facto de que tanto a periogosidade como a exposição são invariáveis, vulnerabilidade assume um papel fulcral na mitigação do nivel de risco sísmico. Através de intervenções correctas no desempenho de uma estrutura (por exemplo através soluções de reforço estrutural) é possivel reduzir o respectivo nivel de risco sísmico. Avanços nas metodologias de avaliação de desempenho e dano, especialmente em estruturas de betão armado são propostos nesta tese.

Através da análise do desempenho de modelos numéricos de estruturas desenhadas para niveis crescentes de aceleração de pico desde um nivel próximo de zero (desempenho sismico muito limitado) até 0.40g (perigosidade sísmica moderada a elevada), relações simplificadas para cálculo do periodo de vibração a partir da altura e do nível de aceleração de dimensionamento são propostas. Adicionalmente, parâmetros de fragilidade adequados para o cálculo de curvas de fragilidade para edificios de betão armados europeus foram desenvolvidos no âmbito de um estudo *risk-targeted hazard assessment*. Estudos estatisticos para definir intervalos para a probabilidade de colapso para edificios sujeitos à aceleração de dimensionamento e para a variabilidade da curva de fragilidade. Um estudo detalhado acerca da influência destes parâmetros no valor do nivel de risco associado é igualmente apresentado.

Através de um estudo detalhado do dano e das respectivas técnicas de reparação as perdas de edificios reais de betão armado foram calculadas tendo por base custos de construção actualizados. Através de análises dinâmicas não lineares um modelo de consequência desenvolvido para a construção portuguesa foi desenvolvido. Uma metodologia para cálculo da vulnerabilidade directamente a partir da distribuição de perdas por intensidade sísmica é igualmente proposta.

Seguindo uma metodologia *event-based* um novo mapa de risco sismico para Portugal é também apresentado.

Palavras-chave: Edificios de betão armado; Metodologias analiticas de vulnerabilidade; Risco sismico

TABLE OF CONTENTS

LIST OF TABLES

LIST OF FIGURES

1

INTRODUCTION

1.1 THE NEED FOR AN EARTHQUAKE LOSS ASSESSMENT STUDY

Earthquakes are amongst the natural hazards responsible for the highest number of human casualties and economic losses throughout mankind's history. Recently the world's population reached the seven billion mark with the prospect of surpassing nine billion by the year 2050 (Silva 2013). The exponential growth in the world's population has led to an increase in the number of megacities (i.e. cities with a population larger than two million) many of them in earthquake prone regions and potentially at risk (Crowley *et al.* 2006). In the past century alone it has been estimated that on average nearly seventeen thousand people have lost their lives annually as a direct result of strong ground motion (Sen 2009). Seismic events also have had a significant impact on the economy both at the country level and globally in recent years. For example, following Haiti's Earthquake in 2010 the total economic losses were estimated to be around 120% the country's gross domestic product (GDP) and in 2011 after the Great East Japan Earthquake a worldwide rise in the prices of electronics was observed due to disruptions in the supply chain to several factories (Silva 2013).

Figure 1.1 presents the global economic losses due to natural disasters from the past few decades. From the figure it can be observed that the total insured losses are usually less than half the total portfolio's value. Earthquakes are usually responsible for about 20% of the global monetary losses (Silva 2013), nonetheless it has been observed that monetary losses due to earthquakes are increasing rapidly. Taking the past century as an example, if the total economic losses are averaged over the one hundred years time span the resulting annual value is about ten billion dollars. However considering only the last decade the annual losses have been estimated at around twenty billion dollars, double the average for the entire twentieth century (Elnashai and Di Sarno 2008).

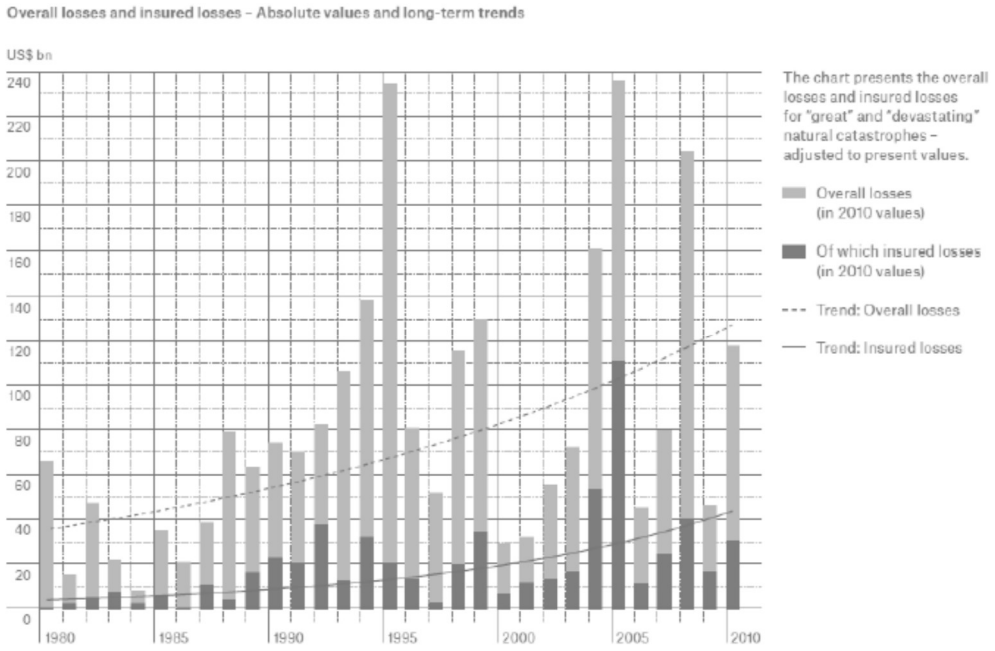

Figure 1.1 - Overall and insured losses due to natural catastrophes from 1980 to 2011 (MunichRe 2012).

Modern seismic design codes prescribe different performance levels for different ground shaking intensity levels that the structures must fulfil. Usually these performance criteria are translated into a given demand parameter or damage level that must not be exceeded and are defined based on a given accepted level of risk. The origins of this approach to seismic design, known as *Performance-based Earthquake Engineering (PBEE)*, can be traced back to 60's (Priestley *et al.* 2007, Sen 2009) and yet current design techniques used by most engineering practitioners are still unable to correctly assess the risk level associated with the performance criteria. Seismic codes require new structures to be designed for a ground motion intensity level, associated with a prescribed return period, under the assumption that the resultant collapse probability is uniform throughout a given region. The uncertainty on the collapse probability distribution and the variability on the shape of the hazard curves often results on a seismic risk level that is site and structure specific, thus invalidating the previous hypothesis. Despite the obvious need for collapse prevention when designing and constructing new structures, it is also important to minimize the potential losses due to extensive damage for more frequent events. Observation of past events has revealed regions where modern seismic design regulations are well established, but still high economic losses have been reported. For

example, the 1994 Northridge Earthquake is deemed as one of the costliest seismic events in recent history (Elnashai and Di Sarno 2008) and most of the economic losses came from severely damaged structures, and not due to its limited number of collapses.

The situation is even more complex when applying the concepts of performance-based design to existing buildings. Even today is not unusual to find several codes of practice that simply state that existing structures must comply with the same level of performance as of a new construction, which in practice is usually not feasible. Moreover, this often leads to significant negative consequences because those accountable for the safety of the structure generally choose not to know the risk level rather than being informed and fail to meet the required performance (Calvi 2013).

Much has been learnt from the past and great advances in the field of seismic risk assessment have been made in the last decades, nonetheless seismic risk is heavily influenced by numerous sources of uncertainty. From the discussion in this section is clear that research in earthquake loss estimation is still a very relevant topic with the capability of reducing the impact of seismic events. The activities developed within this thesis aimed the development and verification of techniques that contribute for a reduction in the level of uncertainty in seismic risk assessment studies.

1.2 OVERVIEW ON SEISMIC RISK ASSESSMENT

Seismic risk is usually defined as the probability of exceeding a given level of loss of a set of assets within a reference time period as a consequence of strong ground motion (Di Pasquale *et al.* 2005). The loss metrics (e.g. number of human casualties, total repair cost, downtime, etc) vary depending on the nature of the exposed assets (e.g. people, buildings, infrastructures, business, etc).

Any seismic risk assessment study is inherently influenced by uncertainty ranging from uncertainties in the spatial, temporal occurrence and size of earthquakes, to the uncertainties in the structural performance for a given ground shaking and the subsequent damage and losses. Despite the efforts to minimize the global level of uncertainty in the field of seismic risk a complete probabilistic assessment of all the variables involved is often not possible. The

current practice is to account only for the uncertainties in the dominant factors and ignore those either deemed negligible or difficult to measure (Di Pasquale *et al.* 2005). Some frameworks have been proposed over the years to account for the aforementioned uncertainties, probably the best known of these is the so-called *PEER Framing Formula* originally presented by Deierlein *et al* (2003). The proposed formula provides an explicit methodology for considering the sources of uncertainty that directly contribute to a given *Decision Variable (DV*). The process begins by defining a ground motion *Intensity Measure (IM)* that defines in a probabilistic sense the main attributes of the ground motion that affect the structural performance. The next variable, *Engineering Demand Parameter (EDP)*, describes the structural response to the earthquake loads from the outputs of numerical analysis (e.g. floor accelerations, drift ratios, etc). The final quantity is the *Damage Measure (DM)* that describes the physical condition of the structure as a function of EDP. The *PEER Framing Formula* is mathematically expressed by the triple integral given in Eq. (1.1). This equation is a direct application of the total probability theorem where the uncertainties in each variable are described as independent conditional probabilities. The terms $G(DV|DM)$, $G(DM|EDP)$ and $G(EDP|IM)$ are conditional probabilities relating one quantity with another while $d\lambda(IM)$ is the derivative of the hazard curve (i.e. a curve with intensity level *vs* frequency of occurrence). The left side of the equation gives the probabilistic description of the chosen decision variable (Deierlein *et al.* 2003).

$$\lambda(DV) = \iiint \left(G(DV \mid DM) \cdot dG(DM \mid EDP) \cdot dG(EDP \mid IM) \cdot d\lambda(IM)\right) \qquad (1.1)$$

The three main components of an earthquake risk model are: *seismic hazard*, *exposure* and *vulnerability*. A brief discussion on each one of these components is provided below.

i. Seismic hazard

The objective of seismic hazard assessment is to estimate the rate of exceedance of a given ground motion intensity for a given return period. A standard approach to hazard analysis is to perform a site specific *Probabilistic Seismic Hazard Assessment (PSHA)* considering all the possible expected earthquakes within a region. A typical PSHA analysis usually has four main steps (Kramer 1996): (i) identification of the seismic sources and characterization of the distribution of the probability for generating strong ground motion within the area; (ii)

characterize the seismicity of each source by a *recurrence relationship* (i.e. the average rate at which an earthquake of a given size is exceeded); (iii) compute the ground motion at the site of interest for any possible earthquake of any possible size and distance through *Ground Motion Prediction Equations (GMPE);* and finally (iv) combine the uncertainties from earthquake size, location and ground motion prediction and compute the probability of the ground motion parameter being exceeded during a specified time span.

The fundamentals of probabilistic seismic hazard assessment (PSHA) were first established during late 60's and early 70's and nowadays PSHA has become common practice for hazard studies. Notwithstanding that still some level of clarification is required on how the computations should be performed (Bommer and Abrahamson 2006).

In the same way as many other subjects in earthquake engineering, hazard assessment is often undermined by uncertainties. The inherent variability considered directly in the hazard computation is called the *aleatory variability* while the uncertainty arising from the scientific models (e.g. models for earthquake recurrence and ground motion prediction) is called *epistemic uncertainty*. The main difference between these concepts is that aleatory variability determines the shape of the hazard curve, whilst considering epistemic uncertainty produces alternative hazard curves (Abrahamson and Bommer 2005). The common practice to account for these sources of variability is to consider a *logic tree*. After the logic tree has been defined the hazard computations are performed following each one of the branches and the associated weight is given by multiplying the weights in the respective path. The weights assigned to each individual branch are usually a decision of the analyst and represent the relative level of confidence in one model with respect to another and its applicability to a particular project. From the hazard estimates and associated weight, hazard curves can be computed for any desired percentile. At this point, and usually for design purposes, the most common approach is to consider only the mean hazard curve; nonetheless some authors have questioned this practice. For example, Abrahanson and Bommer (2005) claim that the use of the mean hazard curve for design purposes *'blurs the distinction between aleatory variability and epistemic uncertainty'*. It must be noted that according to the authors this practice only creates an issue for special structures (e.g. nuclear power plants and infrastructures) for which the design ground motion is pushed to much lower annual frequencies of occurrence than in regular

buildings. At longer return periods the mean hazard curve is pushed to higher fractiles and this shift is neither systematic nor predictable.

ii. Exposure

Exposure data is defined herein as the description of assets exposed to seismic hazard such as people, buildings and infrastructures. The parameters required to develop an exposure model are the value of the asset, its taxonomy and geographic coordinates (Silva *et al.* 2014b). Taxonomy is defined as a classification system that contains very different attributes (such as construction material, height, age, etc) and is used to assign the asset with an appropriate vulnerability curve. The geographic coordinates are required to compute the ground shaking at the site.

The most common and detailed source of information for building the exposure module are usually the different national census. The recent developments in satellite imaging technology have provided new tools for fast assessment of the distribution and classification of assets at risk. There are global databases with information about the distribution of population that combines the information from the national census and satellite data (namely night images) (e.g. *GRUMP- Global Urban and Rural Mapping Project* and *GWP - Gridded Population of the World*). Currently the only available database for the building stock at a global level is PAGER (Jaiswal and Wald 2008)

iii. Vulnerability

Vulnerability is defined as the probability of loss for a given ground shaking intensity. Physical vulnerability of the exposed elements plays a crucial role in the magnitude of losses of a given seismic event, because despite being natural events most of consequences of earthquakes are caused by the poor structural performance of buildings. This realization implies that it is possible to minimize the expected losses by designing new structures capable of withstanding the dynamic loads and correctly improving the performance of existing ones through careful retrofitting.

The understanding of the important role that structural performance plays during an earthquake event meant that during the past decades a significant effort has been made in developing more accurate methodologies for assessing physical vulnerability. The several methods for vulnerability assessment found in the literature can be grouped in two main categories: (i) empirical and (ii) analytical methods (Calvi *et al.* 2006).

The first category makes use of the information of past seismic events in order to compute fragility functions for a given typology. The second group relies on the results given by numerical simulations of the structural response of buildings for increasing levels of ground shaking. This latter group of methods has as its main advantage not depending on the availability of damage or loss data from historical earthquakes. Depending on the level of detail of the numerical models and the analysis algorithm, the analytical methods can also include key aspects of the structural response such as: nonlinear behaviour, structural irregularities and the influence of higher modes of vibration (Silva 2013). Despite the recognition of these methods as a reliable tool for vulnerability assessment, some drawbacks of the analytical methods must be mentioned the most relevant being the computational effort and total number of analyses required to have meaningful results.

The first stage of an analytical vulnerability assessment is to employ the results from structural analysis to establish a relation between a meaningful engineering demand parameter and a structural damage threshold. Then, the evaluation of the evolution of damage with increasing ground shaking intensity can be used to derive structural fragility functions, which provide the probability of exceeding a set of structural damage states, conditional on a set of ground motion levels. The issue of defining damage from structural performance parameters has been addressed in previous studies, (Park and Ang 1985, Calvi 1999, Borzi *et al.* 2008, Benavent-Climent 2011, Fardis *et al.* 2012), or technical guidelines and design recommendations (CEN 2005, FEMA 2014). However, whilst EDP-to-damage estimation is well documented and deals with concepts that are easily recognized by most engineering practitioners and researchers, the same cannot be said regarding the relationship between damage and a level of loss, usually defined by the so-called damage-to-loss or consequence models (e.g. (Kappos *et al.* 2006, Bal *et al.* 2010b)). Despite efforts from a number of researchers to improve the field of loss assessment (e.g. (Gunturi 1993, Kappos *et al.* 1998, Di Pasquale and Goretti 2001, Kappos *et al.* 2006, Bal *et al.* 2008, Ramirez *et al.* 2012)), in general, the majority of available consequence models are still

deterministic and/or based on limited empirical data. Furthermore, it is also important to emphasize that the majority of the existing damage-to-loss models were developed and calibrated to represent the reality of a small number of countries and corresponding building stock, which may lead to a misleading vulnerability evaluation when applied to other regions of the world.

In traditional approach to analytical vulnerability assessment one has to firstly develop a fragility model and then combine it with an available damage-to-loss model. Too frequently this is performed without much thought for the compatibility between both models. A recent study by Martins *et al* (2016) demonstrated how this practice can have a significant impact on the final expected loss value. The findings of this study point towards the recommendation that ideally risk modellers should seek to develop vulnerability models purely based on the distribution of loss ratio per intensity measure levels (IML), for example following an approach based on the cost of repair and cost of replacement. This way the compatibility issue is completely avoided. If this is not feasible it should be at least ensured that the selected damage criteria and fragility model are as much compatible as possible with the damage-to-loss model.

1.3 SCOPE AND MOTIVATION

Portuguese territory is considerate to have moderate seismicity with several destructive earthquakes being recorded in the past. For example, it is believed that about 50% of Lisbon's buildings collapsed or suffered heavy damage during the well-known 1755 earthquake, and that in 1909 the 6.6 Mw earthquake with an epicentre in Benavente caused damage to over 3000 dwellings. Despite the great developments on the field of seismic risk assessment and prevention developed over the past few decades, it has been estimated that large economic losses would still be expected if such historical events were to occur (Sousa 2006).

Reinforced concrete has become the most predominant construction material for structural elements in Portugal. From the last national Census (INE 2011) has been estimated that reinforced concrete construction accounts for nearly 50% of the Portuguese building stock with the vast majority being residential buildings. As previously mentioned physical vulnerability plays an important role on minimizing seismic risk. The main goal of the studies presented in

this thesis is to improve the field of analytical vulnerability assessment of RC buildings. Hence it is expected that the methodologies presented herein provide a reliable source for estimating (and possibly minimize) the risk level for the majority of Portuguese building stock.

1.4 THESIS' LAYOUT

The present thesis has been divided in six different chapters. The first, and current, chapter provides a general introduction to several aspects addressed in the thesis and the main scope and motivation.

The second chapter introduces some general concepts about analytical vulnerability assessment methodologies that are the foundation of the techniques used on this this study.

The third chapter provides a study on the development of simplified period-height relationships for reinforced concrete buildings. Estimating the period of vibration of a structure is essential for computing seismic demands, however this is often not always a simple procedure, and in the cases of large scale assessments analysing every single structure is simply not feasible. For these cases simplified relationships that allow to estimate the period of vibration have proven to be of great value. In this section sets of reinforced concrete buildings designed according to the most up-to-date European regulations and for increasing levels of ground motion have been analysed. For these sets of structures both the elastic and inelastic period have been computed and simplified relationships have been proposed. The findings of this study allowed for developing functions that allow to estimate the period of vibration from not only using the height of the building as the main input parameter but also considering the seismic design level (measured as the design peak ground acceleration)

Chapter four examines the influence of fragility parameters within a risk-targeted assessment framework. From sets of structures designed according to the same criteria and increasing design ground motion levels, fragility parameters (namely the probability of collapse at the design ground motion and lognormal standard deviation) suitable for European R.C. moment resisting frame buildings have been proposed. The expected average annual probability of collapse for the entire European continent has also been computed.

The fifth chapter presents a study on the development of damage-to-loss models for Portuguese reinforced concrete buildings. Damage-to-loss models were developed from the damage prediction of real buildings and the correspondent expected repair cost estimated from real market values taken from a construction technique database. An investigation on the influence of using non compatible fragility and damage-to-loss models on the final loss metrics is also provided.

Chapter number six takes the main results computed in the previous sections and applies them to a seismic risk assessment of mainland Portugal.

The final chapter summarizes the main conclusions of the thesis while providing guidelines for future works intended to extend and improve the subjects addressed herein.

2

ANALYTICAL METHODOLOGIES FOR FRAGILITY AND VULNERABILITY ASSESSMENT

2.1 SUMMARY

Physical vulnerability plays an important role in minimizing seismic risk. This realization meant that significant improvements on the field of analytical vulnerability assessment methodologies have been proposed in the past few decades. Comments on the methodologies currently used within a seismic vulnerability assessment framework are provided in this section. This discussion also serves the purpose of introducing the general concepts used throughout the remaining sections of this thesis.

A discussion on the process of analytical vulnerability assessment from the performance and fragility estimation to damage assessment is provided. An overview on nonlinear static and dynamic analyses is presented highlighting the major advantages and pitfalls of each methodology.

2.2 PERFORMANCE ASSESSMENT METHODOLOGIES

2.2.1 Pushover analysis

In pushover analysis the structure's performance is assessed by applying incremental lateral loads at the floor levels until a collapse mechanism is reached. Despite being usually simpler and less computational demanding than nonlinear dynamic analysis, pushover analysis have demonstrated to be useful for vulnerability assessment, especially to identify regions where significant plastic deformations are expected (Elnashai and Di Sarno 2008). The best results

given by pushover algorithms are usually obtained on structures with regular distribution of stiffness and mass for which the influence of higher modes is negligible.

The objective of these analyses is solving the nonlinear system in Eq. (2.1) where K_T is the tangent stiffness matrix, R_T is the unbalanced force vector and F is the vector of external loads. The algorithm starts by taking the last converged tangent stiffness matrix (in the first load increment this is the elastic stiffness matrix) and nodal displacement vector. Within a load increment the unbalanced forces are recalculated and reintroduced until equilibrium is reached. At this point the structure's tangent stiffness matrix and geometry are updated and stored in order to become the initial conditions for a new load increment. This is repeated until the development of a collapse mechanism, i.e. up to the point where no longer is possible to balance the equation.

$$[K]\cdot\{\Delta u\}=\{\Delta F\}\Leftrightarrow[K_T]\cdot\{\Delta u\}+\{R_T\}=\{F\} \tag{2.1}$$

Pushover algorithms are usually grouped in two main categories based on how the applied lateral load profile is handled during the analysis. If the load profile remains constant this is known as *conventional pushover algorithm* whilst if the load profile is updated in order to take in consideration the changes in the structure's dynamic properties this is known as *adaptive pushover algorithm*. Unlike nonlinear dynamic analysis for which the seismic demand is implicit considered from the ground motion records in nonlinear static methodologies seismic demand is taken into consideration using the so-called *Nonlinear Static Procedures*. A brief discussion on these subjects is provided in the following sub-sections.

2.2.1.1 Conventional pushover algorithms

The origins of pushover analysis can be traced back to the pioneer work of Gulkan and Sozen (1974) in which single degree of freedom (SDOF) systems have been used to capture the nonlinear behaviour of multiple degree of freedom structures.

Conventional pushover methodologies have been praised as a valuable tool for vulnerability assessment due to their simplicity and reduced runtime. However, these methods are unable of reproduce certain phenomena like viscous damping, strength degradation and pinching.

Krawinkler and Seneviratna (1998) have highlighted the constant load pattern as one of the major pitfalls of the this type of pushover algorithms since they ignore deformation modes that are propelled by the dynamic response and are unable to track the changes in the structure's dynamic properties due to nonlinear effects.

In these methodologies the external applied load profile usually adopts a uniform shape or a shape proportional to either the distribution of floor masses (m_i) along height (h_i) (Eq. (2.2)) or to the first mode of vibration components ($\phi_{i,1}$) (Eq.(2.3)) and it is kept constant until collapse is reached.

$$F_i = V_b \cdot \frac{m_i \times h_i}{\sum_{i=1}^{n} (m_i \times h_i)} \tag{2.2}$$

$$F_i = V_b \cdot \frac{m_i \times \phi_{i,1}}{\sum_{i=1}^{n} (m_i \times \phi_{i,1})} \tag{2.3}$$

2.2.1.2 Adaptive pushover algorithms

Adaptive pushover algorithms have been developed as an attempt to overcome the main drawbacks of their conventional counterparts. Over the past few decades some authors, e.g. (Bracci *et al.* 1997, Antoniou and Pinho 2004), have proposed fully adaptive pushover methodologies for earthquake vulnerability assessment. These have the advantage of better accounting for stiffness degradation and the influence of higher modes of vibration. This is accomplished by computing the structure's properties after each load increment and updating the applied load pattern accordingly.

The results from an adaptive pushover for any load increment are given as a combination (often using either *Square Root of the Sum of Squares* (SRSS) or *Complete Quadratic Combination* (CQC)) of the results from the analyses performed with the load pattern (F_{ij}) given by Eq. (2.4) (Γ- participation factor; M- mass matrix) computed for all the significant modes of vibration (Φ).

$$F_{ij} = \Gamma_j \cdot M_i \cdot \Phi_{ij} \cdot g \tag{2.4}$$

2.2.1.3 Nonlinear static procedures

Nonlinear static procedures (NSP) make use of the structure's capacity curve and the ground motion characteristics (frequently by considering the earthquake's response spectrum) in order to estimate the performance point.

i. Coefficient Method of Displacement Modification (CMDM)

The CMDM was firstly proposed in ATC-40 (1996) document and further developed in FEMA-440 (2005).This method allows to compute the maximum displacement of the real MDOF system by modifying the spectral displacement of an equivalent SDOF system at the effective fundament period of vibration through a set of four coefficients C_i (Eq. (2.5)). FEMA-440 provides values for each one of these parameters for different building typologies that have been calibrated from the statistics of dynamic analyses performed in SDOF systems. In Eq. (2.5) C_0 has the purpose of introducing the effect of the difference in the response of SDOF and MDOF systems, C_1 is a measure of the level of ductility, C_2 allows to introduce the effects of pinching and stiffness and strength degradation and lastly C_3 simulates the influence of P-Δ effects. The effective period of vibration is computed from the structure's capacity curve.

$$\delta_t = C_0 \cdot C_1 \cdot C_2 \cdot C_3 \cdot Sa \cdot \left(\frac{T_e}{2\pi}\right)^2 \cdot g \qquad (2.5)$$

ii. Capacity Spectrum Method (CSM)

The CSM method was originally proposed in the 70's by Freeman *et al* (1975) as a tool for fast seismic vulnerability assessment. For this methodology firstly is necessary to transform the capacity curve from its usual displacement *vs.* base shear form to spectral acceleration *vs.* spectral displacement. The procedure for computing the target displacement through the Capacity Spectrum Method compares the capacity and demand using the capacity curve of an equivalent SDOF system and a damped response spectrum, respectively. The inelastic behaviour of the structure is taken in consideration by adjusting the viscous damping of the ground motion spectrum as a function of the displacement level at the point in which the response spectrum intersects the capacity curve. Usually iterations are required in order to match the damping applied to the response spectrum with the equivalent viscous damping

for the structure. The target displacement is given by the final crossing point between the capacity curve and the response spectrum.

Due to some criticisms, e.g. (Fajfar 1999, Chopra and Goel 2000), to the original formulation of the Capacity Spectrum Method for its tendency to underestimate structural deformations, the FEMA-440 (2005) report introduced some modifications to the method with the majority of the changes to CSM recommended in FEMA-440 being related with the way equivalent viscous damping is calculated.

An important aspect worth commenting is the definition of the bilinear relationship and the yield point. The ATC-40 (1996) document defines the slope of the initial segment of the bilinear curve from the initial stiffness. Silva (2013) has mentioned the need to comply with the rule of equal dissipated energy (i.e. the integral of the capacity and the bilinear curves must be equivalent) for some cases, mostly for ground motion of lower intensities, may lead to yielding points located still in the elastic portion of the capacity curve. An alternative that leads to more realistic bilinear curves is to use the effective stiffness of the structure instead, as suggested in FEMA-273 (1997).

iii. N2 Method

Initially proposed by Fajfar and Gašperšič (1996), the N2 method has been incorporated in EN 1998-1 (CEN 2010c) as the recommended NSP for nonlinear static analyses. The N2 method differs from the CSM by using an inelastic response spectrum in order to estimate the performance point instead of an overly damped spectrum. In this method the capacity of idealized SDOF system is characterized through an elastic-perfect plastic relationship determined based on equilibrium of areas.

In order to compute the target displacement using the N2 method is necessary to define if the equivalent SDOF system is in the short-period or medium/long-period range (i.e. the period of the equivalent system (T^*) is lower or greater than the corner period (T_C)). If the structure is considered to be in the medium/long period range the target displacement is taken as by the *equivalent displacement rule*. If on the other hand the structure is on the short period range an additional procedure is required to determine if the structure's yielding capacity has been exceeded. If the structure has remained in the elastic range the target displacement is once

again considered as equal to the elastic spectral displacement at the equivalent period of vibration. If the structural response is inelastic the target displacement is given by Eq. (2.6) where q_u is the ratio between the spectral acceleration at the period T^* and at the yield point.

$$\delta_t = \frac{S_d(T^*)}{q_u}\left[1 + (q_u - 1)\frac{T_C}{T^*}\right] \geq S_d(T^*) \tag{2.6}$$

2.2.2 Nonlinear dynamic analysis

Amongst the scientific community there is a general consensus that nonlinear dynamic analysis is the most accurate technique for assessing the structure's response due to earthquake loading, however this approach requires more computational effort and can become numerically unstable. Silva (2013) has estimated that to achieve comparable levels of confidence in the vulnerability assessment, nonlinear dynamic analyses may require up to six times the runtime of pushover algorithms.

The main objective in nonlinear time-history analysis is to solve the dynamic equilibrium equation (Eq. (2.7)) in which *[M]*, *[C]* and *[K]* are the mass, damping and stiffness matrices respectively, *{u(t)}* is the displacement time series and $\ddot{u}_g(t)$ is the ground acceleration. For linear systems this can be achieved through modal superposition or spectral analysis, however for nonlinear systems solving the dynamic equations often requires numerical integration methods like Newmark or Hilber-Hughes-Taylor (Clough and Penzien 1993, Chopra 2007). These integration methods solve the nonlinear dynamic equations by computing the structural response between discrete time increments for which the system is handled as linear elastic. Once equilibrium is reached the geometry and stiffness properties are updated and a new load increment is applied. The accuracy and stability of these methods is closely related with the size of the time increment, however choosing too small time increments leads to unreasonable runtimes. It is generally considered sufficient to choose a time increment that ensures both numerical stability and the integration of the last significant mode of vibration.

$$[M]\cdot\{\ddot{u}(t)\} + [C]\cdot\{\dot{u}(t)\} + [K]\cdot\{u(t)\} = -[M]\cdot\{1\}\cdot\ddot{u}_g(t) \tag{2.7}$$

2.3 FRAGILITY AND VULNERABILITY ASSESSMENT

2.3.1 Damage assessment

Current seismic design provisions allow for some level of damage in the building to occur during an earthquake considering the performance and safety criteria are not exceeded.

Correctly predicting the damage level is a crucial step in computing a fragility model. However, despite the contributions to this field proposed in the past few decades, defining a unified damage assessment methodology universally accepted amongst the scientific community has yet to be reached. One of the main difficulties still to overcome with developing a uniform damage criterion being defining the concept of *damage* itself since it is not uncommon that this concept is used with subjectivity (Kappos 1997). Most of the available damage scales for reinforced concrete have overcome this by being based on some level of observable physical anomaly such as cracking, spalling or buckling of the rebar recorded from inspections performed after real seismic events (e.g. (Park and Ang 1985).

2.3.1.1 Assessing local damage

One of the most common methods to assess local damage is through damage indices. A complete list of all available damage indices is out of scope of this thesis, however a brief presentation on the Park and Ang (1985) index is provided. This is one of the most commonly referenced indices for damage assessment in R.C. structures and has provided the foundations for the development of other indices like the one used in section 5.3 of this thesis.

Park and Ang damage index (PADI) establishes the damage in reinforced concrete elements as a linear combination of the damage due to excessive deformation with the damage due to hysteresis. Eq. (2.8) shows the general mathematical formula for the damage index where δ_M and δ_u are the maximum and ultimate deformation for the element, Q_y is the yield capacity under static loading and dE is the dissipated energy. The β parameter is a function of the plastic hinge length, the axial load and the total amount of rebar and stirrups in the element.

$$D = \frac{\delta_M}{\delta_u} + \frac{\beta}{Q_y \cdot \delta_u} \int dE \tag{2.8}$$

From observations of damage on real buildings, Park *et al* (1987) have established 0.40 as the threshold marking the damage level from which repairing is no longer economically viable. These observation also allowed the authors to propose thresholds for other damage levels ranging from *undamaged* to *collapse* (Table 2.1). Williams and Sexsmith (1995) highlighted the fact PADI has been calibrated from real damage from past earthquakes as one of the main advantages of this index. However, some authors, e.g. (Chung *et al.* 1987), have raised questions on the definition of the β parameter and on the legitimacy of linearly combining the damage due to deformation and due to dissipated energy.

Table 2.1 - Damage state limits proposed by Park *et al* (1987).

Damage state	Threshold
Undamaged	$D<0.1$
Light damage	$0.1\leq D<0.25$
Moderate damage	$0.25\leq D<0.4$
Severe damage	$0.4\leq D<1.0$
Collapse	$D\geq 1.0$

2.3.1.2 Assessing global damage and the collapse DS

Probably one of the most significant damage states to any seismic vulnerability study is collapse. Firstly, a distinction between element collapse and global structural failure should be made since the first often does not immediately lead to the latter because well-designed structures are expected to be able to redistribute the loads between the remaining elements. Thus, analytically assessing the global collapse of a structure is often a complex task with considerable uncertainty. Generally it is assumed that structure has collapsed when it is no longer able to support the permanent loading or when its repair is no longer a cost effective option (Kappos 1991, Ibarra and Krawinkler 2005). Several approaches for estimating collapse within an analytical performance assessment framework have been suggested. One criteria commonly used in analytic performance assessment is to consider a structure as collapsed when a reduction on 20% on the lateral load bearing capacity is observed, e.g (Silva *et al.* 2014d). Criteria based on the local damage have also been proposed to estimate global collapse, e.g. (Bal *et al.* 2010a), these are usually connected to a prescribed collapse mechanism (e.g. soft storey linked to the failure of the columns at a given floor). It should be noted that Silva *et al*

(2014d) have discussed on the use of local criteria to define limit states for fragility assessment and have concluded that this path may not be adequate for generating curves for a population of buildings

In a vulnerability assessment framework, the residual deformations of the structure should also be considered for evaluating collapse since severely deformed structures may require to be demolished meaning a complete loss of the structure (i.e. for all practical purposes the structure should be considered as collapsed) (Ramirez and Miranda 2012).

2.3.2 Computing fragility and vulnerability curves

Fragility curves provide the probability of a structure reaching or exceeding a given damage conditional on the ground shaking intensity level.

Traditionally, fragility curves are assumed to follow a cumulative lognormal distribution given by Eq. (2.9), where Φ is the standard normal distribution, β logarithmic standard deviation and θ the median (Cimellaro *et al.* 2011). According to Shinozuka *et al* (2000), the wide spread of the two-parameter lognormal model in fragility assessment was due to its mathematical convenience in relating with the structure's real strength capacity. The actual capacity of a structure can generally be described through a safety factor which in turn can be factored into a multiplicative of safety factors, each one associated with a given source of uncertainty. Applying the lognormal assumption for each one of these factors ensures that the overall seismic safety factor also follows a lognormal distribution due to the multiplicative reproducibility of the lognormal variables. The two parameters of the lognormal distribution (i.e. θ and β) are generally assessed through *Maximum Likelihood Estimation* (MLE), with the likelihood function being given in Eq. (2.10) in which F is the fragility function for a specific damage state and x_i a parameter that can take the value of 0 or 1 depending whether the structure is capable or not of sustaining a given damage state at the intensity level y_i.

$$F(y) = \Phi\left[\left(1/\beta\right)\cdot \ln\left(y/\theta_y\right)\right]; y \geq 0 \tag{2.9}$$

$$L = \prod_{i=1}^{nIML} \left[\left(F\left(y_i\right) \right)^{x_i} \cdot \left(1 + F\left(y_i\right) \right)^{1-x_i} \right] \tag{2.10}$$

Vulnerability curves provide the distribution of loss conditional on the level of ground shaking. Often vulnerability curves are computed through the convolution fragility with an available damage-to-loss model, which correlates the level of damage with the respective expected loss. Damage-to-loss models, also known as consequence models, are probably one of the main sources for uncertainty in the vulnerability assessment. Damage-to-loss models simultaneously fully compatible with the fragility model and developed for the region and building typology under assessment are often not available. This, obviously, has an impact on the final loss estimates. Martins *et al* (2016) have studied these effects and proposed an alternative way to compute vulnerability curves directly from the cost of repairing the damage on the different elements.

3

DEVELOPMENT OF PERIOD-HEIGHT RELATIONSHIPS FOR ASSESSMENT OF REGULAR CODE-COMPLIANT REINFORCED CONCRETE BUILDINGS

3.1 SUMMARY

Simplified relationships to compute the period of vibration are useful in the estimation of seismic loads during the design process of new structures, in the assessment of the structural vulnerability of existing buildings, or in the estimation of earthquake losses of large portfolios of assets. The height of a structure (or in alternative the number of storeys) has been traditionally used as the main parameter to quickly estimate the period of vibration. A brief examination of existing height-period relationships demonstrates that more often than not they are specific to a given region and therefore with limited applicability. By analysing a large number of buildings with varying heights and designed according to increasing levels of ground motion, this study proposes simplified relationships suitable for assessment of regular code-compliant European reinforced concrete moment frame buildings.

3.2 INTRODUCTION

Estimating the period of vibration of a structure is an essential step for the calculation of the seismic demand in the design process. However, this is often not always a simple procedure. While numerical modelling is a suitable alternative, for estimating the period of vibration for single structures, when assessing a region containing a large number of buildings this is simply

not feasible. For these large-scale assessments is not unusual to apply simplified relationships (i.e. requiring no numerical modelling) to predict the expected period of vibration, (Bal *et al.* 2010a). The vast majority of these models use the height of the structure (or in alternative the number of storeys) as the main input parameter to estimate the period of vibration and although not innovative, the simplicity of the height-dependent empirical relationships contributed greatly to their widespread dissemination.

Traditionally, these relationships have been developed from either monitoring the dynamic properties of real buildings, (Oliveira and Navarro 2010), or from numerical analysis, (Crowley and Pinho 2004). The former approach allows a more realistic estimation of the periods of vibration, but it might be too structure-specific, and in the vast majority of the cases it only allows the estimation of the elastic period of vibration. Moreover, the experimental measurement of the dynamic properties of a statistically sufficient sample of structures can be considerably expensive and time-consuming. The latter approach enables considering a wider variety of structures, and the estimation of the period of vibration at various stages of damage (from elastic (undamaged), to yielding or even near collapse).

The majority of the proposed models to estimate the fundamental period of vibration have the form given by Eq. (3.1), in which H is the building's height and C_t and α are constants. A detailed examination and discussion on existing period-height relationships is presented in Crowley and Pinho (2004, 2010). For the sake of synthesis, in this study a summary of previously published relationships for European constructions is provided in Table 3.1.

Common limitations of current period-height relationships are, for example, the reduced number of structures and/or the need to consider more storeys. Moreover, structures designed and built according to different seismic regulations and to distinct levels of ground shaking are often analysed together in order to attain a statistically significant sample. One of the justifications for this study was to evaluate in a consistent manner the variations that different design accelerations can induce on the period estimates within the scope of large scale seismic assessment studies. Furthermore, despite the significant number of simplified period-height relationships, it is clear that European structures designed according to the Eurocodes have yet been the target of limited scrutiny. Additionally, the current version of Eurocode 8 (CEN 2010c) uses a formula initially developed for Californian buildings during the 70's decade. This

study offers the opportunity to revise its applicability. Moreover, the mathematical model included in Eurocode 8 was intended to underestimate or the period of vibration in order to be used with the lateral force method, as observed by Gallipoli *et al* (2009) and remarked by Crowley and Pinho (2010), This approach, albeit valid for design, is not suitable for assessing the behaviour of existing structures where the mean value for the period of vibration is required. Hence, the present study improves upon former ones by addressing these issues and providing updated mathematical models for predicting the expected period of vibration of reinforced concrete structures designed according to the most recent European regulations, and considering different design shaking, with and without infill panels.

For this study the first mode elastic and inelastic periods of vibration of reinforced concrete moment frame buildings were estimated from a significant number of finite element models. The total number of floors of these structures ranged between 3 and 10, and the influence of infill panels has also been considered. The elastic period was computed from eigenvalue analysis whilst the inelastic period was estimated from pushover analysis. This study expands on previous endeavours by: (i) including the seismic design level rather than just the total height as an input parameter for estimating the period of vibration, (ii) considering both the elastic and inelastic (at the yielding point) periods of vibration, (iii) considering the influence of infill panels and the number of bays, (iv) propagation of the building-to-building variability in the period estimates, and (v) evaluation of the impact in the calculation of and derivation of fragility models and on the final risk metrics.

$$T = C_t H^{\alpha} \tag{3.1}$$

Table 3.1 - List of proposed period-height relationships.

Region	Elastic period (T_{el})		Yielding period (T_y)		Reference
	Bare frame	Infilled	Bare frame	Infilled	
Spain		$T = 0.051N$			(Kobayashi *et al.* 1996)
Spain		$T = 0.049N$			(Navarro *et al.* 2002)

France		$T = 0.015H$			(Dunand *et al.* 2002)
Southern Europe			$T = 0.1H$ *		(Crowley and Pinho 2004)
Southern Europe				$T = 0.055H$	(Crowley and Pinho 2006)
Southern Europe			$T = 0.07H$ **		(Crowley *et al.* 2008)
Italy		$T = 0.016H$			(Gallipoli *et al.* 2009)
Turkey			$T = 0.083H$		(Bal *et al.* 2010b)
Portugal	$T = 0.022H$	$T = 0.013H$			(Oliveira and Navarro 2010)
Southern Europe			$T = 0.014H$		(Ricci *et al.* 2011)

N - Total number of storeys; H - Height
(*) non ductile structures
(**) ductile structures

3.3 CASE STUDY

According to the global building database developed by the PAGER group (Jaiswal et al. 2010), on average, reinforced concrete moment frames (with or without masonry infill walls) host 51% of the population in Southern Europe, where seismic hazard is highest. Silva et al (2014) indicated that reinforced concrete construction accounts for approximately 50% of the Portuguese building stock and hosts 60% of the national population. The vast majority of these structures are composed by moment frames with masonry infills, and 51% have been designed following either to latest Portuguese design regulation or the Eurocodes. This type of construction has been increasing significantly in the last decades in Southern Europe. For example, reinforced concrete was rare in Italy, Portugal and Greece in the 1920's, and in the last decade it accounted for (on average) 68% of the new construction. The growing acceptance and enforcement of the Eurocodes suggests an expected increase on the number of *Eurocode-compliant* structures.

The calculation of the elastic or inelastic period of vibration using analytical approaches is usually performed using 2D models or equivalent single-degree-of-freedom systems, and less frequently 3D structures. Considering the structures covered in this study, (Crowley and Pinho 2004, Silva *et al.* 2014d, Ulrich *et al.* 2014) used 2D moment-resisting frames with 1 to 8 storeys and 1 to 7 bays (on average, 3.5 bays). Similarly, Silva *et al.* (2014) assessed the dynamic

response of 2D frames with a number of storeys ranging from 1 to 8, with 3 bays. Bal et al. (2010b)and Ulrich *et al.* (2014) instead modelled 3D structures with 2 to 8 storeys and 2 to 4 bays (on average, 3.1 bays). The present study considered sets of 3 to 10 storeys moment-resisting frame reinforced concrete structures designed according to the most recent European standards (CEN 2009, CEN 2010a, CEN 2010b, CEN 2010c) and for increasing levels of ground shaking. The majority of the case study structures were 3-bay moment resisting frames. However, for the taller buildings, an extra bay was added, as the footprint of buildings with a higher number of storeys tends to be larger (e.g. Oliveira and Navarro (2010)). The structures were designed to be regular in height and symmetrical in both horizontal axes, as recommend by modern design regulations. The chosen concrete class has a characteristic compressive strength of 25 MPa, whilst the characteristic yield strength of the rebar steel is 500 MPa. A permanent vertical load of 6.25 kNm^{-2} has been considered in the design in order to represent the expected weight of the concrete slab. An additional live load of 2.80 kNm^{-2} has also been included. Following the recommendations in Eurocode 1-1 (CEN 2009), the absolute value of the live load has been lowered at the roof level to 0.40 kNm^{-2}. In addition to the vertical loads, all structures have been designed to withstand the horizontal loading due to the wind excitation, considering a wind velocity of 25ms^{-1} and a Class II terrain, according to the Eurocode 1-4 (CEN 2010a). Five levels of ground motion intensity were considered with design peak ground acceleration ranging from 0.05g (i.e. low seismic hazard) to 0.40g (i.e. high seismic hazard) selected to cover the range of expected design ground motion levels for the European continent .

To avoid excessive deformations under static loading, the minimum height for the beams was set to 1/12 of the respective span while the minimum cross section for the columns was 0.25x0.25 m^2. For the 10-storey structures, a vertical element has been added to account for the increase in stiffness of a lift shaft. For each intensity level, 25 structures were generated and both the span length and storey height have been randomly sampled from the probability distributions found in Silva *et al* (2014d). For the sake of simplicity, the same beam length was used for each bay within the same structure, which is a common assumption in other similar studies(e.g. (Ulrich *et al.* 2014)).

Brick infill panels were considered on the building's facade. These have been modelled with a double diagonal struts system with the strength and stiffness properties computed according to the recommendations of Crisafulli and Carr (1997) and Smyrou *et al* (2006, 2011).

The numerical models have been constructed using force-based beam elements with distributed plasticity and five integration points using the open-source finite element software OpenSees (McKenna *et al.* 2000). The nonlinear material behaviour of the concrete was modelled following the stress-strain relationship proposed by Mander *et al* (1988), whilst the steel reinforcement was modelled following Menegotto and Pinto (1973) recommendations.

3.4 USING EIGENVALUE ANALYSIS TO COMPUTE ELASTIC UNCRACKED PERIOD

Although unlikely to find any structure responding with its uncraked stiffness, using period estimates based on gross stiffness can still be useful especially within a force-based design framework where an overestimation of the expected shear forces is recommended. This also provides a suitable lower boundary for the true value of the expected fundamental period of vibration.

Figure 3.1 depicts the fundamental periods of vibration computed from the 3D finite element models for both the bare frame and infilled structures. The results have been sorted in total number of storeys and design ground motion. As expected, the average period increases with the number of storeys and decreases with the seismic design level.

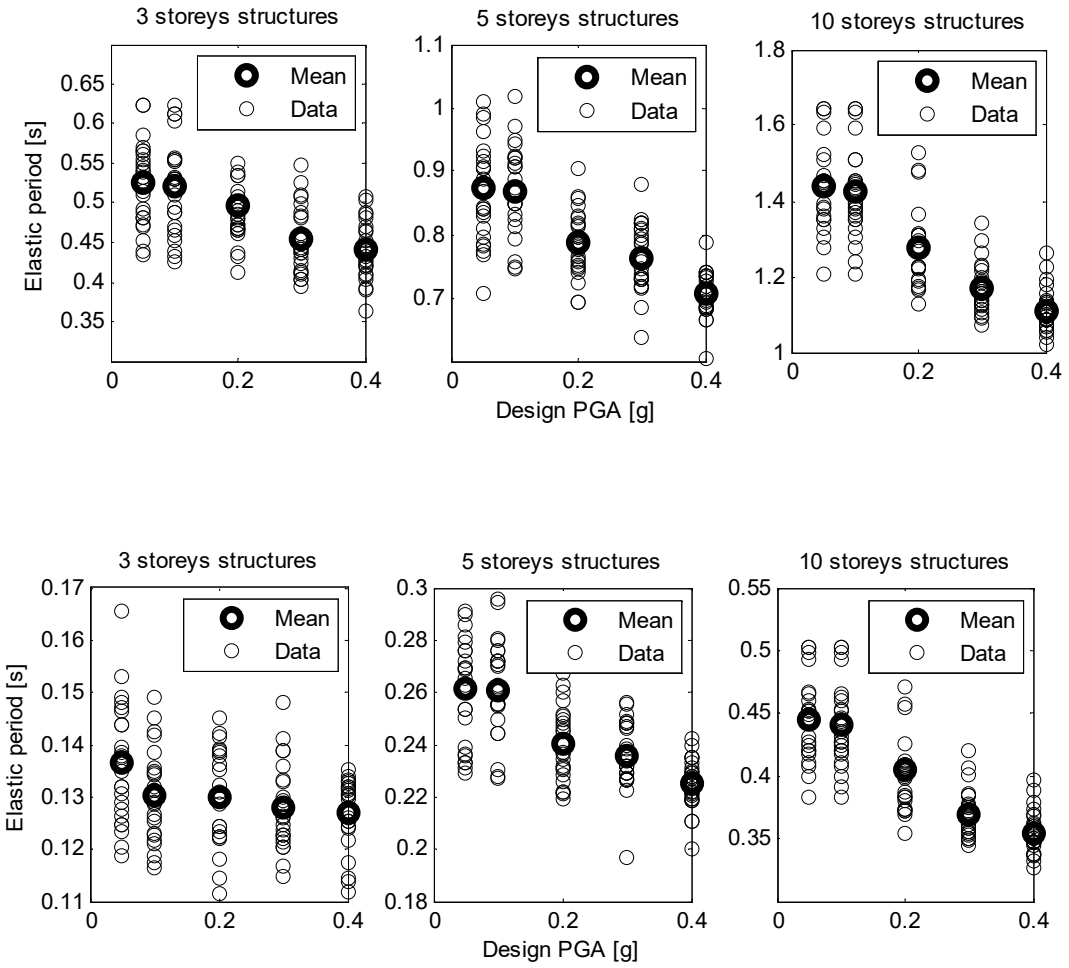

Figure 3.1 - First mode elastic period *vs* design ground motion. Top: Bare frame structures; Bottom: Infilled structures

Figure 3.1 shows a decrease of around 20% on the average period from the lowest ground motion level to the highest due to the need for having elements with larger cross section (and consequently with greater inertia and stiffness). These differences are obviously non-negligible and are quite significant for the development of fragility functions, e.g. (Silva *et al.* 2013), or employment of displacement-based earthquake loss assessment methodologies, e.g. (Bal *et al.* 2010a), further supporting the claim for including the seismic design level on the period estimates.

Moreover, comparing between the top and bottom plots indicate a decrease of more than 50% in the period of vibration. Silva *et al* (2014d) in a former study has also found a reduction on the elastic period due to the introduction of the infill panels in the same order of magnitude.

An additional comment on Figure 3.1 is that the decrease in the mean period of vibration between from 0.05g to 0.10g is comparably smaller than the decrease for the remaining design levels. This is probably due to the fact that for these levels of ground shaking the lateral load resisting system design is often governed by a combination of permanent load and live loads (e.g. wind).

Fitting unconstrained power laws to the complete datasets the models yielded the models plotted in Figure 3.2. The accuracy of the fits was quantified by the standard error of estimate (S_{est}) which provides an indication on the on the error introduced when predicting the period of vibration from the proposed models for any possible value for the building's height (Crowley and Pinho 2004). This parameter is calculated using Eq. (3.2) where $r_{Tpred,Tobs}$ represents the correlation between the observed periods (Tobs) and their predicted counterparts (T_{pred}) with a sample with size n. The error was found to be equal to 0.094s and 0.048s for the bare-frame and infilled structures, respectively. These reasonably low values indicate an acceptable fitting of the mathematical model.

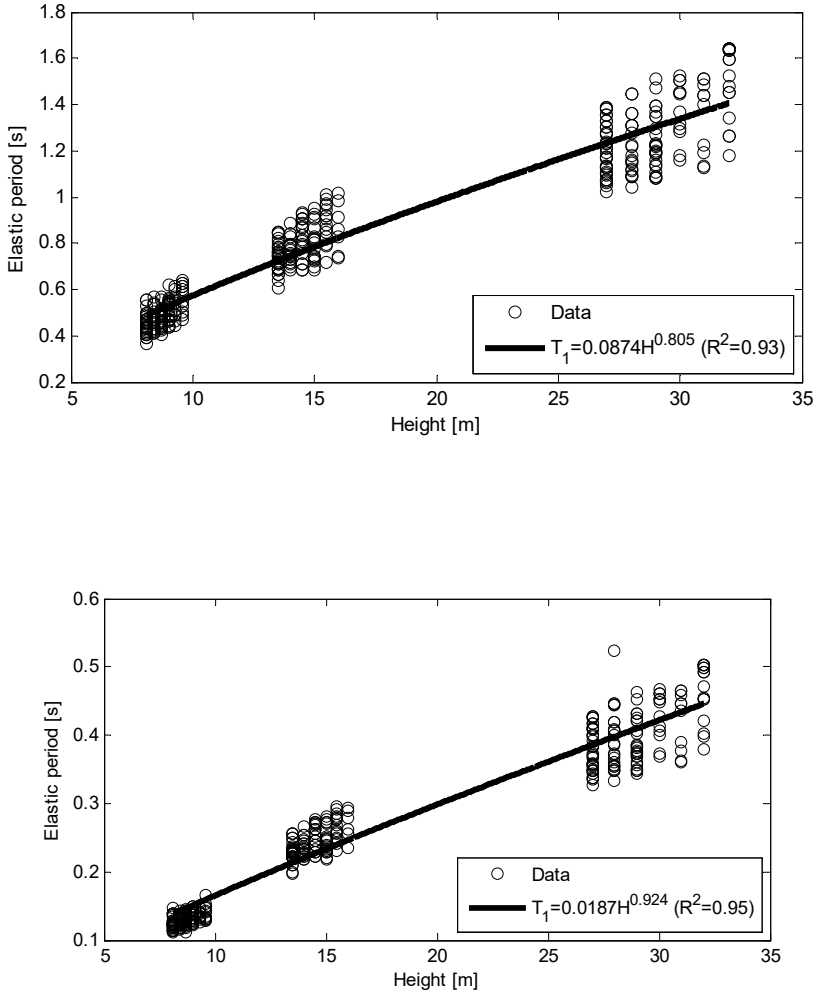

Figure 3.2 - Power law fitting to first mode elastic period. Top: Bare frame structures; Bottom: Infilled structures

$$S_{est} = S_{T_{pred}} \cdot \sqrt{1 - r^2_{T_{pred},T_{obs}}} \cdot \sqrt{\frac{n}{n-2}} \cdot \tag{3.2}$$

Although the models in Figure 3.2 yielded relatively small standard errors of estimate and exceptionally good correlation factors (R^2>0.90), the dispersion around the best-fit curve is still considerably large (especially for the taller buildings). Therefore, it seems obvious that in order to have the best possible period estimate, prior to fit any mathematical model the data should be firstly sorted by seismic design level. Figure 3.3 depicts the results of fitting an unconstrained power laws (C_t and α in Table 3.2 and Table 3.3) to the elastic periods of vibration given by the Eigenvalue analysis sorted by design ground motion. The results in Table 3.2 and Table 3.3 show, as expected, a decrease of at least 40% on the standard error of

estimate for the new models when comparing with the one computed considering the whole dataset.

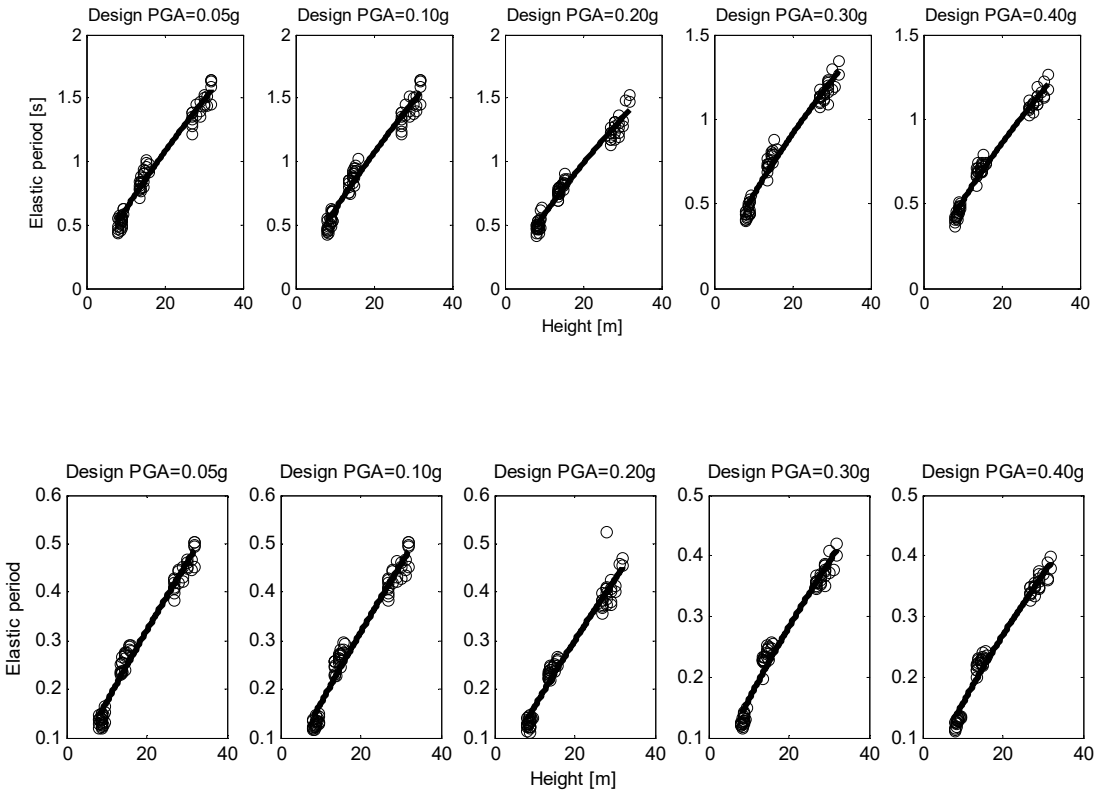

Figure 3.3 - Power law fitting to first mode elastic period sorted by design PGA. Top: Bare frame structures; Bottom: Infilled structures

Table 3.2 - Models parameters (elastic period-bare frame structures)

Design PGA [g]	C_t	α	S_{est} [s]
0.05	0.0986	0.7972	0.0645
0.10	0.0989	0.7934	0.0671
0.20	0.0995	0.7641	0.0526
0.30	0.1015	0.7327	0.0518
0.40	0.0945	0.7349	0.0368

C_t and α - Model parameters; S_{est} - Standard error of estimation

Table 3.3 - Models parameters (elastic period-infilled structures)

Design PGA [g]	C_t	α	S_{est} [s]
0.05	0.0223	0.8896	0.0200
0.10	0.0214	0.8997	0.0220

0.20	0.0221	0.8696	0.0219
0.30	0.0259	0.7962	0.0164
0.40	0.0257	0.7838	0.0137

C_t and α - Model parameters; S_{est} - Standard error of estimation

The mathematical models presented in Table 3.2 and Table 3.3 have been calibrated to discrete values of design ground motion. However, one of the objectives of this study to generalize the results to any design ground motion. To this end, a surface model was fitted considering the entire dataset as illustrated in Figure 3.4. Due to the physics of the problem it is obvious that the best-fit surfaces must not yield negative values for the period of vibration for any realistic combination of design ground motion and height within the region of interest (i.e. non-negative design ground motion and non-negative height values lower than 40 metres), therefore any best-fit surface must contain the origin. Consequently, and if one assumes a two parameter polynomial function to represent the best-fit surface, this constraint was met by setting the constant of the function to zero. The degree of the polynomial function was defined after some iterations and evaluating the maximum degree without parameters with non-meaningful coefficients. The best-fit surface that complied with these conditions was found to be the polynomial function shown in Eq. (3.3) and (3.4). For this case the computed standard errors of estimate for the surface fit were 0.054s and 0.018s for the bare frame and infilled structures.

$$T_1(PGA, H) = -0.06 \cdot PGA + 0.07 \cdot H + 0.17 \cdot (PGA)^2 - 0.03 \cdot PGA \cdot H \qquad (3.3)$$

$$T_1(PGA, H) = -0.11 \cdot PGA + 0.02 \cdot H + 0.25 \cdot (PGA)^2 - 0.01 \cdot PGA \cdot H \qquad (3.4)$$

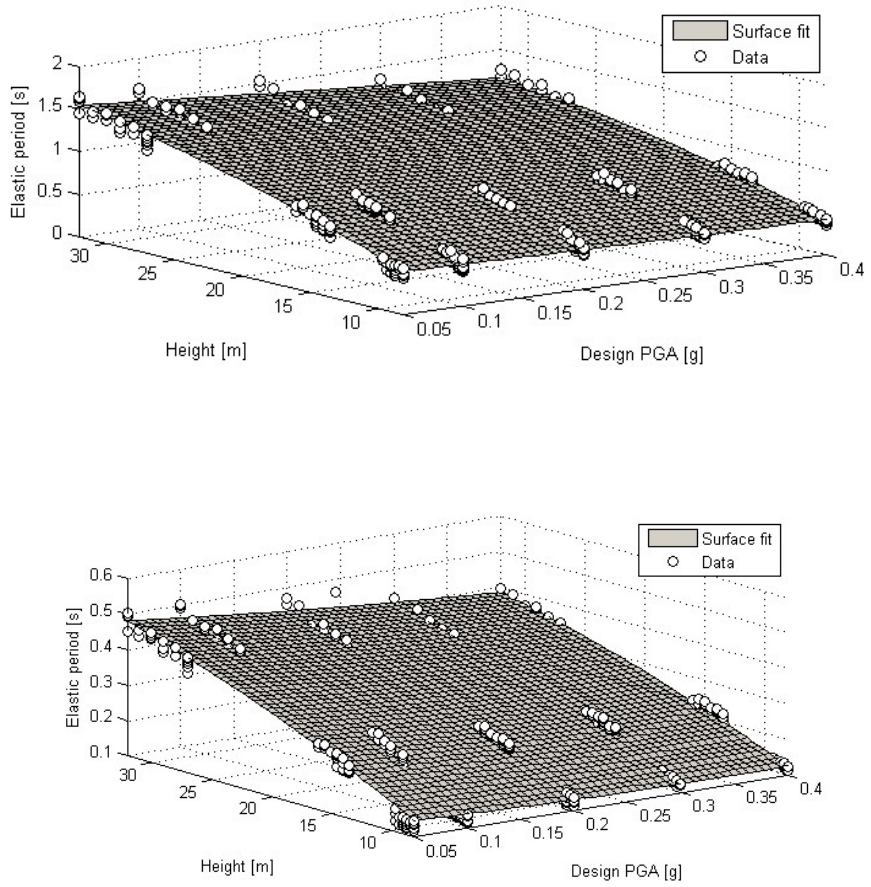

Figure 3.4 - Surface fitting to first mode elastic period. Top: Bare frame structures; Bottom: Infilled structures

3.5 USING PUSHOVER ANALYSIS TO COMPUTE YIELD PERIOD

While using period estimates based on the uncracked stiffness could be acceptable to compute a lower boundary of the true value of the period of vibration for displacement-based assessment the expected yield rather than the elastic period is often necessary. In reinforced concrete buildings, cracking in critical elements (e.g. beams) is expected to occur under permanent loading alone. Even in the unlikely cases where cracking has not occurred it is unreasonable to believe that a structure would respond with its gross stiffness under an earthquake since cracking will occur at the early stages of the dynamic response and therefore stiffness will reduce rapidly. Moreover, the derivation of fragility models (Silva *et al.* 2013) or the direct assessment of earthquake losses (Bal *et al.* 2010a) may require the calculation of the yield period of vibration. All the case study structures are symmetrical in plan and regular in height and as a consequence the influence of the higher modes is negligible. Therefore,

pushover algorithms have been considered an acceptable alternative to the more accurate, but also more computational demanding, nonlinear time-history analysis for estimating the yield period. An approach to compute the expected yield period of the structure can be to firstly compute the yield displacement of the equivalent single degree of freedom system. In this study the bilinearization of the capacity curve using the N2 method (Fajfar and Gašperšič 1996) has been used to compute such yield displacement. Knowing the yield displacement and the correspondent structure's deformed shape the expected yield period is computed from Eq. (3.5) where M_{eff} is the effective mass of the equivalent system calculated by the means of Eq (3.6), V_y is the base shear at the point of yield and $d_{y,eff}$ is the correspondent displacement measured at the height of centre of the seismic forces (h_{eff}). Figure 3.5 depicts the yield period computed from the capacity curves for bare and infilled structures.

$$T_y = 2\pi \sqrt{\frac{M_{eff}}{V_y / d_{y,eff}}} \tag{3.5}$$

$$M_{eff} = \frac{\left(\sum_{i=1}^{n} m_i \delta_i\right)^2}{\left(\sum_{i=1}^{n} m_i \delta_i^2\right)} \tag{3.6}$$

$$h_{eff} = \frac{\left(\sum_{i=1}^{n} m_i \delta_i h_i\right)}{\left(\sum_{i=1}^{n} m_i \delta_i\right)} \tag{3.7}$$

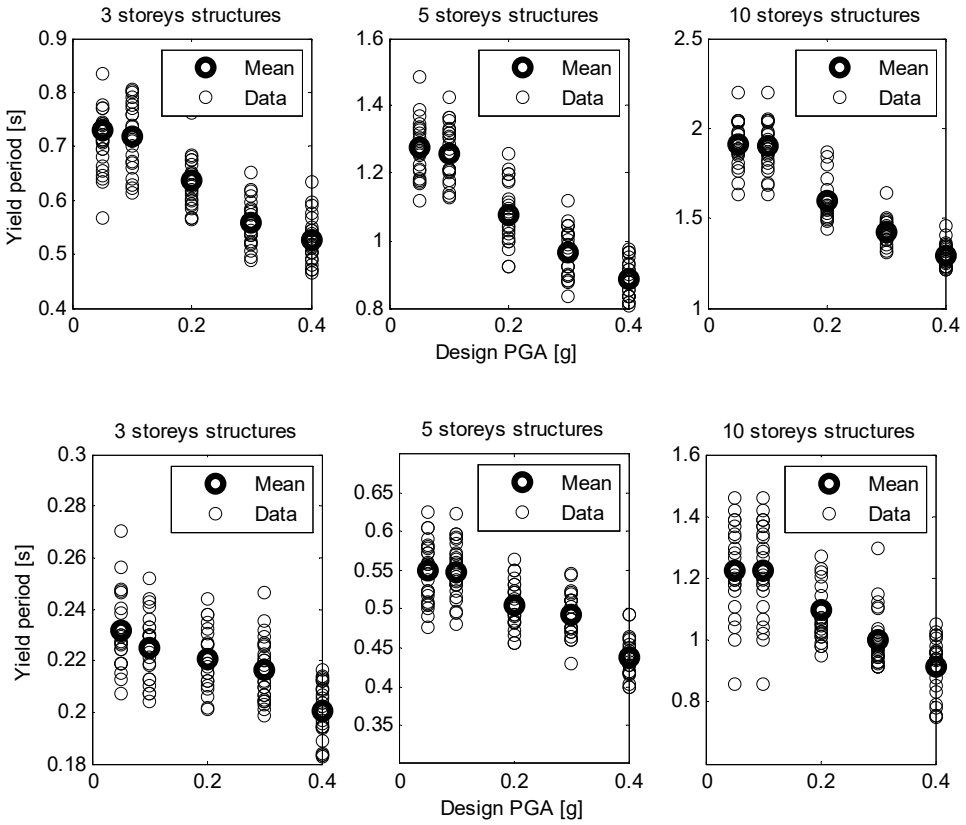

Figure 3.5 - Yield period vs design ground motion. Top: Bare frame structures; Bottom: Infilled structures

It should be noted that, in this context, T_y could also be calculated following a mechanical approach, in which $d_{y,eff}$ is estimated following the formulae for the calculation of the displacement (or curvature) at the yielding point, e.g. (Sullivan and Calvi 2012).

The results from Figure 3.5 indicate a decrease on the yield period of vibration with the design ground shaking in the order of 39% for bare frames and 24% for infilled frames. This decrease is also more pronounced for taller structures, as also observed in the assessment of the elastic period.

When unconstrained power laws were fitted to the analytical results (see Figure 3.6), the standard error of estimate for the yield period were found to be equal to 0.201s and 0.105s, which is about double the error computed for the uncracked elastic period. This was to be expected since the nonlinear behaviour of the structure inherently introduces additional variability on the response. However, it should be noted that the standard error of estimate found is still relatively small.

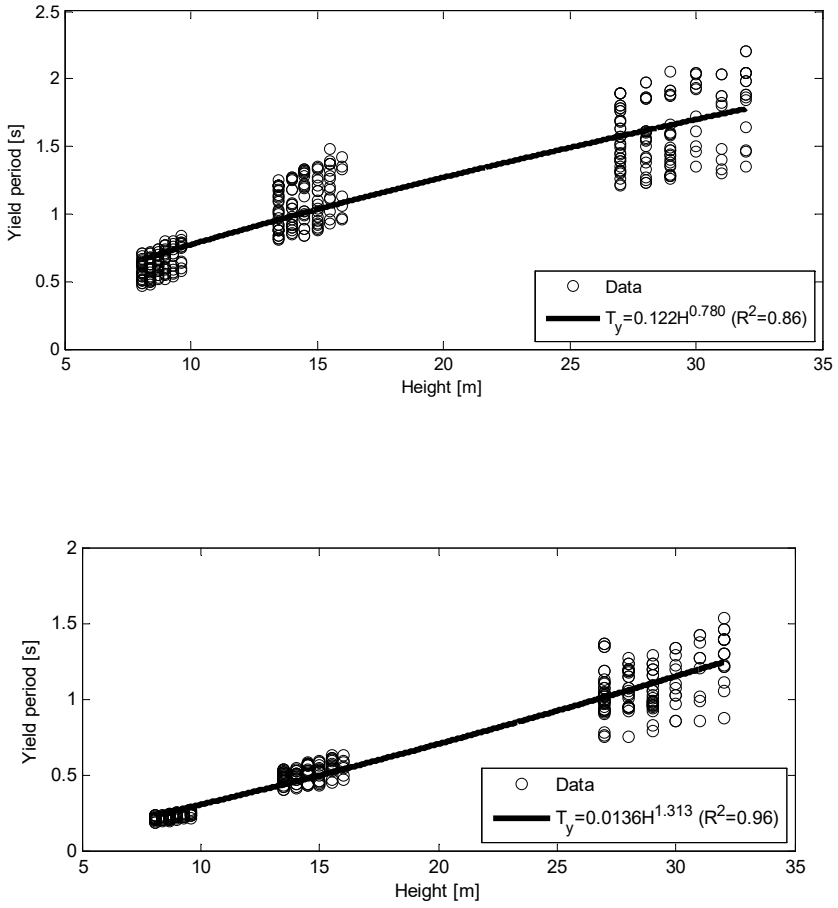

Figure 3.6 - Power law fitting to yield period. Top: Bare frame structures; Bottom: Infilled structures

Similarly to what has been presented in section 3.4, it has been decided to fit different mathematical laws according to the considered seismic design levels (see Figure 3.7). The standard error of estimate described in Table 3.4 and Table 3.5 indicate a significant decrease in comparison with the one computed from the data prior to be sorted by seismic design level.

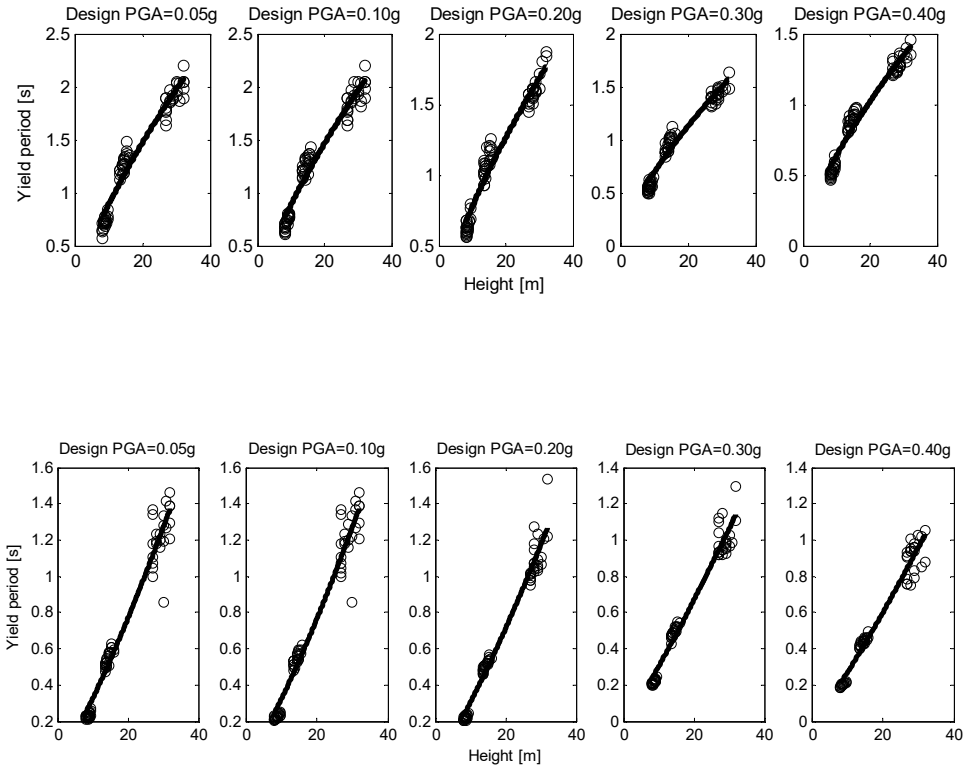

Figure 3.7 - Power law fitting to yield period sorted by design PGA. Top: Bare frame structures; Bottom: Infilled structures

Table 3.4 - Models parameters (yield period -bare frame structures)

Design PGA [g]	C_t	α	S_{est} [s]
0.05	0.1647	0.7302	0.1032
0.10	0.1657	0.7267	0.0984
0.20	0.1529	0.7054	0.0771
0.30	0.1352	0.7068	0.0690
0.40	0.1320	0.6829	0.0571

C_t and α - Model parameters; S_{est} - Standard error of estimation

Table 3.5 - Models parameters (yield period- infilled structures)

Design PGA [g]	C_t	α	S_{est} [s]
0.05	0.0188	1.2367	0.0784
0.10	0.0179	1.2513	0.0798
0.20	0.0179	1.2296	0.0570
0.30	0.0217	1.1427	0.0565
0.40	0.0183	1.1632	0.0511

C_t and α - Model parameters; S_{est} - Standard error of estimation

The same criteria presented in section 3.4 to estimate the best-fit surface was employed to model the inelastic period for the bare frame and infilled structures, as shown in Eq. (3.8) and (3.9) and depicted in Figure 3.8. For these best-fit surfaces the computed standard error of estimate were 0.104s and 0.077s for bare frames and infilled structures, respectively. As previously discussed increasing the design ground motion level naturally decreases the structure's period of vibration. This decrease is more apparent for the inelastic period (see Figure 3.8) since structures designed for lower levels of PGA are expected to develop a mechanism at earlier stages of loading. Considering that the inelastic period is especially suited within a displacement-based assessment framework, where the main goal is to correctly predict the displacements, it is recommended that at least on these cases to use mathematical models that also consider the seismic design level rather than just the height, like the ones presented herein.

$$T_y(PGA,H) = -0.74 \cdot PGA + 0.11 \cdot H + 0.98 \cdot (PGA)^2 - 0.05 \cdot PGA \cdot H \qquad (3.8)$$

$$T_y(PGA,H) = -0.16 \cdot PGA + 0.03 \cdot H + 0.30 \cdot (PGA)^2 - 0.03 \cdot PGA \cdot H \qquad (3.9)$$

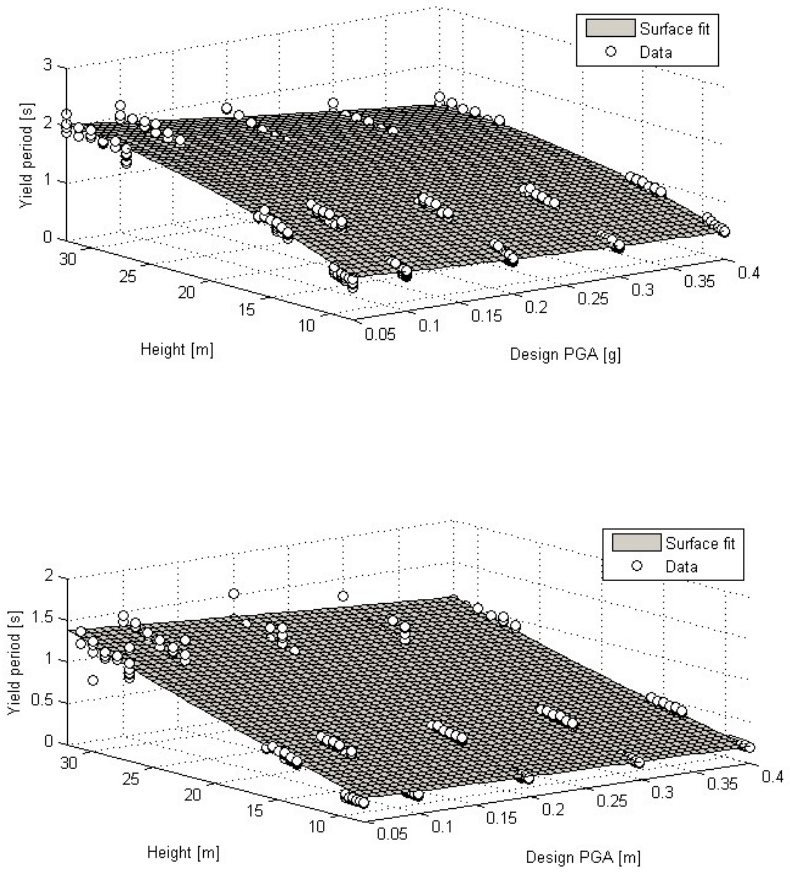

Figure 3.8 - Surface fitting to yield period. Top: Bare frame structures; Bottom: Infilled structures

3.6 COMPARISON WITH PREVIOUS MODELS

This section presents a comparison with the models derived herein and previous proposals. As previously mentioned, the vast majority of the existing studies on this subject are region-specific. Since the structures generated in this study have been designed according to European regulations, it was decided to limit this comparative study only to models developed for this region. For the relationships listed in Table 3.1 where the number of storeys rather than height was used as the input parameter to compute the expected period an average storey height of 3 metres was considered.

The majority of the previous models were developed based on the results from structures with very limited (if any) seismic design, therefore in this section and for comparison purposes, only the models developed for the lowest ground motion level have been considered. The study from Oliveira and Navarro (2010) contains structures built in Portugal (mainly in the

region of Lisbon) between 1940 and late 2000's with the majority being post 1980's buildings, consequently with some degree of seismic design. For this reason, when comparing the period estimates proposed by this study with the models from Oliveira and Navarro, only functions developed for peak ground acceleration equal to 0.20g (i.e. the expected acceleration for the 475-year return period at the city of Lisbon) have been used.

Most of the models listed in section Table 3.1 have been developed from data collected using monitoring systems installed on buildings under low amplitude motion. Under these circumstances is safe to assume that these models are most likely best suited for estimating the elastic period of vibration. Only Crowley and Pinho (2004) propose different models for both the elastic and inelastic period of vibration. Figure 3.9 summarizes the main findings of this comparative study.

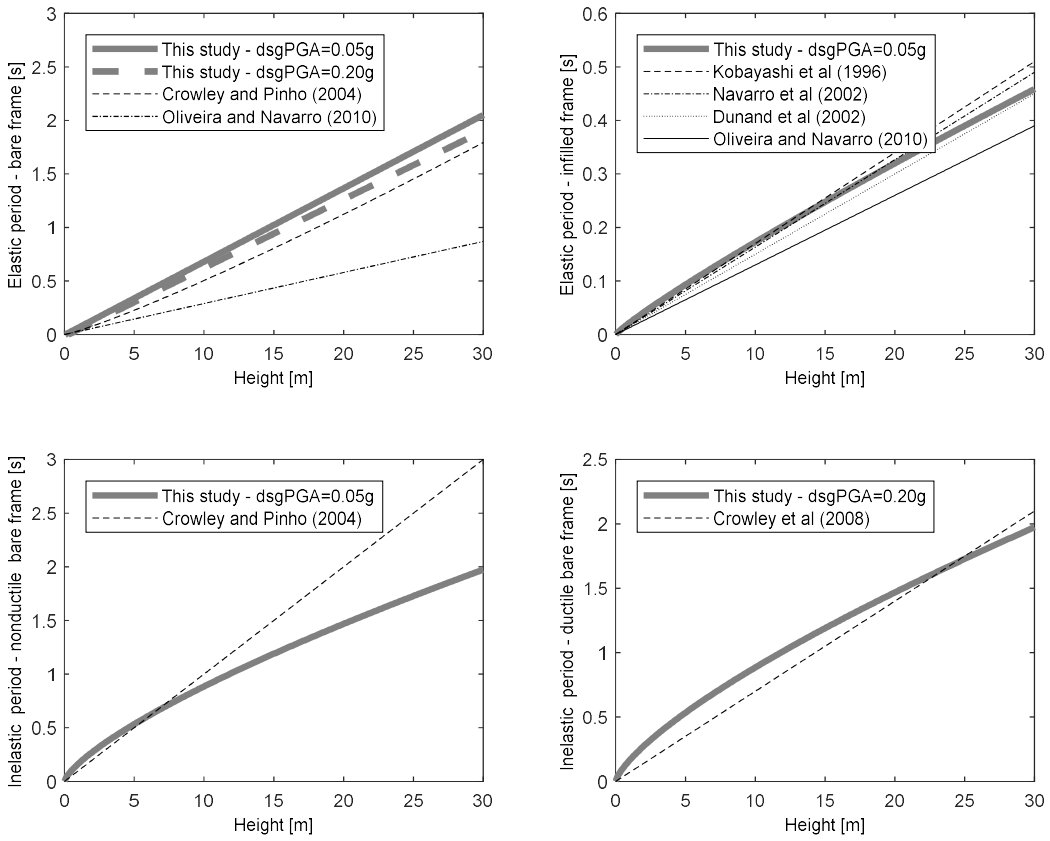

Figure 3.9 - Comparative study.

As previously mentioned, the differences on the period of vibration introduced by the seismic design level can on average reach about 20%. This is consistent with the results shown on the

top-left plot of Figure 3.9 where the differences between both curves become more discernible with increasing heights. Another comment on the results depicted in Figure 3.9 is that the period predictions obtained with the model from Oliveira and Navarro (2010) for bare frame structure are clearly set apart from the remaining mathematical models with significantly lower estimates. One of the reasons for this discrepancy could be the poor correlation between the periods of vibration and height indicated by Oliveira and Navarro (2010), due to the limited number of analysed structures. When analysing the results for the infilled frames, a stronger correlation between all the models for heights up to 10 metres (i.e. around 3 storeys) was found. For higher structures, the models start to deviate considerably. When considering the elastic period, the relationships proposed herein generally yielded slightly more flexible solutions than the remaining studies. This could result from the fact that some building collections considered in previous studies have also included buildings with a greater number of bays than the ones considered in this study (more commonly observed in taller buildings, e.g. Oliveira and Navarro (2010). However, as previously mentioned the total number of bays considered herein was selected based on existing literature and is a commonly seen building typology. An additional factor to possibly have contributed for this observation was the fact that the buildings analysed in this study have been designed according to modern design codes that generally favour more flexible solutions for better energy dissipation. With regards to the inelastic period, the models developed herein and the ones proposed by Crowley and Pinho (2004) provided period estimations with remarkable correlation for the heights up to 10 metres, but after this point the models start to diverge and the model proposed herein consistently produces lower estimates of the expected period of vibration. This behaviour is most likely to have occurred due to the period saturation expected to happen in taller buildings that cannot be captured using a linear function as proposed by Crowley and Pinho (2004), and the addition of the influence of stiff structural elements such as staircases or lift shafts.

3.7 IMPACT ON THE DERIVATION OF FRAGILITY AND SEISMIC RISK

The derivation of fragility functions (establishing the probability of exceeding a number of damage states conditional on a set of ground shaking levels) using simplified approaches often

relies on period-height relationships (e.g. Borzi et al. (2008), Silva et al. (2013), Villar-Vega et al. (2017)). Thus, the accuracy and reliability of these relationships will affect directly the resulting fragility functions. A simple demonstration is provided herein, in which two single-degree-of-freedom systems were created considering the expected periods of vibration, using the formulae proposed in this study. These two SDOF systems represent two mid-rise (5 storeys) structures, and will have distinct periods of vibration due to the different design ground shaking (0.20g and 0.40 g – see Figure 3.6). In order to appraise the differences in the structural response only due to the distinct periods of vibration, the same yielding (1%) and ultimate (3%) global drifts were considered. However, it is acknowledged that distinct designs would certainly lead to different displacement capacities. The resulting capacity curves are presented in Figure 3.10. These two SDOF systems have been tested (using nonlinear time history analysis) against the European database of strong motion (Akkar *et al.* 2014) in order to derive a fragility function for the yielding and collapse damage states, as illustrated in Figure 3.11. Additional information about this methodology can be found in Villar-Vega et al. (2017). Finally, these fragility functions were used to calculate the average annual probability of exceeding yielding (AAPY) or reaching collapse (AAPC), considering a hazard curve for the city of Istanbul (www.efehr.org), as described in Table 3.6.

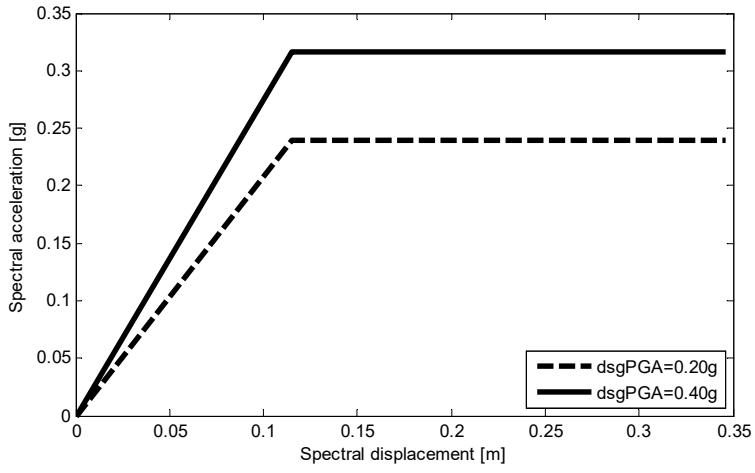

Figure 3.10 - Example differences introduced in the of capacity curves.

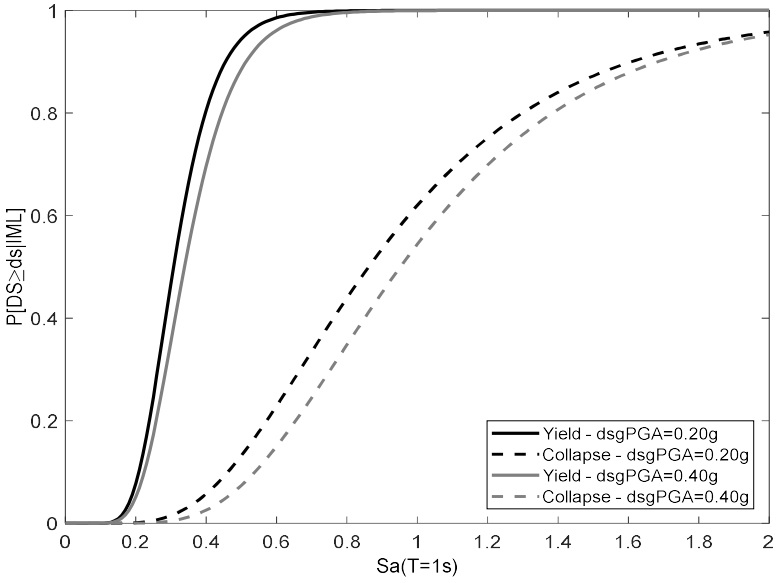

Figure 3.11 - Fragility curves for 5 storeys building.

Table 3.6 - Annual average probability of exceeding yield and reaching collapse.

AAPY		AAPC	
dsgPGA=0.20g	**dsgPGA=0.40g**	**dsgPGA=0.20g**	**dsgPGA=0.40g**
2.36×10^{-3}	2.03×10^{-3}	4.37×10^{-4}	3.319×10^{-4}

These results shown in Figure 3.11 and Table 3.6 demonstrate that the variability in the fragility and risk metrics would have been underestimated should a single period-height relationship had been used for the derivation of the SDOF systems, as opposed to account for the effects due to the consideration of distinct design ground shaking.

3.8 FINAL REMARKS

Period of vibration versus height relationships have been used for several decades for the design of new structures or the assessment of large portfolios of buildings, where individualized numerical analyses are not practical. One of the major limitations of the existing height-period relationships is that often they have limited applicability outside of the region where they have been developed or calibrated, and no distinction is made regarding the design acceleration.

In this study, sets of reinforced concrete frames (bare and infilled) were created and their period of vibration was estimated using an analytical approach. These structures have been designed to be compliant with the most up-to-date European regulation and different levels of design ground motion. Tridimentional finite elemental models were created and the elastic and inelastic periods were evaluated by the means of eigenvalue and pushover analysis respectively.

The results presented herein allowed developing functions that consider both the building's height and the design ground motion as input parameters. Considering these two parameters together has led to a reduction of about 50% in the standard error of estimate when comparing with models were the data had not been sorted by seismic design level.

The findings on this study suggest a reduction of the period of vibration of around 20% from the lowest to the highest design peak ground acceleration levels considered. For the elastic period of vibration, the introduction of the infill panel lead to a decrease in the period of vibration for about one third of its equivalent for the bare frame structures. With regards to the inelastic period, the introduction of the infill panels leads to a minimum reduction of about 30% in the period.

The models presented in this study have been compared with existing studies developed for European constructions. The results revealed slightly more flexible period predictions given by the models developed herein, which may be a result of the fact of the other models contained structures with a higher number of bays.

Finally, an evaluation of the impact in seismic risk introduced by the period of vibration has been included. The analysis allowed to identify and illustrate (i) the need for correct period estimations to avoid erroneous demand predictions potentially resulting in biased assessment, and (ii) the variability on the fragility and risk metrics can be significantly underestimated if a single period-height equation is applied.

4

ADVANCES IN THE DERIVATION OF FRAGILITY MODELS FOR THE DEVELOPMENT OF RISK-TARGETED HAZARD MAPS

Martins, L., Silva, V., Bazzurro, P. and Marques, M. (2016) *Advances in the derivation of fragility models for development of risk-targeted hazard maps*, Engineering Structures (under review).

4.1 SUMMARY

Risk-targeted hazard assessment aims at estimating the design ground shaking that leads to a uniform distribution of the collapse probability of buildings within a given region. An essential aspect of this methodology relies on the definition of the relationship between the collapse probability of buildings designed according to modern seismic regulations and the considered design ground motion. This study adds to previous research on the topic of seismic risk-targeted hazard assessment by investigating how the collapse probability varies with the design level of ground motion, and how this variability influences the resulting seismic risk across Europe. A large number of structures designed according to the most recent seismic regulation in Europe have been analysed. These structures were designed for increasing levels of peak ground acceleration ranging from values close to zero (i.e. buildings located in regions with very low seismic hazard) up to 0.40 g (i.e. moderate to high seismic hazard). Each structure was modelled as a tri-dimentional finite element model, and tested against a set of ground motion records using nonlinear dynamic analyses. Several fragility functions were derived for yielding and collapse damage states, and combined with the seismic hazard curves from the European project SHARE to calculate the spatial distribution of earthquake risk across Europe.

4.2 INTRODUCTION

Current seismic design codes require buildings to be designed for a given ground motion intensity level that is determined from a prescribed return period. The implicit assumption is that this design criterion ensures that the probability of collapse of different types of buildings, although often unknown, is comparable if not uniform. This is unfortunately not true. Uncertainties in the fragility of structures and on the shape of the local hazard curves often lead to an associated seismic risk level that is not only site-specific but also structure-specific, thus invalidating the previous hypothesis (Luco *et al.* 2007, Douglas *et al.* 2013).

Luco *et al* (2007) has described a methodology, known as risk-targeted hazard assessment, that aims at computing the ground motion intensity that in fact leads to an uniform distribution of the seismic risk within a region, usually at national level. The target seismic risk level is directly correlated to the risk a given community or society is willing to accept, and should be established by decision makers, such as politicians with the support of engineers and sociologists.

In this context, it is clear that following a design methodology based on the principles of risk-target assessment has several advantages in comparison with the current procedures. However, a significant obstacle in the implementation of this methodology still needs to be overcome. An essential aspect of this methodology relies on the relationship between the design ground motion (a_{des}) and the expected collapse probability of the structure given a ground motion intensity ($P_c \mid a_{des}$). Low values for the probability of collapse at the design ground motion are to be expected for newly designed structures. However, a literature review has revealed an extremely high variability in this parameter, ranging from 10^{-7} to 10^{-2} (Luco *et al.* 2007, Douglas *et al.* 2013, Silva *et al.* 2014a, Ulrich *et al.* 2014, Martins *et al.* 2015, Sinković *et al.* 2016). These studies, however, considered different types of buildings and design regulations, which often required the use of values of a_{des} corresponding to distinct return periods. Appropriate boundaries for $P_c \mid a_{des}$ and its associated dispersion can be defined by analysing large suits of structures designed according to the same criteria. The ground motion intensity, a_g, at which the collapse is reached is usually modelled as a random variable with a cumulative lognormal distribution, defined by a logarithmic standard deviation (β) and by

any quantile of the distribution (e.g. the 50th quantile, namely the median, $\hat{a}_c$ for which $P_c|a_{des}=0.5$). High dispersion for β has also been found with proposed values ranging from 0.4 to 1.0 (Silva *et al.* 2016). This parameter has a significant influence on the resulting risk-targeted hazard results, as it affects directly the slope of the fragility curve. For example, although not often recognized, large values of β in the widely adopted lognormal distribution modelling framework cause non-negligible values of P_c for levels of ground motion that are hardly felt by humans and certainly of no harm to engineered structures such as those considered here. This large variability and its direct impact in the resulting earthquake risk strengthens the need to further investigate reasonable ranges for $P_c|a_{des}$ and β.

Despite the obvious need for providing an adequate safety margin against collapse when designing and constructing new structures, it is also important to minimize the potential losses due to extensive damage for more frequent events. Observations of past events have revealed regions where modern seismic design regulations are well established, but still high economic losses have been reported. For example, the 1994 Northridge earthquake is deemed as one of the costliest seismic events in recent history, and most of the economic losses came from severely damaged structures, and not due to the very limited number of collapses. These considerations have already been accounted for in some design regulations, such as the Eurocode 8 (CEN 2010c), which establishes a damage limitation requirement for a design ground motion corresponding to a probability of exceedance of 50% in 50 years. However, such an approach, once again, leads to an uneven distribution of damage risk across different structures and regions.

This study investigates the structural fragility of new buildings designed according to the European regulation, within the context of risk-targeted hazard assessment. This goal is achieved through numerical modelling of a number of structures designed considering different seismic ground motion hazard levels, which are then utilized to perform numerous nonlinear dynamic analyses (NDA). The building responses resulting from the NDAs are combined with a damage model to derive fragility functions for yielding (representing the onset of damage) and structural collapse. A comparison is also made between existing fragility functions and those developed herein. Conclusions are drawn regarding the impact that fragility curves with different characteristics have on the annual probability of collapse or of reaching structural damage for different buildings across Europe. Moreover, the findings

presented herein also allow estimating fragility curves for any region in Europe, provided that the buildings have been designed according to the Eurocode.

4.3 NUMERICAL MODELLING AND GROUND MOTION SELECTION

4.3.1 Structural design and 3D finite element modelling

For this study a pre and post-processing Matlab® (MathWorks 2013) algorithm has been developed and all the structural analyses have been performed with the open-source finite element software OpenSees (McKenna *et al.* 2000).

The case study buildings are reinforced concrete moment frames designed according to the most up-to-date European regulations (CEN 2009, CEN 2010a, CEN 2010b, CEN 2010c). All the structures are regular in height and symmetric along both horizontal main axes. The concrete class chosen for the structural design has a characteristic strength of 25MPa, whilst the characteristic yield stress of the rebar steel considered herein was 500MPa. A permanent load of 6.25 kNm^{-2} has been considered on all floors to reproduce the weight of a reinforced concrete slab of average thickness. Following the guidelines of Eurocode 1-1 (CEN 2009) for residential buildings, an additional live load of 2.80 kNm^{-2} has also been considered in the design stage. For the top floor (roof) the absolute value of the live load has been lowered to 0.40 kNm^{-2}. In addition to the vertical loads, all structures have been designed to withstand horizontal loading due to the wind excitation, considering a wind velocity of 25ms^{-1} and a Class II terrain, according to the Eurocode 1-4 (CEN 2010a).

To avoid excessive deformations under static loading, all beams have been designed with a minimum height equal to 1/12 of the span length, while the minimum cross section considered for columns was 0.25x0.25 m^2. Standard values for the reinforcing bars diameters have been used (i.e. 6, 8, 10, 12, 20, 25 and 32 mm). The adopted rebar pattern was the one that minimized the difference between the required rebar area and the actual rebar area while ensuring sufficient spacing between rebars in the most congested cross sections. When designing the structural elements, if the cross section of any structural components had to be updated, the minimum increment in the section's dimensions considered was 0.05 m.

Five sets of 10 structures with 3 and 5 storeys designed for 5 increasing levels of ground motion ranging from peak ground acceleration (PGA) of 0.05g (i.e. very low seismic hazard) up to 0.4 g (i.e. moderate to high seismic hazard) have been analysed herein. Eurocode 8 (CEN 2010c) performance requirements and recommendations have been followed during the design phase. In order to introduce variability in the design, the span length and storey height have been randomly sampled from the probability distributions found in Silva *et al* (2014d). An example of the numerical model is presented in Figure 4.1.

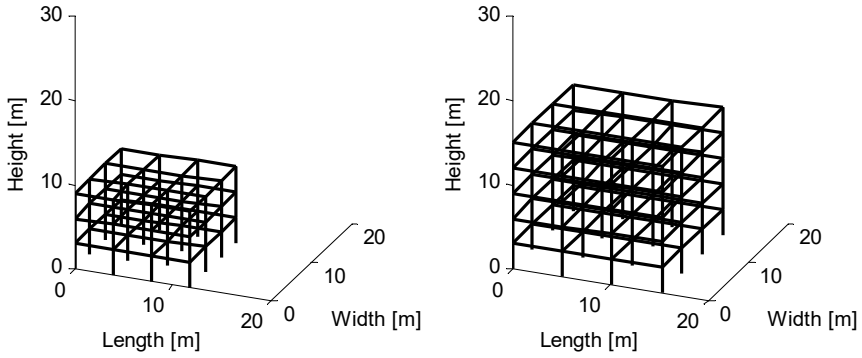

Figure 4.1 - Representation of the numerical models Left) 3 storeys building; Right) 5 storeys building

Being regular structures, a simpler procedure with 2D frames and lateral forces has been used during the design stage, which is also in agreement with the common practice. The design ground motion levels and, consequently, the lateral earthquake loads assumed that the structures are constructed on rock sites (i.e. average shear wave velocity in the top 30m greater than 800ms^{-1}). Both types of seismic action currently included in Eurocode 8 (i.e. Type 1 – far field earthquakes, and Type 2 – near field earthquakes) were considered, and the one that led to the higher base shear was utilised in the design process. Furthermore, all the structures were assumed to have medium ductility.

The 3D structural models developed for assessing the seismic performance of each building were defined using force-based fibre elements, each with five Gauss-Lobatto integration points. The nonlinear material behaviour of the concrete was modelled following the stress-strain relationship proposed by Mander *et al* (1988), whilst the steel reinforcement was

modelled following Menegotto and Pinto (1973) recommendations. Figure 4.2 displays the natural periods of vibration for the different sets of structures assuming uncracked sections.

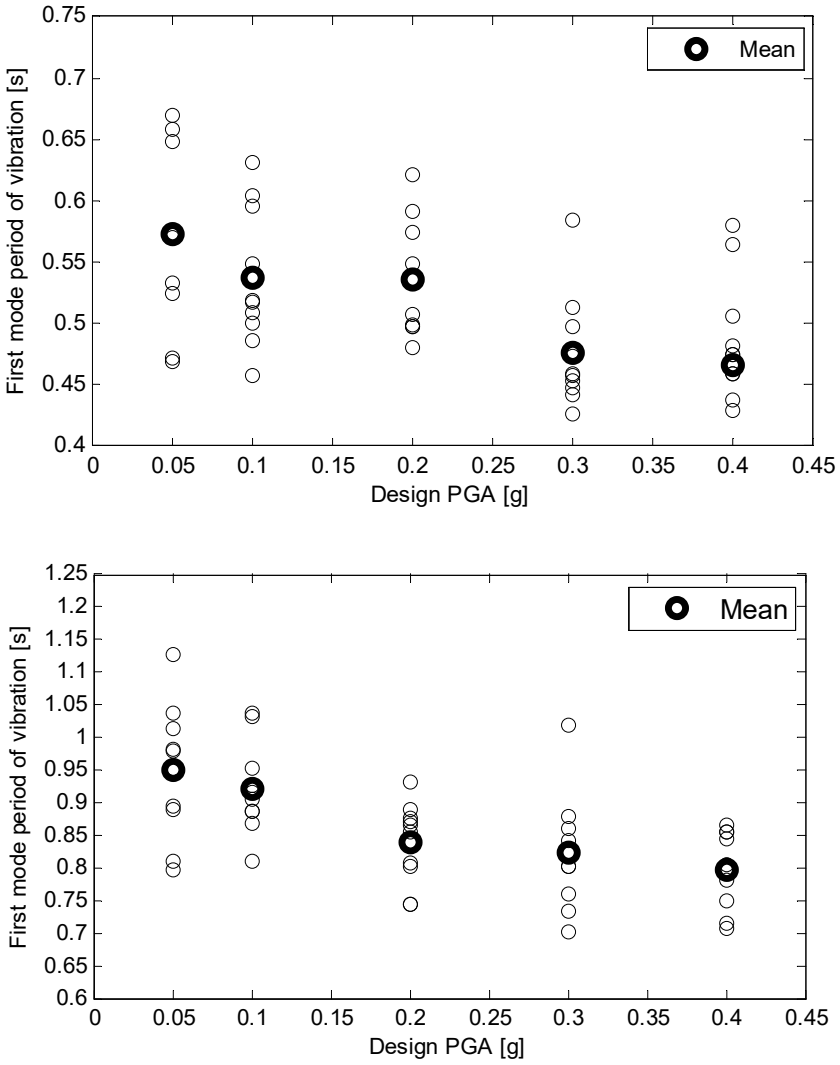

Figure 4.2 - First mode period of vibration [s] Top) 3 Storeys buildings; Bottom) 5 Storeys buildings

4.3.2 Analysis algorithm and ground motion selection

For this study, a modified version of the Incremental Dynamic Analysis (IDA) (Vamvatsikos and Cornell 2002) often called multiple stripe analysis, e.g. (Lin and Baker 2013), has been applied. In this study, fragility curves were derived considering two intensity measures (IM): peak ground acceleration (PGA) and Spectral Acceleration (SA) at the mean first mode period of vibration (T) each set of structures. Whilst Sa yields a better correlation with structural

damage in comparison with PGA (e.g. (Silva *et al.* 2013, De Biasio *et al.* 2014)), most of the seismic hazard maps are defined in terms of PGA. Thus, fragility curves using the former IM can lead to risk metrics with higher accuracy and lower dispersion, but the latter allows a direct estimation of the collapse probability and the design ground motion.

The seismic loads were introduced using scaled real ground motion records, applied to the structure's foundations in both horizontal directions. The combination of effects given by the bidirectional loading was done with one of the horizontal components being multiplied by 0.30, whilst the other remained unchanged, as recommended by the Eurocode 8 (CEN 2010c). Calabrese *et al* (2010) have demonstrated that distributed plasticity elements can become numerically unstable at high ductility levels, especially if the structure exhibits softening behaviour. Therefore, before reporting a numerical collapse, the implemented framework tested several nonlinear solution algorithms (regular Newton-Raphson, modified Newton-Raphson and Newton-Raphson with line search), before reducing the time step given by the ground motion record by a factor of 10 and increasing the tolerance from 10^{-6} to 10^{-4} in order to try to attain convergence.

Ground motion is known to be one of the main sources of uncertainty in structural vulnerability assessment, (Shome and Cornell 1999). For this reason, special consideration has been given to the selection of the ground motion records. The framework developed by Sousa *et al*. (2014) has been used herein to select a large number of accelerograms. This framework is strongly based on the Conditional Spectrum (CS) method developed by Baker and co-workers (Baker 2011, Jayaram *et al.* 2011, Lin *et al.* 2013), which relies on the empirically verified assumption that the set of (log) spectral accelerations at various periods follow a random multivariate normal distribution. By defining the target spectral acceleration, one can obtain from disaggregation the parameters, such as magnitude and source-to-site distance, of the controlling scenarios. The values of such parameters inserted in a ground motion prediction model (GMPM) provide the conditional mean and variance of *S*a at the vibration periods of interest. The methodology proposed by Sousa *et al.* (2014) improves on the original CS method by using several GMPM at the same time to compute the full distribution of magnitude and distance given by the disaggregation.

4.4 SEISMIC PERFORMANCE ASSESSMENT

4.4.1 Capacity assessment and definition of damage states

In this study the damage states thresholds used for fragility assessment have been calculated from the individual capacity curve of each structure, which were derived using an adaptive pushover algorithm (Antoniou and Pinho 2004). As mentioned, two limit states were considered in this study, yielding (marking the onset of damage) and collapse, which are the main damage states of significance for risk-targeted hazard assessment.

Yielding was assumed to have occurred for the interstorey drift (ISD) level at which the relationship with the normalized base shear departs *considerably* from linearity (hence, not at the first crack in the first member that yields). The exact interstorey drift threshold was computed from bilinearization of the capacity curve. The buildings were considered to have reached their ultimate lateral load bearing capacity when a 20% reduction in base shear is observed (Silva *et al.* 2014d). Some of the structures displayed excessive ductility, with this drop in the base shear capacity only occurring for maximum interstorey drift levels at which the structures are most certainly unstable and/or un-repairable (e.g. interstorey drifts higher than 4%). For these structures, the drift thresholds proposed by Ghobarah (2004) for ductile moment resisting frames have been followed (i.e. for these structures collapse was assumed to have occurred for ISD >3%). Figure 4.3 depicts the evolution of the base shear (normalized by its peak value) with the maximum interstorey drift for all seismic design levels.

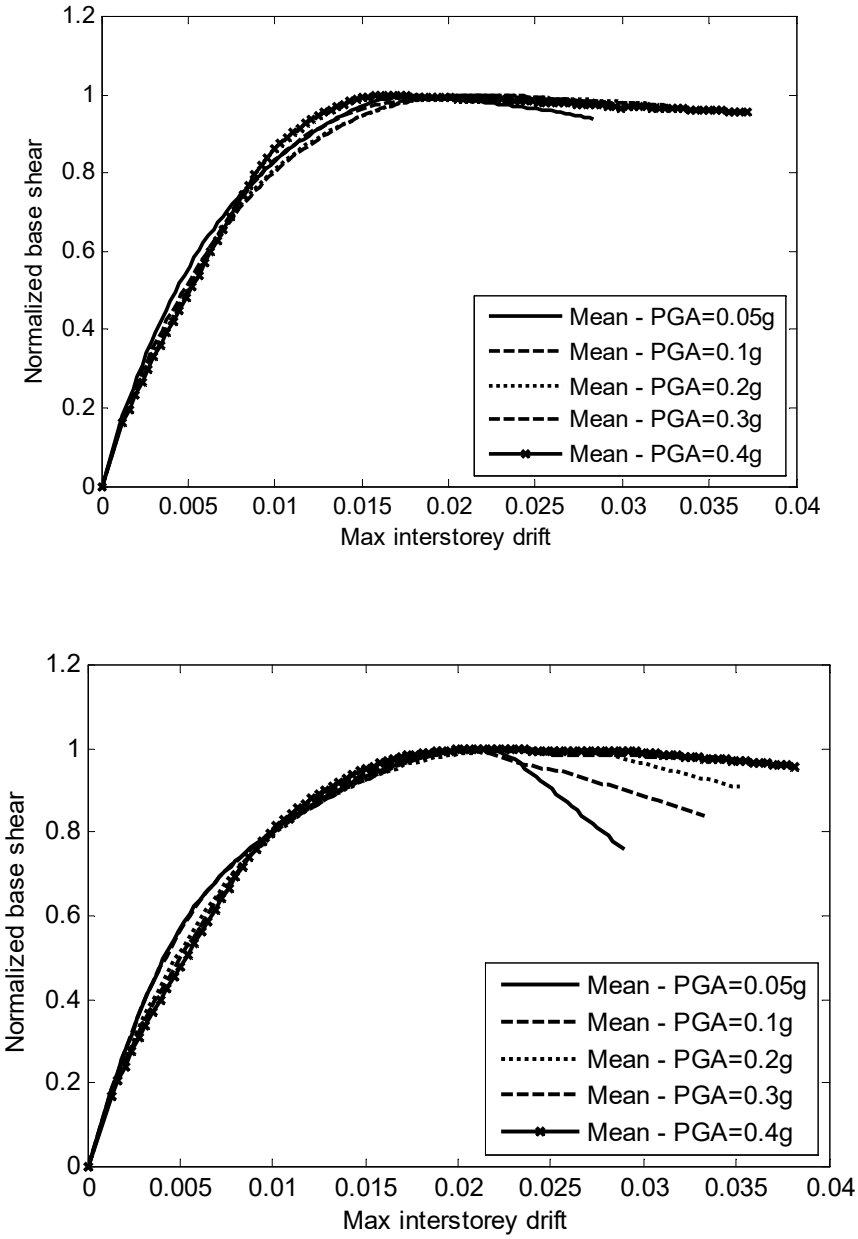

Figure 4.3 - Mean capacity curves expressed as Maximum interstorey drift *vs* Normalized base shear Top) 3 Storeys structures; Bottom) 5 storeys structures.

The mean capacity curves plotted in Figure 4.3 display, as expected, an increase on the ultimate displacement capacity and a reduction on the level of post yield softening with the increase on the design acceleration. It is relevant to note that the capacity curves computed for the lowest level of design acceleration (i.e. applicable to regions with low seismic hazard or for buildings with low seismic provisions) have an average collapse drift level around 3%, which is in line

for example with the threshold proposed by Rossetto and Elnashai (2003) (2.8%) for non-ductile structures.

4.4.2 Fragility assessment

Considering the performance thresholds computed from the capacity curves and the results from the nonlinear dynamic analyses, a number of fragility curves were calculated as depicted in Figure 4 to Figure 4.7. As previously mentioned, a lognormal distribution has been assumed for the acceleration, a_g, at which the damage state is reached (in the collapse case) or exceeded (in the onset of damage case) using two intensity measures: *PGA* and *Sa* at the mean period of vibration of each set of structures (T_{avg}) illustrated in Figure 4.2. The associated parameters for the collapse damage state (θ, β) are provided in Table 4.1 and Table 4.2 for *PGA*, and in Table 4.3 and Table 4.4 for *Sa*.

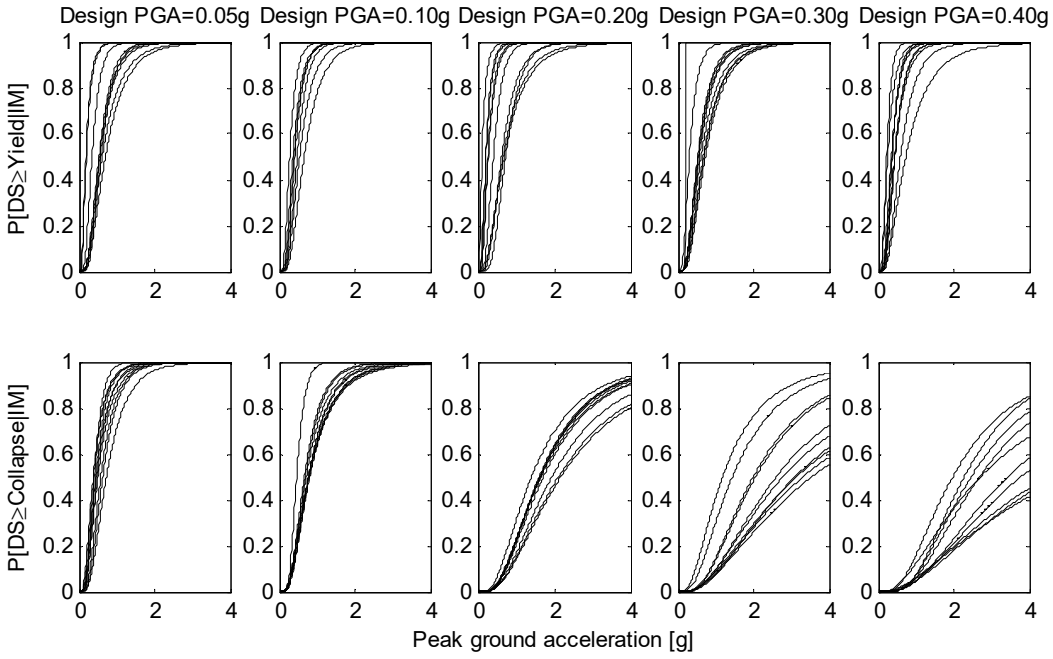

Figure 4.4 - Fragility curves for 3 storeys frames (IM=PGA) for onset of damage (top row) and collapse (bottom row).

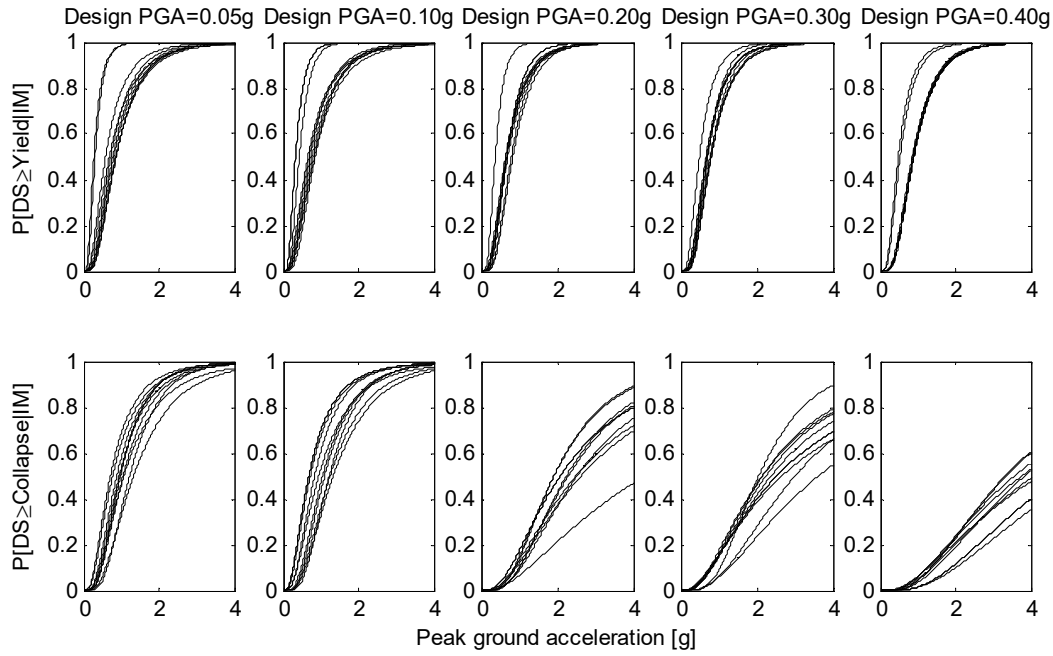

Figure 4.5 - Fragility curves for 5 storeys frames (IM=PGA) for onset of damage (top row) and collapse (bottom row).

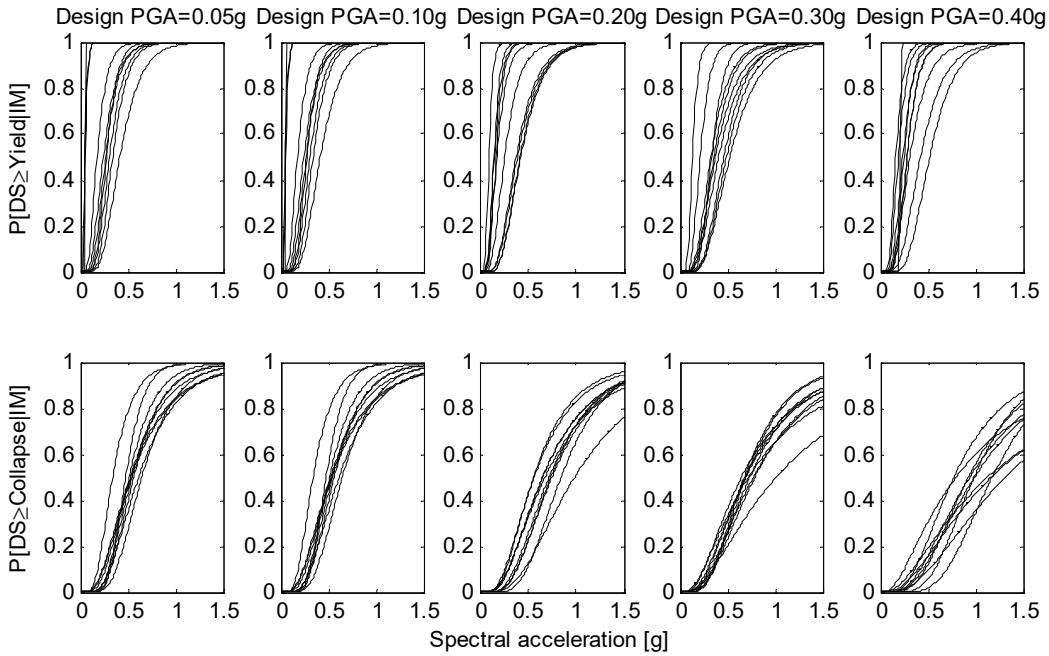

Figure 4.6 - Fragility curves for 3 storeys frames (IM= $Sa(T_{avg})$) for onset of damage (top row) and collapse (bottom row).

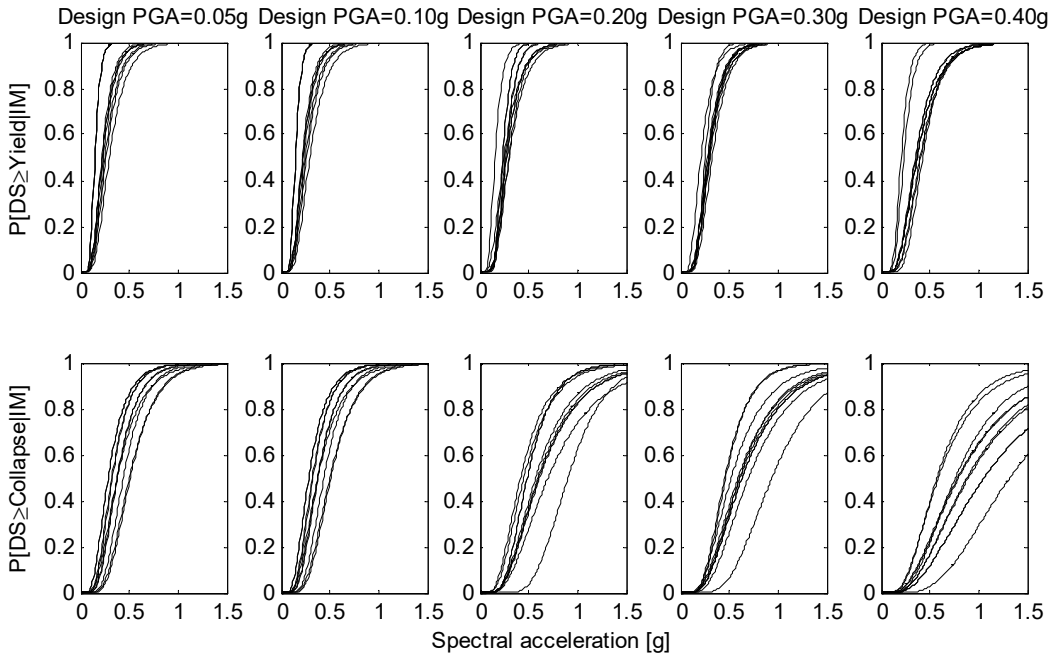

Figure 4.7 - Fragility curves for 5 storeys frames (IM= $Sa(T_{avg})$) for onset of damage (top row) and collapse (bottom row).

Table 4.1 - Fragility parameters for the collapse (3 storeys structures, IM=PGA).

Str. #	PGA=0.05g		PGA=0.10g		PGA=0.20g		PGA=0.30g		PGA=0.40g	
	θ	β	θ	β	θ	β	θ	β	θ	β
1	0.479	0.552	0.771	0.566	2.106	0.714	3.109	0.785	1.968	0.684
2	0.436	0.543	0.775	0.645	1.605	0.624	1.987	0.662	2.457	0.623
3	0.383	0.589	0.792	0.651	1.931	0.680	3.552	0.885	2.678	0.642
4	0.571	0.548	0.454	0.383	2.173	0.724	3.323	0.869	3.439	0.738
5	0.373	0.632	0.661	0.538	1.654	0.673	3.153	0.848	2.713	0.869
6	0.402	0.433	0.767	0.590	1.630	0.651	2.598	0.734	5.010	1.041
7	0.721	0.574	0.801	0.616	1.405	0.681	1.435	0.706	4.694	0.922
8	0.444	0.622	0.685	0.539	1.632	0.626	2.784	0.792	3.791	0.792
9	0.624	0.525	0.772	0.685	1.616	0.629	2.048	0.665	4.515	0.952
10	0.493	0.610	0.709	0.585	1.715	0.654	1.177	0.733	2.270	0.573
Mean	0.493	0.563	0.719	0.580	1.747	0.666	2.517	0.768	3.354	0.784
CoV.	0.218	0.098	0.137	0.138	0.132	0.050	0.308	0.100	0.311	0.191

θ - Median; β - Logarithmic standard deviation; CoV - Coefficient of variation

Table 4.2 - Fragility parameters for collapse damage state (5 storeys structures; IM=PGA).

Str. #	PGA=0.05g		PGA=0.10g		PGA=0.20g		PGA=0.30g		PGA=0.40g	
	Θ	β	θ	β	θ	β	θ	β	θ	β
1	0.944	0.643	0.833	0.657	1.913	0.601	2.143	0.770	4.089	0.849
2	0.880	0.640	1.004	0.590	2.633	0.823	2.372	0.825	3.576	0.813
3	1.330	0.639	0.943	0.693	2.518	0.688	2.533	0.917	3.326	0.701

4	0.768	0.724	0.788	0.736	2.078	0.787	3.631	0.814	3.848	0.738
5	1.047	0.605	1.220	0.523	1.910	0.622	2.271	0.785	4.821	0.730
6	0.707	0.715	1.330	0.639	2.078	0.787	2.047	0.534	3.773	0.850
7	0.962	0.575	0.778	0.747	2.491	0.819	2.533	0.917	5.348	0.761
8	1.220	0.523	1.043	0.614	2.288	0.646	3.009	0.702	4.249	0.938
9	1.067	0.702	0.778	0.747	4.333	0.962	2.672	0.978	3.356	0.705
10	0.977	0.565	1.246	0.628	2.241	0.628	2.144	0.813	4.821	0.730
Mean	0.990	0.633	0.996	0.657	2.448	0.736	2.536	0.806	4.121	0.782
CoV.	0.181	0.101	0.199	0.107	0.274	0.151	0.180	0.148	0.158	0.095

θ - Median; β - Logarithmic standard deviation; CoV - Coefficient of variation

Table 4.3 - Fragility parameters for collapse damage state (3 storey structures; IM= Sa(T)).

Str. #	**PGA=0.05g**		**PGA=0.10g**		**PGA=0.20g**		**PGA=0.30g**		**PGA=0.40g**	
	θ	**β**	**θ**	**β**	**θ**	**β**	**θ**	**β**	**θ**	**β**
1	0.382	0.547	0.559	0.436	0.654	0.607	0.684	0.643	0.924	0.530
2	0.431	0.507	0.537	0.634	0.845	0.428	0.673	0.523	0.982	0.428
3	0.630	0.539	0.611	0.536	0.679	0.652	0.718	0.842	0.770	0.590
4	0.336	0.400	0.475	0.326	0.565	0.604	1.010	0.843	0.988	0.619
5	0.687	0.589	0.509	0.428	0.559	0.566	0.644	0.743	1.164	0.848
6	0.350	0.237	0.525	0.548	0.722	0.542	0.689	0.684	1.127	0.942
7	0.604	0.474	0.338	0.490	0.740	0.504	0.786	0.618	1.315	0.736
8	0.654	0.521	0.540	0.468	0.751	0.527	0.769	0.679	0.937	0.636
9	0.405	0.350	0.526	0.637	0.987	0.593	0.690	0.519	0.793	0.916
10	0.465	0.512	0.646	0.426	0.653	0.614	0.732	0.588	1.173	0.407
Mean	0.494	0.468	0.526	0.493	0.715	0.564	0.739	0.668	1.017	0.665
CoV.	0.259	0.218	0.149	0.188	0.170	0.110	0.134	0.164	0.163	0.272

θ - Median; β - Logarithmic standard deviation; CoV - Coefficient of variation

Table 4.4 - Fragility parameters for collapse damage state (5 storey structures; IM= Sa(T◎)).

Str. #	**PGA=0.05g**		**PGA=0.10g**		**PGA=0.20g**		**PGA=0.30g**		**PGA=0.40g**	
	θ	**β**	**θ**	**β**	**θ**	**β**	**θ**	**β**	**θ**	**β**
1	0.353	0.542	0.326	0.449	0.478	0.517	0.463	0.421	0.880	0.593
2	0.317	0.432	0.372	0.452	0.697	0.567	0.606	0.512	0.794	0.614
3	0.510	0.402	0.376	0.525	0.595	0.525	0.632	0.542	0.572	0.519
4	0.309	0.490	0.320	0.463	0.484	0.428	0.936	0.419	0.760	0.538
5	0.451	0.418	0.438	0.408	0.416	0.530	0.590	0.551	1.054	0.632
6	0.299	0.431	0.510	0.402	0.484	0.428	0.453	0.445	0.895	0.603
7	0.368	0.495	0.283	0.515	0.612	0.534	0.632	0.542	1.312	0.504
8	0.438	0.408	0.377	0.439	0.605	0.539	0.697	0.522	0.783	0.624
9	0.397	0.491	0.361	0.505	0.901	0.333	0.611	0.551	0.587	0.561
10	0.405	0.485	0.499	0.428	0.571	0.513	0.520	0.528	1.055	0.632
Mean	0.385	0.459	0.386	0.459	0.584	0.491	0.614	0.503	0.869	0.582
CoV.	0.179	0.102	0.194	0.095	0.238	0.147	0.223	0.107	0.260	0.083

θ - Median; β - Logarithmic standard deviation; CoV - Coefficient of variation

For the yield damage state, little variation between the average value for θ and β has been found for all the case study structures. This behaviour is most likely due the fact that the vast majority of the structures reach yield for a similar value of interstorey drift ratio (around 1.5%).

The values of β were found to range from 0.60 up to 0.80 when using peak ground acceleration, and from 0.40 to 0.60 when using spectral acceleration. This higher dispersion for the fragility curves defined in terms of PGA is due, as demonstrated by De Biasio *et al* (2014) and Silva *et al* (2014d), to the lower efficiency of PGA in estimating interstorey drift, which is the engineering demand parameter adopted here to set the thresholds of the two damage states. Previous authors (Haselton *et al.* 2011, Lazar and Dolšek 2014, Silva *et al.* 2014d), have also analysed the fragility of groups of structures and have proposed a range for the logarithmic standard deviation between 0.35 and 0.50 when *Sa* is used as the intensity measure and between 0.50 and 0.75 for PGA. The boundaries found in this study are slightly higher than the ones previously proposed, likely due to the variability in the structural design within each set of structures not accounted for in previous studies.

4.5 IMPACT ON RISK-TARGETED HAZARD ASSESSMENT

4.5.1 Correlation between collapse probability ($P_c|a_g$) and design ground motion

The fragility curves in terms of *PGA* were used to calculate the probability of collapse at the design ground motion, $P_c|a_{des}$, for values of PGA from 0.05g to 0.40g, as indicated in Table 4.5 and Table 4.6. The data for each design class indicates that the average $P_c|a_{des}$ should be placed in the interval of 10^{-5} to 10^{-3}. An analysis of the results of the five sets of structures shows that structures designed for PGA=0.05g generally exhibit values of $P_c|a_{des}$ lower than those of the remaining case study structures. Although this behaviour was expected, it should be noted that for some of these structures the loads controlling the design were due to wind and not seismic activity. This explains some of the lowest values seen in this study (i.e. in the order of magnitude of 10^{-10} to 10^{-7}). It is also relevant to note that the same behaviour was reported by Ulrich *et al* (2014).

Table 4.5 - Probability of collapse at design ground motion (3 storey structures).

Str.#	$P_c \mid a_{des}$				
	PGA=0.05g	**PGA=0.10g**	**PGA=0.20g**	**PGA=0.30g**	**PGA=0.40g**
1	$2.123x10^{-5}$	$1.536x10^{-4}$	$4.871x10^{-4}$	$1.442x10^{-3}$	$9.884x10^{-3}$
2	$3.261x10^{-5}$	$7.461x10^{-4}$	$4.233x10^{-4}$	$2.148x10^{-3}$	$1.786x10^{-3}$
3	$2.713x10^{-5}$	$7.440x10^{-4}$	$4.252x10^{-4}$	$2.619x10^{-3}$	$1.538x10^{-2}$
4	$4.379x10^{-6}$	$3.811x10^{-5}$	$4.919x10^{-4}$	$2.832x10^{-3}$	$1.772x10^{-3}$
5	$7.327x10^{-4}$	$2.256x10^{-4}$	$8.512x10^{-4}$	$2.772x10^{-3}$	$1.382x10^{-2}$
6	$7.650x10^{-7}$	$2.781x10^{-4}$	$6.284x10^{-4}$	$1.639x10^{-3}$	$7.597x10^{-3}$
7	$1.673x10^{-6}$	$3.652x10^{-4}$	$2.101x10^{-3}$	$1.331x10^{-2}$	$3.796x10^{-3}$
8	$2.217x10^{-5}$	$1.766x10^{-4}$	$3.999x10^{-4}$	$2.456x10^{-3}$	$2.258x10^{-3}$
9	$7.471x10^{-7}$	$1.430x10^{-3}$	$4.473x10^{-4}$	$1.946x10^{-3}$	$5.431x10^{-3}$
10	$8.704x10^{-5}$	$4.041x10^{-4}$	$5.073x10^{-4}$	$3.107x10^{-2}$	$1.220x10^{-2}$
Mean	$9.305x10^{-5}$	$4.561x10^{-4}$	$6.763X10^{-4}$	$6.223X10^{-3}$	$7.392X10^{-3}$
CoV.	2.307	0.865	0.727	1.434	0.664

CoV - Coefficient of variation

Table 4.6 - Probability of collapse at design ground motion (5 storey structures).

Str.#	$P_c \mid a_{des}$				
	PGA=0.05g	**PGA=0.10g**	**PGA=0.20g**	**PGA=0.30g**	**PGA=0.40g**
1	$2.413x10^{-6}$	$6.312x10^{-4}$	$8.602x10^{-5}$	$5.346x10^{-3}$	$3.075x10^{-3}$
2	$3.645x10^{-6}$	$2.370x10^{-5}$	$8.664x10^{-4}$	$6.120x10^{-3}$	$3.527x10^{-3}$
3	$1.404x10^{-7}$	$6.007x10^{-4}$	$1.150x10^{-4}$	$1.002x10^{-4}$	$1.263x10^{-3}$
4	$7.959x10^{-5}$	$2.533x10^{-3}$	$1.465x10^{-3}$	$1.106x10^{-3}$	$1.082x10^{-3}$
5	$2.417x10^{-7}$	$8.708x10^{-7}$	$1.416x10^{-4}$	$5.227x10^{-3}$	$3.219x10^{-3}$
6	$1.051x10^{-4}$	$2.552x10^{-5}$	$1.465x10^{-3}$	$1.620x10^{-4}$	$4.124x10^{-3}$
7	$1.384x10^{-7}$	$3.028x10^{-3}$	$1.030x10^{-3}$	$1.002x10^{-4}$	$3.252x10^{-3}$
8	$5.105x10^{-10}$	$6.788x10^{-5}$	$8.082x10^{-5}$	$5.081x10^{-4}$	$5.857x10^{-3}$
9	$6.400x10^{-6}$	$3.028x10^{-3}$	$6.964x10^{-4}$	$1.267x10^{-3}$	$1.280x10^{-3}$
10	$7.103x10^{-8}$	$2.969x10^{-5}$	$5.954x10^{-5}$	$7.778x10^{-3}$	$3.219x10^{-3}$
Mean	$1.977x10^{-5}$	$9.970x10^{-4}$	$6.006x10^{-4}$	$2.771x10^{-3}$	$2.990x10^{-3}$
CoV.	1.961	1.320	0.967	1.077	0.493

CoV - Coefficient of variation

The values taken by $P_c \mid a_{des}$ have been the target of limited investigation. Ramirez *et al* (2012) analysed a large number of reinforced concrete structures designed according to modern seismic provisions for Western US that prescribe a design ground motion equal to 2/3 of the acceleration of the Maximum Considered Earthquake (MCE). This ground motion level is similar to what is expected for the 475-year return period. The estimated values of $P_c \mid a_{des}$ varied between 0.4% and 4.2%, which is in agreement with the values proposed by FEMA (2009), Goulet *et al* (2007) and Haselton *et al* (2011). These values are considerably higher than those obtained in this study, probably due to the lower safety margins implicit in the design

provisions for structures in western US, a region with moderate to high seismic hazard. Douglas *et al* (2013) while developing risk-targeted hazard maps for France has proposed a probability of collapse at the 475-year return period ground motion equal to 10^{-5}. Later, Ulrich *et al* (2014) analysed several 3-storeys moment frame reinforced concrete buildings designed for increasing levels of ground motion and proposed an acceptable interval for $P_c|a_{des}$ between 10^{-7} and 10^{-5}. These values, which are lower than those proposed by Douglas *et al* (2013) and those obtained herein, are perhaps too conservative for ordinary structures (ASCE 2005). It should be noted, however, that the study by Ulrich *et al* (2014) focused on buildings in France, where seismic hazard is generally lower than the hazard of Southern Europe. Another recent study for European buildings (Silva *et al.* 2016) has suggested a range of values of $P_c|a_{des}$ similar to those obtained herein.

In order to incorporate the variability of $P_c|a_{des}$ in probabilistic risk analysis of structures, a parametric distribution of this random variable is desirable. This distribution can be empirically estimated via a statistical model of the residuals for all five sets of 3 and 5 storeys structures. The residuals are simply the differences between the value of $P_c|a_{des}$ for every sample structure and the mean value of $P_c|a_{des}$ for all the buildings in the same design structure set. The symmetry of the residuals around the null value suggested that a normal distribution could be used to model this variability (see Figure 4.8). The adequacy of the fitted distribution was assessed through a one-sample Kolmogorov-Smirnov (K-S) test. In addition, the Root Mean Squared Error (RMSE) between the empirical and theoretical Cumulative Distribution Function (CDF) was also calculated. Table 4.7 presents the mean and standard deviation for the best fit probability density function and the significance level at which the K-S test is satisfied.

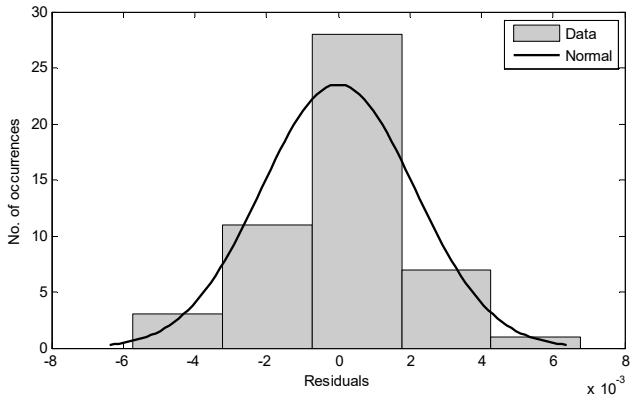

Figure 4.8 - Fitted Gaussian distribution to the residuals around the mean probability of collapse at the design ground motion.

Table 4.7 - Best fitted distribution to the residuals around the mean probability of collapse at the design ground motion.

Probability density model	Parameters	Significance level	RMSE
Normal	μ=0; σ=0.0021	1%	0.0085

RMSE - Root Mean Squared Error; μ - Mean; σ - Standard deviation

4.5.2 Investigation on the logarithmic standard deviation

Similarly, to what done for the probability of collapse at the design ground motion, an investigation on the distribution of residuals around the mean logarithmic standard deviation of β was also performed. The adequacy of the fit to the different probability models has been assessed using the same procedure used for $P_c|a_{des}$. The findings (see Table 4.8, Table 4.9 and Figure 4.9) suggest that a normal probability distribution is sufficient to accurately represent the distribution of residuals around the mean value of β for both damage states (onset of damage and collapse) and intensity measures, PGA and Sa.

Table 4.8 - K-S test and RMSE results from fitting residuals around the mean β (IM=PGA)

Probability density model	Yield DS			Collapse DS		
	Parameters	Significance level	RMSE	Parameters	Significance level	RMSE
Normal	μ=0; σ=0.0481	1%	0.0005	μ=0; σ=0.0915	1%	0.0008

RMSE - Root Mean Squared Error; μ - Mean; σ - Standard deviation

Table 4.9 - K-S test and RMSE results from fitting residuals around the mean β (IM=Sa)

Probability density model	Yield DS			Collapse DS		
	Parameters	Significance level	RMSE	Parameters	Significance level	RMSE
Normal	μ=0; σ=0.0535	5%	0.0046	μ=0; σ=0.0515	5%	0.0044

RMSE - Root Mean Squared Error; μ - Mean; σ - Standard deviation

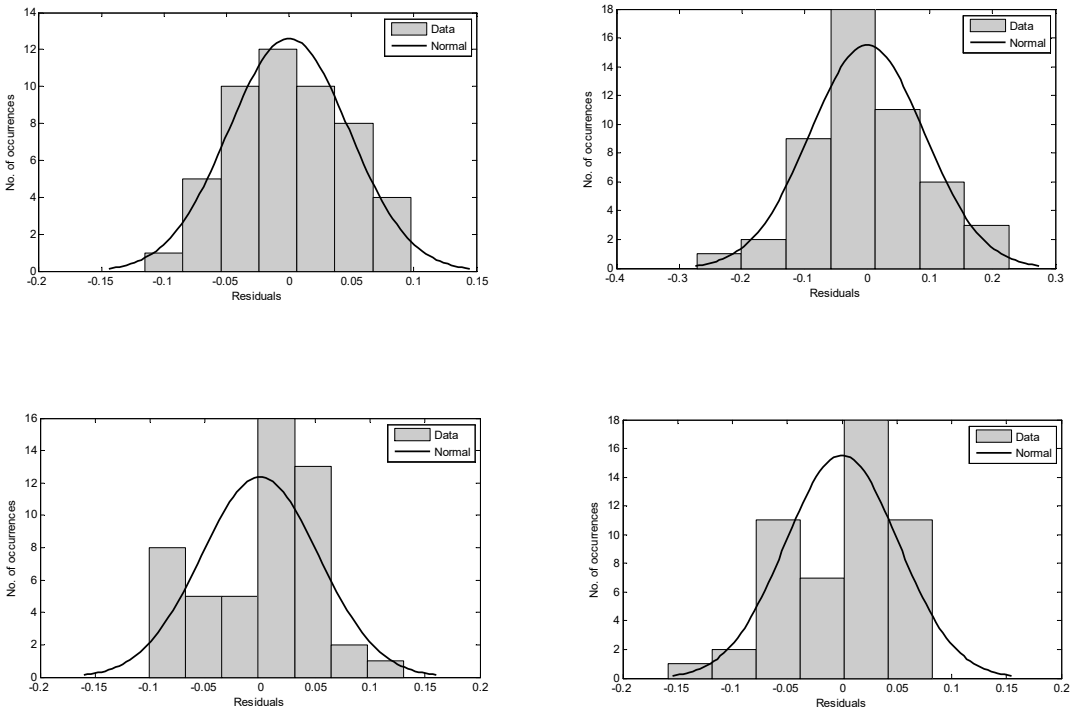

Figure 4.9 - Histogram and fitted probability distributions to the residuals around the mean β for all five design structure sets. Top) IM=PGA; Bottom) IM=Sa; Left) Yield DS; Right) Collapse DS.

Silva *et al* (2016) stated that $P_c|a_{des}$ and β are often positively correlated. In other words, for example, low values of β are usually associated with low values of $P_c|a_{des}$. This study confirms

the same findings. The results suggest that a significant correlation exist (R^2=0.67) between the logarithmic standard deviation and the natural logarithm of $P_c|a_{des}$, as illustrated in Figure 4.10. This result indicates that it is important to consider the correlation between β and $P_c|a_{des}$ in the generation of synthetic collapse fragility curves from the aforementioned probability distributions to prevent unrealistic curves from being generated.

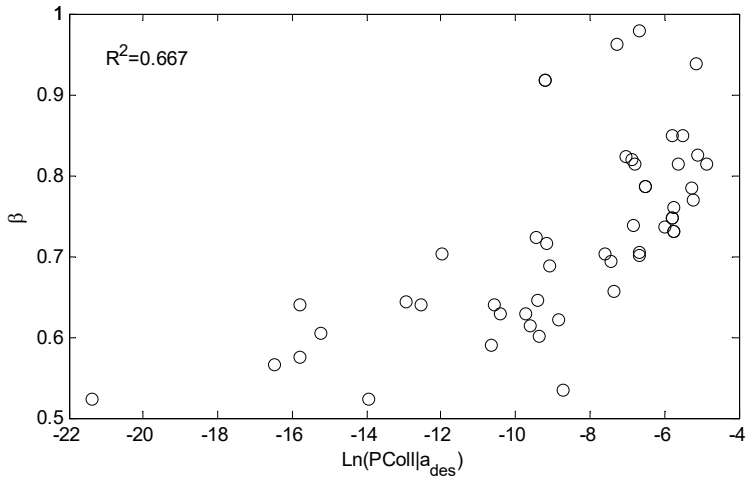

Figure 4.10 - Relationship between the natural log of the probability of collapse at the design ground motion, $P_C|a_{des}$, and logarithmic standard deviation, β.

4.5.3 Sensitivity analysis on the annual probability of collapse

In the previous sections, fragility curves were derived for reinforced concrete structures designed for increasing levels of ground motions. This exercise provided boundaries and probability distributions for both the probability of collapse at the design ground motion ($P_c|a_{des}$) and the variability of the fragility curves (β). In this section we investigate how the variability of $P_c|a_{des}$ and β influences the mean annual rate of reaching the collapse damage state.

The mean annual rate of collapse is also known to be affected by the shape of the local hazard curve (Luco *et al.* 2007). Hence, our investigation considered three different locations (Vienna, Lisbon and Istanbul) with 475-year return period PGA values ranging from 0.10 g (i.e. low hazard) up to 0.40 g (i.e. moderate to high hazard). The required PGA hazard curves (see Figure 4.11) were developed within the FP7 European project SHARE (Woessner *et al.* 2015),

and extracted from the European Facility for Earthquake Hazard and Risk (http://www.efehr.org/en/hazard-data-access/hazard-curves/).

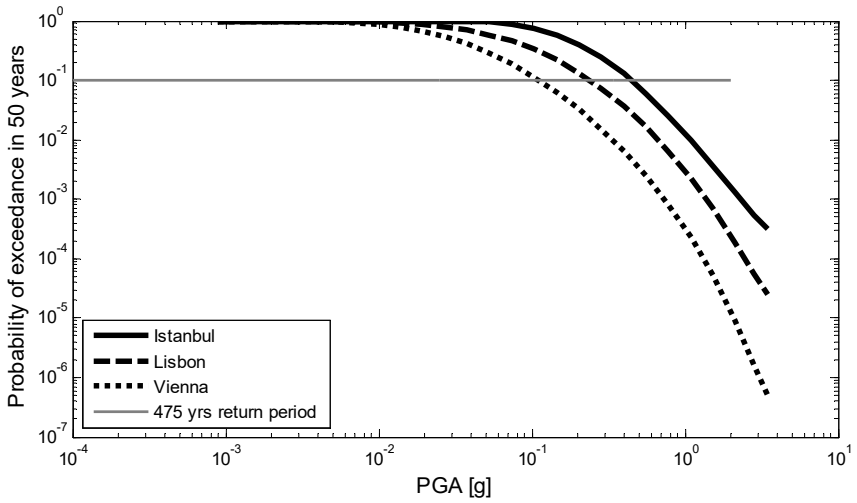

Figure 4.11 - Hazard curves for chosen locations at rock site in terms of peak ground acceleration.

For each location a total of twenty hypothetical fragility curves with $P_c|a_{des}$ ranging from 10^{-5} to 10^{-2} and β ranging from 0.5 to 0.9 were constructed assuming a lognormal probability distribution (see Figure 4.12) for the acceleration a_g at which the damage state is reached (in the collapse case) or exceeded (in the onset of damage case). Section 4.5.2 highlighted that correlation between $P_c|a_{des}$ and β should be considered in a real seismic risk assessment scenario in order to avoid unrealistic fragility estimates. However, the main objective of this section is to provide a sensitivity analysis on the effects that a variation on the fragility parameters introduce on annual rate of collapse, thus for the sake of simplicity and to accentuate any possible trend it was decided not to include the correlation effects in this exercise.

In order to compute the annual rate of collapse, the method proposed by Eads *et al.* (2013), and further explored by Silva *et al.* (2016), was used. The original hazard curves were converted before using them from the native annual probability of exceedance into annual rate of exceedance assuming a Poisson model. The resulting curves were then discretized into several segments and the rate of occurrence associated with the central acceleration value of each segment was calculated. Then, for any given fragility curve the probability of collapse ($P_c|a_{g,i}$)

at the central acceleration value ($a_{g,i}$) of the i^{th} segment was calculated and then multiplied by the rate of occurrence of $a_{g,i}$. The annual rate of collapse is the sum of these products for all n values of $a_{g,i}$ where n are the number of segments in which the hazard curve has been discretized. The results from this sensitivity analysis are provided in Table 4.10 to Table 4.12.

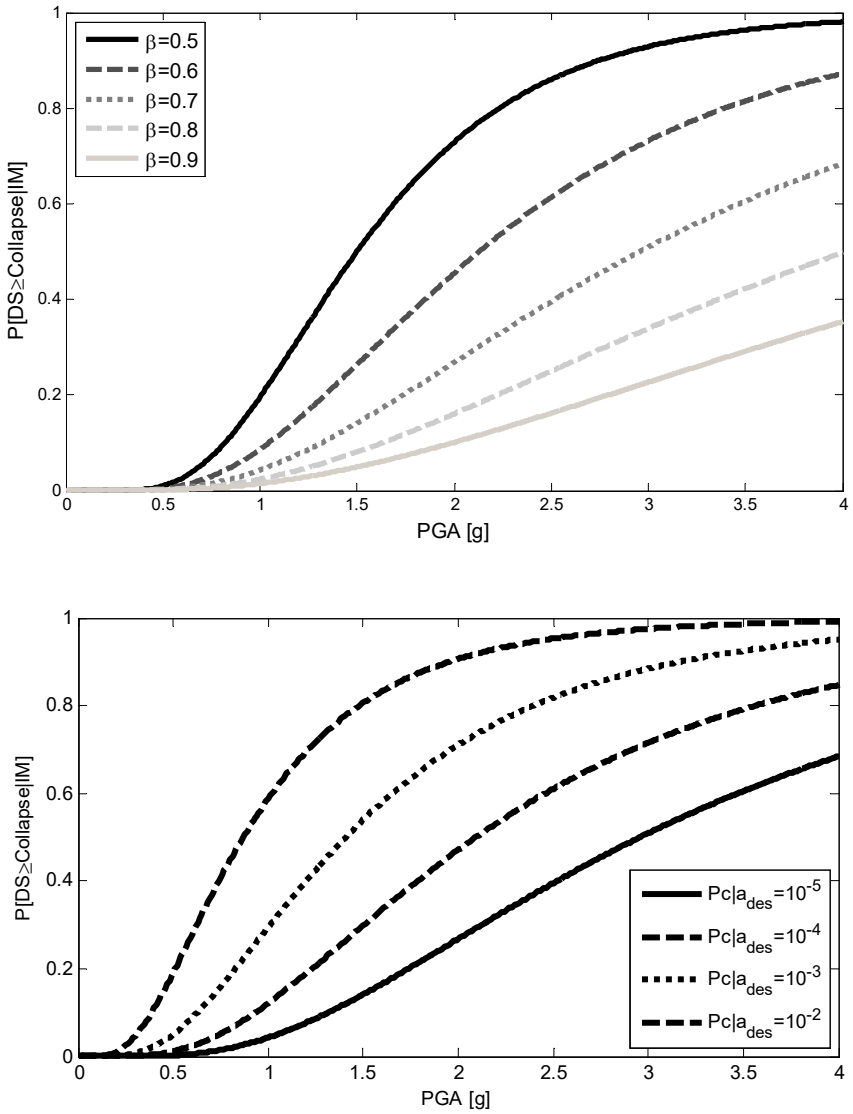

Figure 4.12 - Examples of fragility curves. Top: a_{des}=0.2g; $Pc \mid a_{des}$ =10^{-5} and five values of β; Bottom: a_{des}=0.2g; β=0.7 and four values of $Pc \mid a_{des}$.

Table 4.10 - Sensitivity analysis on the expected mean annual rate of collapse for Vienna.

$P_c \mid a_{des}$	Expected annual rate of collapse (Vienna a_{des}=0.10g)				
	β=0.50	β=0.60	β=0.70	β=0.80	β=0.90
10^{-5}	$4.7x10^{-5}$	$2.4x10^{-5}$	$1.3x10^{-5}$	$7.6x10^{-6}$	$4.8x10^{-6}$
10^{-4}	$9.5x10^{-5}$	$5.5x10^{-5}$	$3.4x10^{-5}$	$2.3x10^{-5}$	$1.6x10^{-5}$
10^{-3}	$2.0x10^{-4}$	$1.3x10^{-4}$	$9.4x10^{-5}$	$7.1x10^{-5}$	$5.5x10^{-5}$
10^{-2}	$4.4x10^{-4}$	$3.4x10^{-4}$	$2.8x10^{-4}$	$2.4x10^{-4}$	$2.1x10^{-4}$

Table 4.11 - Sensitivity analysis on the expected mean rate of collapse for Lisbon.

$P_c \mid a_{des}$	Expected annual rate of collapse (Lisbon a_{des}=0.20g)				
	β=0.50	β=0.60	β=0.70	β=0.80	β=0.90
10^{-5}	$4.0x10^{-5}$	$1.9x10^{-5}$	$9.7x10^{-6}$	$5.7x10^{-6}$	$3.6x10^{-6}$
10^{-4}	$8.7x10^{-5}$	$4.9x10^{-5}$	$3.0x10^{-5}$	$1.9x10^{-5}$	$1.4x10^{-5}$
10^{-3}	$1.9x10^{-4}$	$1.3x10^{-4}$	$9.1x10^{-5}$	$6.8x10^{-5}$	$5.3x10^{-5}$
10^{-2}	$4.6x10^{-4}$	$3.6x10^{-4}$	$2.9x10^{-4}$	$2.5x10^{-4}$	$2.2x10^{-4}$

Table 4.12 - Sensitivity analysis on the expected mean annual probability of collapse for Istanbul.

$P_c \mid a_{des}$	Expected annual rate of collapse (Istanbul a_{des}=0.40g)				
	β=0.50	β=0.60	β=0.70	β=0.80	β=0.90
10^{-5}	$1.2x10^{-5}$	$5.2x10^{-6}$	$2.7x10^{-6}$	$1.6x10^{-6}$	$1.1x10^{-6}$
10^{-4}	$3.5x10^{-5}$	$1.8x10^{-5}$	$1.1x10^{-5}$	$7.5x10^{-6}$	$5.5x10^{-6}$
10^{-3}	$1.0x10^{-4}$	$6.4x10^{-5}$	$4.5x10^{-5}$	$3.5x10^{-5}$	$2.8x10^{-5}$
10^{-2}	$3.0x10^{-4}$	$2.3x10^{-4}$	$1.9x10^{-4}$	$1.7x10^{-4}$	$1.5x10^{-4}$

The results for all three locations indicate, as expected, that the mean annual rate of collapse increases with the values of $Pc \mid a_{des}$. These results are not surprising since a higher value for $P_c \mid a_{des}$ generally indicate more fragile structures, as illustrated in Figure 4.12 by the shift to the left of the curves with the increasing level of $P_c \mid a_{des}$. Increasing β for the same level of $P_c \mid a_{des}$ has instead the effect of reducing the expected annual probability of collapse. This trend can be explained by the flatter shape of fragility curve with higher values of β, that produce lower probabilities of collapse for ground motion levels higher than that of $P_c \mid a_{des}$.

4.5.4 Annual rate of exceeding a given DS

The consideration of several structural models in this study allowed the development of empirically-based probabilistic models for the parameters defining the fragility curves ($P_c \mid a_{des}$, β) and for the correlation between them. The definition of these parameters in a probabilistic manner allows the propagation of the associated uncertainties to the final risk estimates. In

this context, a Monte Carlo simulation was employed to generate a hundred fragility curves for each one of the two damage states using the statistical models previously established for each level of a_{des}. Then, each fragility curve was used to calculate the annual rate of reaching the associated damage state, according to the methodology described in the preceding section. The results are provided in Table 4.13 and Table 4.14.

Table 4.13 - Expected mean annual rate of yield at three locations and respective coefficient of variation.

Location	Annual rate of yield	
	Mean	Coefficient of variation
Vienna (a_{des}=0.1g)	1.86×10^{-4}	0.248
Lisbon (a_{des}=0.20g)	5.29×10^{-4}	0.244
Istanbul (a_{des}=0.40g)	1.39×10^{-3}	0.236

Table 4.14 - Expected mean annual rate of collapse at three locations and respective coefficient of variation.

Location	Annual rate of collapse	
	Mean	Coefficient of variation
Vienna (a_{des}=0.10g)	2.03×10^{-5}	0.322
Lisbon (a_{des}=0.20g)	4.32×10^{-5}	0.320
Istanbul (a_{des}=0.40g)	5.31×10^{-5}	0.301

The average annual rate of exceeding the onset of damage or reaching collapse can be compared with acceptable risk thresholds in order to decide whether risk reduction measures should be pursued. Luco *et al* (2007) in a previous study for the US estimated an acceptable threshold for the annual probability of collapse of around 2×10^{-4}. Douglas *et al* (2013) upon extensive review on existing literature proposed 10^{-5} as an appropriate upper limit for this parameter. After an analysis of several acceptable thresholds for societal risk and fatality rates for inhabitants of reinforced concrete structures, Silva *et al* (2016) proposed an acceptable threshold (5×10^{-5}) in between those of the former two studies.

This threshold determines how the design ground motion at a given site should be adjusted to attain a uniform risk distribution. The accepted risk threshold to be adopted, and consequently the design ground motion, has a profound impact not only on the direct costs of design and construction but also on the expected social and economic losses (e.g. the expected mortality rate or number of damaged buildings) in future earthquakes. Selecting a more conservative threshold increases the initial costs of design and construction and lowers future

losses. The task facing decision makers is determining an adequate balance between a level of safety and the cost necessary to achieve it.

For the locations considered here and assuming the proposal by Silva *et al* (2016), it is possible to observe that in some cases the estimated mean annual collapse rate exceeds the acceptable limit, and in others this value is below. More specifically, the design ground shaking for Istanbul should be increased, whilst the one for Vienna or Lisbon could be reduced. However, if one assumes the threshold proposed by Douglas *et al* (2013) the results indicate that the design ground motion should be increased in all three locations.

4.5.5 Average rate of collapse for new reinforced concrete frames in Europe

An analysis on the expected annual rate of collapse of newly designed reinforced concrete frame buildings has been performed for the European continent. For each location, the expected design ground motion for the 475-year return period has been extracted from the SHARE model. Then, in order to estimate collapse fragility curves for any value of ground motion, the results from Table 4.2 were used to fit linear functions for the median (θ), logarithmic standard deviation (β) and $P_c|a_{des}$ (see Figure 4.13). Strong positive correlation between the design *PGA* and the fragility parameters, $P_c|a_{des}$ and β was found, with values of the coefficients of determination (R^2) above 0.80. Since more than 120,000 locations have been considered in this study, only the mean collapse fragility curve was considered at each site, unlike in the probabilistic procedure explored in the previous section. The computed values for the probability of collapse at the design acceleration for each location are depicted in Figure 4.14.

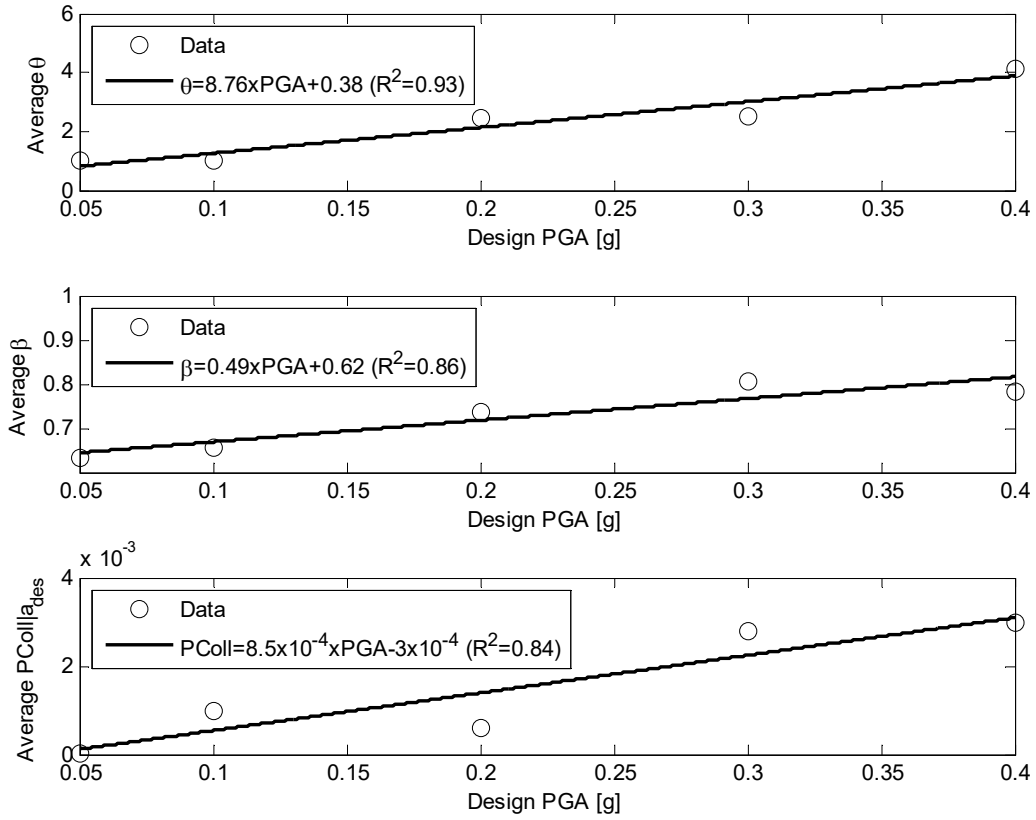

Figure 4.13 - Polynomial functions used to estimate the values of the parameters of the collapse fragility curves.

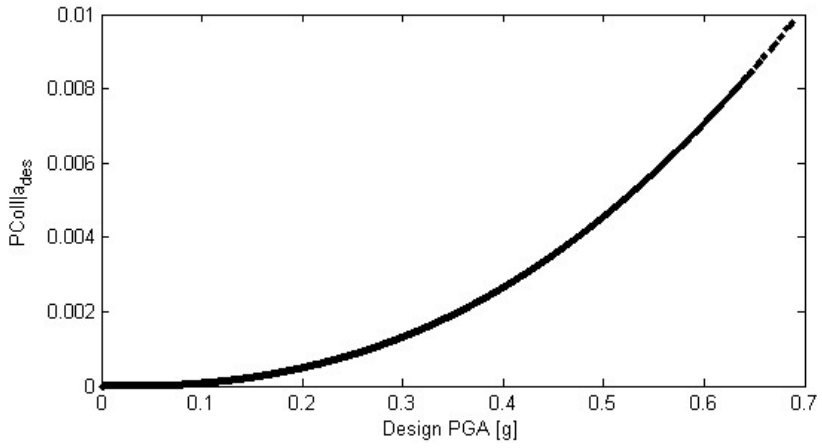

Figure 4.14 - Computed probability of collapse at the design ground motion at site.

The annual probability of collapse across the European territory is illustrated in Figure 4.15. Assuming an acceptable threshold for the annual probability of collapse of 5×10^{-5}, Figure 4.15 suggests that the design ground motion for most of the Northern European countries could be lowered since the mean annual rate of collapse is considerably lower than the proposed

acceptable risk threshold. This finding is not surprising since the design at these latitudes is often not controlled by seismic loads (the seismic hazard is low) but rather by a combination of permanent and live loads (e.g. wind or snow loads).

For South and Southeast Europe (e.g. Southern Italy, Central and Southern Greece and the North Anatolian Fault in Turkey), Figure 4.15, however, exhibits a quite different scenario. Considering the threshold suggested by Silva *et al* (2016), the results would call for an increase of the design ground motion in order to attain an admissible and uniform risk distribution in these regions. It should be noted that in some of these regions the estimated annual rate of collapse peaked to almost double the acceptable risk threshold adopted here.

Finally, the findings of this study also indicate that for the majority of Central Europe the mean annual probability of collapse is between $3x10^{-5}$ and $5x10^{-5}$, very similar to the acceptable threshold value adopted in this study.

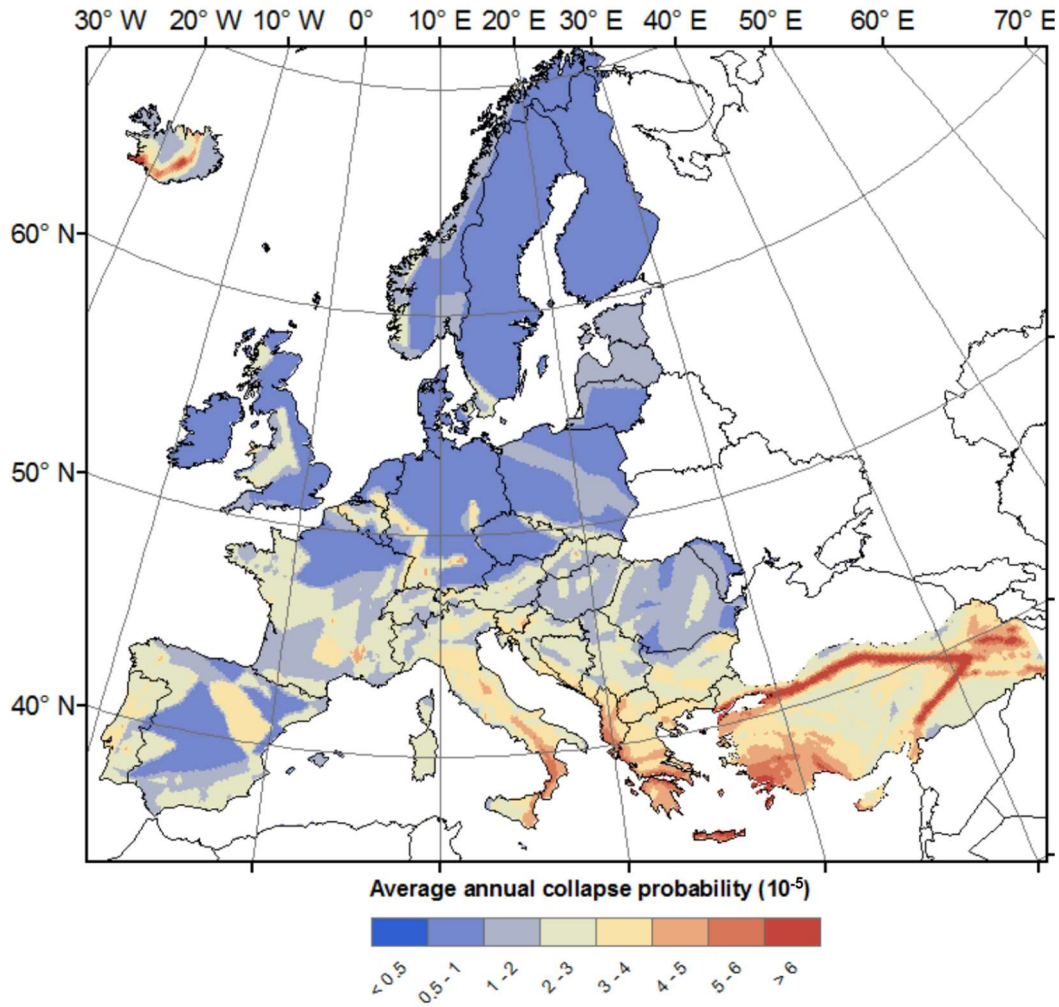

Figure 4.15 - Map for the average annual probability of collapse for newly designed reinforced concrete frame buildings in Europe.

It is interesting to note that the results presented herein differ quite significantly from a previous study for Europe by Silva *et al* (2014a), especially for the Northern European countries. The fragility parameters used by Silva *et al* (2014a) were kept constant across the European territory, whereas those used in this study are conditional on the local design ground motion level. Regardless of the approach for the definition of the fragility curves, it is clear that the spatial distribution of risk across Europe varies considerably, despite the fact that the same return period for the design ground shaking is being considered.

4.6 FINAL REMARKS

This study analysed the influence of the structural fragility on the probability of collapse at the design ground motion level in order to identify key aspects that impact the development of risk-targeted hazard maps, such as the uncertainty in building fragility and the annual probability of reaching (or exceeding) a given damage state.

A set of regular reinforced concrete moment frame structures compliant with the most up-to-date European regulations and designed for increasing levels of ground motion has been created. Each structure was represented using a tridimentional finite element model, and tested against a set of ground motion records using nonlinear dynamic analyses. This study considered two damage states: yielding (onset of structural damage) and the structural collapse. Variability in the structural design has been introduced in order to propagate the building-to-building variability to the risk estimates.

The results presented herein suggest that the mean probability of collapse at the design ground motion for modern code compliant structures lays between 10^{-5} and 10^{-3}. These values are similar to those of other previously published studies, l. Lower values for the probability of collapse at the design ground motion have been found for structures designed for the lowest ground motion level considered herein. In these cases, the design of the lateral load resisting system was generally not controlled by earthquake loading, but by loads due to other actions (e.g. wind loads). These results seem to suggest that in some locations with very low earthquake hazard, the seismic design recommendations enforced by the codes may be unnecessary since the lateral load capacity required by other sources of horizontal excitation could be sufficient to ensure an adequate seismic performance.

The previous observation was later confirmed by analysing the annual rate of collapse for the European continent. Considering the currently enforced 475-year return period design ground motion, most of the regions in Northern Europe exhibited annual rates of collapse below all commonly accepted risk thresholds. On the other end of the spectrum, this study also identified regions (mostly in southern Europe) where the design ground motion would have to be increased in order to bring the expected earthquake risk to an acceptable level. Mapping the expected annual rate of collapse across Europe has also demonstrated one of the main problems with modern seismic design codes. Despite having considered the same return

period for the design ground motion the computed spatial distribution of seismic risk was far from being uniform.

This study also provided probability distributions functions for the residuals around the mean logarithmic standard deviation and probability of collapse at the design ground motion used to develop fragility functions within a probabilistic framework. A sensibility analysis on the influence of the fragility parameters on the final risk metrics has also been included.

Summarizing, the results of this study contribute to the understanding of the seismic performance of new structures designed according to modern codes, and consequently to the increase of the robustness and reliability of the risk-targeted hazard methodology.

5

DEVELOPMENT AND ASSESSMENT OF DAMAGE-TO-LOSS MODELS FOR MOMENT-FRAME REINFORCED CONCRETE BUILDINGS

Martins, L., Silva, V., Marques, M., Crowley, H. and Delgado, R. (2016) *Development and assessment of damage-to-loss models for moment-frame reinforced concrete buildings.* Earthquake Engineering & Structural Dynamics, **45**(5): p. 797-817. DOI: 10.1002/eqe.2687.

5.1 SUMMARY

In this section a methodology for computing losses induced by earthquake loads in reinforced concrete structural elements is presented. Structural damage has been correlated with the element's chord rotation through a modified version of the Park and Ang (1985) damage index. Damage levels are correlated with an appropriate repair technique and the expected loss is computed as a combination of expected repair cost per technique weighted by the probability of the element being in a given damage state.

The proposed method relies on a comprehensive study on the cost of repair of damaged structures. Real and up-to-date repair costs suitable for Portuguese RC buildings are presented. The methodology described in this section has been drafted for the Portuguese building stock; however, the general principals presented herein are still applicable to any region of the globe provided a reliable source of repair costs is available.

The methodology has been applied to two real Portuguese reinforced concrete structures built during the late 50's and early 60's. From the estimated structural losses suitable damage-to-loss models have been produced. A study between the differences in the expected annual

losses computed with the proposed methodology and the traditional methodology has also been included.

5.2 INTRODUCTION

Seismic risk analysis should be performed with the highest possible level of accuracy, in order to provide decision makers with reliable information that can be used for risk mitigation purposes. However, the process of performing risk analysis still involves a number of steps which could benefit from further improvements, mainly in the definition of the relationship between damage and loss, arguably one of the highest sources of uncertainty within an analytical vulnerability assessment.

The first stage of an analytical vulnerability assessment is to employ the results from structural analysis to establish a relation between a meaningful engineering demand parameter - EDP (e.g. drift ratios, dissipated energy, floor acceleration) and a structural damage threshold. Then, the evaluation of the evolution of damage with increasing ground shaking intensity can be used to derive structural fragility functions, which provide the probability of exceeding a set of structural damage states, conditional on a set of ground motion levels. The issue of defining damage from structural performance parameters has been addressed in previous studies, (Park and Ang 1985, Calvi 1999, Borzi *et al.* 2008, Benavent-Climent 2011, Fardis *et al.* 2012), or technical guidelines and design recommendations (CEN 2005, FEMA 2014). However, whilst EDP-to-damage estimation is well documented and deals with concepts that are recognized by most engineering practitioners and researchers, the same cannot be said regarding the relation between damage and a level of loss, usually defined by the so-called damage-to-loss or consequence models (e.g. (Kappos *et al.* 2006, Bal *et al.* 2010b)).

Despite efforts from a number of researchers to improve the field of loss modelling (e.g. (Kappos *et al.* 1991, Gunturi 1993, Kappos *et al.* 1998, Di Pasquale and Goretti 2001, Kappos *et al.* 2006, Bal *et al.* 2008, Ramirez *et al.* 2012)), in general, the majority of available consequence models are still deterministic and/or based on limited empirical data. Furthermore, it is also important to emphasize that the majority of the existing damage-to-loss models were developed and calibrated to represent the reality of a small number of countries and

corresponding building stock, which may lead to a misleading vulnerability evaluation when applied to other regions of the world, as demonstrated herein.

This study presents a procedure to estimate the expected level of damage for a given ground shaking intensity, through the employment of numerical modelling and nonlinear dynamic analysis. A comprehensive study on the repair of reinforced concrete structural elements was used as the starting point to compute the expected structural losses due to seismic excitation. For what concerns the non-structural vulnerability, a decision was made to account for the possible damage in the infill walls, openings, plumbing and electrical network. Different repair techniques were adopted based on the extent of damage in the various components, and vulnerability functions were derived combining the losses given by the component structural damage and the complete structural collapse. By relating the estimated losses back to global damage states, it has been possible to define damage-to-loss models for the case study structures.

Two moment-frame reinforced concrete buildings located in Portugal have been considered for these analyses. Currently, no studies seem to exist in the literature concerning consequence models for Portugal, which makes the present study a significant contribution for future loss studies. The need for an adequate damage-to-loss model for Portuguese buildings has been addressed by Martins *et al* (2014). In the latter study, a vulnerability analysis was presented using a component-based consequence model developed for the Californian building stock, which was deemed to lead to a significant overestimation of losses in Portugal, especially for greater ground shaking intensity levels. Likewise, the findings of the present study also demonstrate that the assessment of probabilistic risk using damage-to-loss models developed for other countries might lead to erroneous results, often by a factor of two. Hence, the present investigation improves upon existing studies by using repair costs that are specific to the Portuguese reality, and also provides a general methodology to compute structural losses that can be easily adapted to other countries.

5.3 METHODOLOGY FOR COMPUTING STRUCTURAL LOSSES

5.3.1 Element damage assessment

In order to determine the damage level of each structural element, a modified version of the Park and Ang (1985) damage index originally proposed by Beck *et al* (2002) (Eq. (5.1)) was applied. The Deformation Damage Index (*DDI*) is defined as the ratio of the maximum plastic hinge rotation attained during seismic loading ($\theta_{p\_transient}$), and the difference between the ultimate rotation capacity (θ_u) and the recoverable rotation at unloading (θ_r).

$$DDI = \frac{\theta_{p\_transient}}{\theta_u - \theta_r} \tag{5.1}$$

In monotonic loading, the recoverable rotation may be approximately determined assuming the initial stiffness path as the unloading path. However, in dynamic analysis, the computation of plastic hinge rotations is not straightforward as the unloading path is a function of the loading history, which varies from record to record (Chen and Lui 2006). By providing additional runtime for the structure to stabilize after the seismic excitation, it is possible to estimate the plastic rotations (θ_{pl}) due to residual deformation. Computing the recoverable rotation is then just a matter of subtracting the residual rotation from the maximum recorded rotation. The ultimate rotation capacity is dependent on the section geometry, reinforcing steel pattern and the internal stresses, which are combined through Eq. (5.2), originally proposed by Priestley and Park (1987), where Φ_y and Φ_u are the yield and ultimate curvature, L_s is the shear-span and L_{pl} is the plastic hinge length.

$$\theta_u = \phi_y \frac{L_s}{3} + \left(\phi_u + \phi_y\right) L_{pl} \left(1 - \frac{L_{pl} \diagup 2}{L_s} \right) \tag{5.2}$$

5.3.2 Repair cost estimation

The deformation damage index for each structural element was used to assign a damage state (DS) using the component fragility functions proposed by Haselton *et al.* (2008) (Figure 5.1 and Table 5.1). It should be mentioned that these fragility functions have been developed for code compliant structures, for which no failure due excessive shear is expected. For gravity-

designed structures the shear forces must be controlled and in case of excessive shear, the element should automatically be assigned to the *Collapse* damage state.

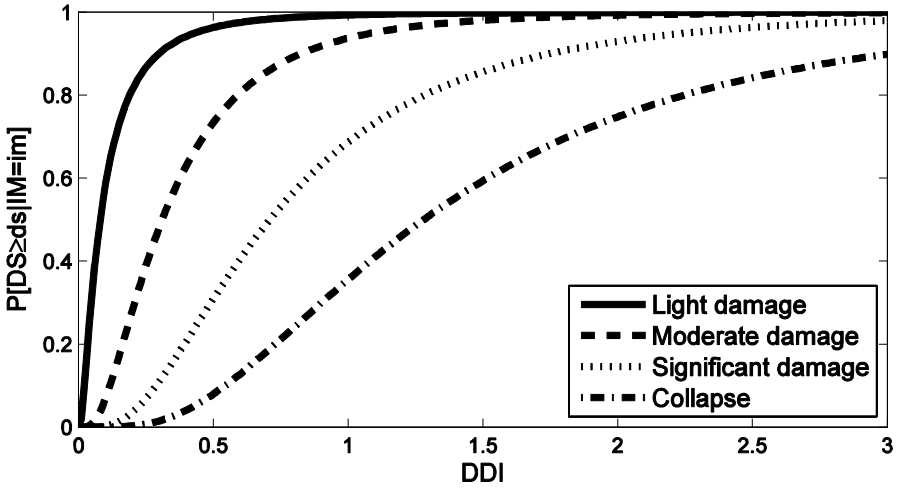

Figure 5.1 - Probability of exceeding a given damage state as a function of the DDI (Haselton *et al.* 2008).

Table 5.1 - Lognormal distributions proposed by Haselton *et al* (2008).

Damage State	Fragility parameters	
	Median (X_m)	Logarithmic Standard Deviation (β)
Light damage (DS1)	0.08	1.36
Moderate damage (DS2)	0.31	0.89
Significant damage (DS3)	0.71	0.80
Collapse (DS4)	1.28	0.74

By identifying a damage state to each structural member, it is possible to establish the most appropriate repair technique. Knowing the probability of being in a particular damage state at a given ground shaking level (*P[DS=ds|IM])*, and provided that a reliable estimate of the cost of the associated repair technique (C_{rpr_ds}) is available, one can estimate the expected total repair cost per element ($E[C_{rpl\_elem}|IM]$) using Eq. (5.3). In this equation, DS=0 corresponds to the undamaged state for which no repair costs are expected.

$$E\left[C_{rpr\_elem} \mid IM\right] = \sum_{ds=0}^{nDS} \left(P\left[DS = ds \mid IM\right] \cdot C_{rpr\_ds}\right) \tag{5.3}$$

According to Haselton *et al* (2008), structural elements assigned to the light damage state can be repaired with epoxy injection. On the other hand, elements that have suffered moderate

damage require a more expensive intervention in order to be restored to their previous undamaged state, with a recommendation given for jacketing-based techniques. For more severe damage states, a complete replacement of the structural element (i.e. rebuilding the whole element) is recommended. It is worth mentioning that the complete replacement of a damaged element is possible but often a difficult operation to execute in practice. The feasibility of this repair job in real life conditions should always be determined through a careful inspection of the damaged element and its surroundings on site. Regardless of this, determining the practicability of the element replacement has been considered out of the scope of this work and incompatible with the definition of a generalized and methodology for loss assessment (i.e. the main objective of this section) thus for it has been assumed that this operation could always be performed.

In sections 5.3.2.1 to 5.3.2.3 a more detailed description on the procedure adopted to compute the cost associated to each repair technique is presented. In order obtain realistic loss estimates a real up-to-date online database specialized in construction costs has been used (http://www.geradordeprecos.info/).

5.3.2.1 Expected epoxy injection cost

It has been determined that, unsurprisingly, the global cost of an epoxy injection is closely related with the amount of structural adhesive applied. In regular injections the quantity of epoxy varies from 0.2kg to 3.0kg per linear metre of repaired element. For Portuguese construction this translates to a repair cost ranging from 9.18€/m to 74.26€/m.

The amount of adhesive is correlated to the width and length of the cracks in the concrete, and therefore it is reasonable to assume that the cost of epoxy injection must be related with the damage (herein assumed to be measured by the DDI). Thus, lower values of DDI will lead to less expensive repair costs.

In order to incorporate this variability in the cost estimation, a relationship between the deformation damage index and the unit cost of the epoxy injection has been assumed. From the parameters in Table 5.1 for the light damage state, the DDI values that lead to a probability of exceedance of 0.10 and 0.90 were computed. Due to lack of data regarding the cost of repair,

a linear variation of the repair cost has been arbitrarily assumed between these values, whereas outside this interval the repair cost was presumed to remain constant and equal to the minimum and maximum costs respectively (Figure 5.2).

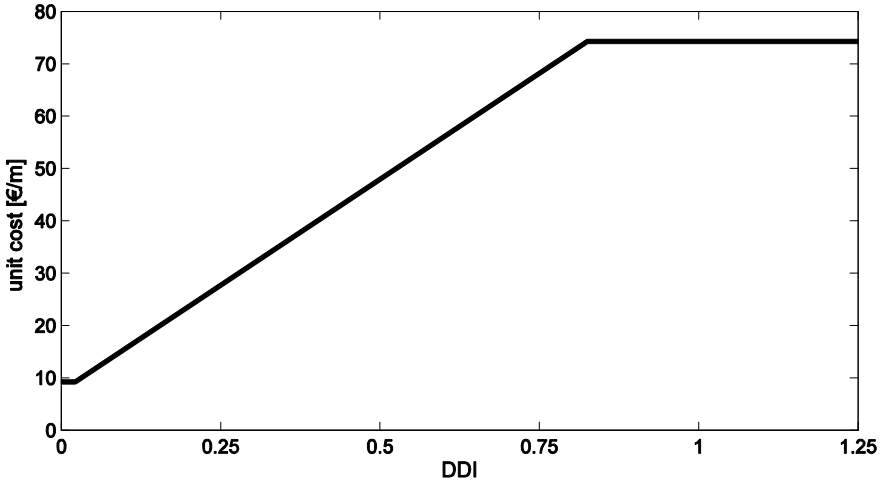

Figure 5.2 - Epoxy injection cost *vs.* DDI relationship.

5.3.2.2 Expected jacketing cost

Jacketing is one of the most frequently used techniques for repairing and/or strengthening structural elements (Waghmare 2011). The jacketing cost is dependent on the type and geometry of the structural element. Thus, in order to make an informed judgment on the cost of a jacketing operation, a decision was made to divide the total cost into a number of individual costs.

For columns, a four-sided RC jacket executed with a cast-in-place technique was assumed. For the sake of simplicity, the width of the jacket was kept at the recommended minimum of 0.10m and 8 new longitudinal rebars were added (Fardis 2009, Waghmare 2011). The same diameter of the existing corner rebar has been used as reference for the size of the additional reinforcing steel, with a minimum of 12 mm for the steel bars at the corners of the RC jacket (Waghmare 2011). The transverse reinforcement spacing has been halved within the jacket, as suggested by Julio *et al.* (2003). Waghnare (2011) recommends that the compressive strength of the concrete jacket should be at least equal to that of the existing structure, or up to 5 MPa higher. For the majority of ordinary building structures in Portugal this translates into a compressive strength between the classes C25/30 and C30/37 of Eurocode 2 (CEN 2010b), and thus the price

used to compute the jacketing repair cost was given by the average of these two classes. This assumption is in agreement with the work of Silva *et al.* (2014d) that from the results of core drilling tests in 76 Portuguese buildings has proposed a model for estimating the compressive concrete strength based on a gamma distribution with an average value of 23.8 MPa and Coefficient of Variation (CoV) of 49%. Most guidelines and published literature on RC jacketing highlight the need for preparing the interface between the concrete on the original column and the added jacket. This task serves the purposes of increasing the surface roughness of the original column, which is usually followed by the application of a bounding agent like an epoxy based compound. In order to provide a good estimate of the complete repair cost, in addition to the cost of the aforementioned materials, the expenditure of formwork and labour were also considered.

Knowing the geometry of the jacket and the number of additional rebars, one can determine most of the quantities needed for the repair job, with the exception of the labour and bounding agent that are not directly correlated with the dimensions of the jacket. In this context, a number of possible column cross sections were considered and the associated amount of labour and adhesive were estimated using the aforementioned database. Then, using these possible scenarios, a regression analysis was performed to approximate several polynomial functions establishing a relation between the column cross section area and the amount of labour and adhesive, as illustrated in Figure 5.3.

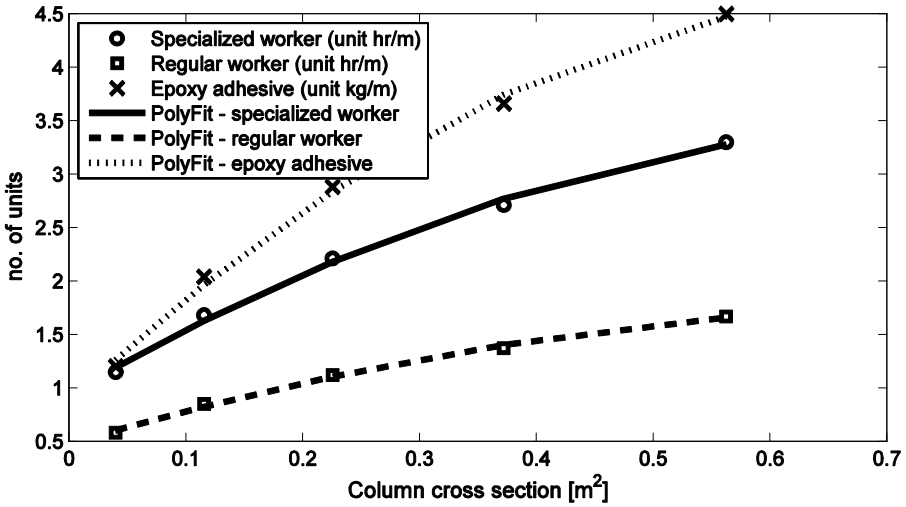

Figure 5.3 - Model for labour and bounding agent estimates as a function of column cross section.

For what concerns the repair of the beams, in order to avoid creating a strong beam - weak column mechanism, the maximum stiffness and strength should be kept in the columns. For this reason, the chosen repair technique for beams was steel jacketing, with the steel sheet being applied only at the bottom of the beam. Prior to the jacketing, it is necessary to repair any possible damage sustained by the beams due to the seismic loads, and thus the application of repair mortar in the surface area of the beam has been included in the total repair cost. According to the queried database, the cost for steel jacketing of beams is solely dependent on the thickness of the steel sheet, with all other costs (labour and additional materials) remaining constant. For simplicity, an average thickness of 3mm of S355 grade steel for the repair job has been assumed herein. Table 5.2 and Table 5.3 describe the unit costs of all the aforementioned repair tasks, which were used to compute the expected structural repair costs.

Table 5.2 - List of unit costs for column repair.

Description	**Unit**	**Unit cost [€/un]**
Concrete	m^3	107.56
Reinforcing Steel	kg	0.82
Formwork	m^2	10.50
Surface roughening	m^2	40.52
Bonding agent (epoxy)	kg	11.25
Specialized worker	hr	17.69
Regular worker	hr	17.27

Table 5.3 - List of unit costs for beam repair.

Description	**Unit**	**Unit cost [€/un]**
Repair mortar	m^2	90.02
Surface preparation	m^2	40.52
Steel jacket (3mm S355 steel sheet)	m^2	92.02

5.3.2.3 Computing replacement cost

Herein the element's replacement cost (C_{rpl_elem}) has been computed as a function of the structures's replacement cost (C_{rpl_str}), assumed to be a percentage of the building's replacement cost. It is reasonable to assume that a smaller and less important element should have a lower replacement cost. In this work the ratio between the element's volume (V_{elem}) and the whole structure's volume has been used in order to estimate the element's replacement cost (Eq. (5.4)). It should be mentioned that although completely acceptable whenever no additional information is available, the cost estimates given by Eq. (5.4) may be considered over simplistic. Nonetheless this equation has been suggested in this study because it enables the development of an entirely universal methodology for loss assessment that is independent of the structure being analysed and easily adaptable to other regions of the globe.

An approximation of the building's replacement cost may be achieved using the average construction cost per square metre. These are usually readily available and frequently updated, for example the Portuguese government publishes on a regular basis this information for tax purposes. According to the Portuguese Ministry of Finance (2003) the average construction cost accounts for all the direct and indirect costs associated with the construction industry namely labour, materials, equipments and energy. Herein the average construction cost suggested by the Portuguese government (603€/m²) (Finanças 2013) has been used. It should be noted that this value can be further updated to account for the building's location and age. However, for the sake of simplicity in this work it has been decided to ignore this and adopt the default value.

$$C_{rpl\_elem} = C_{rpl\_str} \cdot \frac{V_{elem}}{\sum_{i=1}^{nElem} (V_{elem})_i} \tag{5.4}$$

5.4 COMPUTING NON-STRUCTURAL LOSSES

Recent events have indicated that a large portion of the direct losses are due to damage in the non-structural components, and not in the structural elements (e.g. (Taghavi and Miranda 2003, Miranda *et al.* 2012)). Recent studies (Pinto 2007, Mendes 2011, Mêda 2014) regarding the typical construction practices in Portugal has revealed that, on average, structural components account only for 32% of the building's total value. The remaining costs are distributed amongst

infill panels (33%), plumbing and electricity (15%), openings (i.e. windows, doors) (12%) and other elements (8%). The monetary value of each of these categories of non-structural components can be estimated by multiplying the building's total replacement cost by the respective percentage.

For the assessment of the losses due to damage in the brick infill walls, the normalized economic damage index proposed by Kappos *et al* (1998) has been used. This index establishes the onset of damage in the panels at interstorey drift ratios of 1‰ and the complete loss of the panels at 4‰. Although important, the combination of in-plane and out-of-plane excitation has not been considered herein for computing losses in the walls and only the former has been considered. Once the economic damage index has been computed for each floor and each direction, the final economic loss due to damage in the infill walls is given by the sum of the product of these coefficients by the expected masonry monetary value.

The calculation of the expected losses for the remaining non-structural components followed a similar approach to the one used for the infill walls. The limit states proposed by HAZUS (FEMA 2014) have been adopted, considering whether the expected damage is drift or acceleration sensitive. A deterministic loss analysis has been considered herein with the median value for each damage state being assumed to be the performance threshold.

The monetary loss due to non-structural damages ($E[Loss_{nonStruc}]$) was obtained by summing the expected losses for each non-structural element. It should be mentioned that different thresholds could have been used to estimate the damage in the non-structural components (e.g. those proposed by the FEMA P58), but the general procedure remains unaltered regardless of the adopted damage criteria.

Despite consisting the majority of the building replacement cost, the methodology to compute loss in non-structural elements is clearly less detailed than the methodology followed for structural elements. This is in large amount due to the less evolved state of current scientific knowledge when comes to non-structural elements (e.g. the simple double strut models for modelling infills) and the very different behaviour between all the different types of non-structural elements (e.g. drift sensitive *vs* acceleration sensitive).

5.4.1 Computing global losses

Having computed the expected repair cost for all the structural elements the expected loss for the building can be obtained through a weighted sum of the building's replacement cost and the total repair cost for the whole structure (Eq. (5.5)). It should be mentioned that computing the repair cost for the whole structure as a sum of the individual repair costs for each element may lead to an overestimation of the actual repair cost. All real repair operations have variable costs (e.g. the cost for transporting materials and equipments to the site) that decrease with the number of repaired elements. These costs are usually dependent on the resources put at disposal by the construction companies and their overall level of expertise and therefore are difficult to assess *a priori*. Despite being an important issue that needs to be properly addressed, including these considerations in the proposed methodology would probably widen too much the scope this work.

Another critical aspect of Eq. (5.5) that needs further commenting is the correct evaluation of the building's collapse probability (*P[Coll | IM]*). When performing a vulnerability analysis, the structural behaviour might not be completely characterized by the peak transient response due to excessive residual deformations, which might lead to the need for demolition, resulting in its complete loss. Ramirez and Miranda (2012) have addressed this issue and proposed to model the probability of demolition as a function of the residual interstorey drift, using a lognormal distribution with median of 0.015 and logarithmic standard deviation of 0.30. Thus, if the structure has not collapsed due to the earthquake loads, the probability of demolition is calculated using the residual deformation and the aforementioned probability distribution.

$$\begin{aligned} E[Loss \mid IM] &= P[Coll \mid IM] \cdot C_{rpl\_bld} + \\ &+ (1 - P[Coll \mid IM]) \cdot \left(\sum_{i=1}^{nElem} \left(E\left[C_{rpr\_elem} \mid IM\right] \right)_i + E\left[Loss_{nonStruct}\right] \right) \end{aligned} \tag{5.5}$$

5.5 CASE STUDY AND DERIVATION OF A DAMAGE-TO-LOSS MODEL

5.5.1 Numerical models and analysis algorithm

This section summarises the most relevant findings of the application of the aforementioned methodology to two real Portuguese residential buildings. Both structures are mid-rise

reinforced concrete (RC) moment frame buildings (see Figure 5.4) built between the late 50's and early 60's. Given their date of construction, both buildings were mainly designed to withstand only gravity loads.

The first structure, henceforth referred to as Str1, is a five storey moment-frame with a maximum height of 14.25m, a floor area of 151m^2 and a natural (uncracked) period of vibration of 0.36s. The second structure, from now on referred to as Str2, is a six storey moment-frame with a maximum height of 18.0m, a floor area of 254.8 m^2 and a natural (uncracked) period of vibration of 0.46. The façade of both buildings consists in a double layered hollow brick wall. For the nonlinear dynamic analyses, in addition to the permanent loads, the live loads acting on the structure were also considered. For the nonlinear dynamic analyses, in addition to the permanent loads, the live loads acting on the structure were also considered.

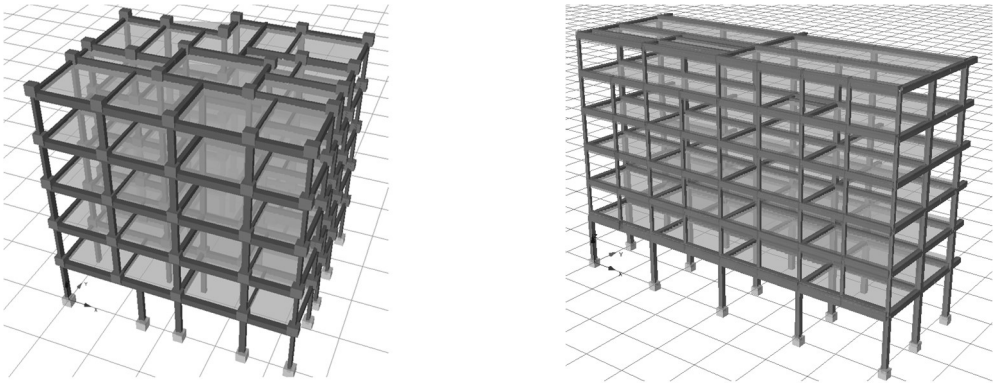

Figure 5.4 - Left: Perspective view of Str1; Right: Perspective view of Str2.

In order to assess the structural performance of each building, 3D finite element models have been created using the open-source software OpenSEES (McKenna *et al.* 2000). The models were defined using force-based fibre elements, each with five Gauss-Lobatto integration points. As demonstrated by Calabrese *et al* (2010), distributed plasticity elements can become numerically unstable at high ductility levels, especially if the structure exhibits softening behaviour. Therefore, before reporting a numerical collapse, the implemented framework tested several nonlinear solution algorithms (regular Newton-Raphson, modified Newton-Raphson, Newton-Raphson with line search and Broyden-Fletcher-Goldfarb-Shanno), before reducing the time step given by the ground motion record by a factor of 100 and increasing the tolerance from 10^{-6} to 10^{-4} in order to try to attain convergence. The infill walls were

modelled with two nonlinear single-struts connecting the opposing corners of the panel. The strength and stiffness properties of the struts were computed following the proposals of Crisafulli and Carr (1997) and Smyrou *et al* (2006). To improve numerical stability while avoiding spurious damping, a 2% tangent stiffness proportional damping was considered with the damping matrix being updated at all converged time steps. After applying the earthquake loading, the structure was allowed to vibrate freely until it finally stabilized in order to determine potential residual drifts and rotations.

Using the spectral acceleration at the fundamental period of vibration (Sa (T_1)) as the intensity measure (IM), a modified version of the incremental dynamic analysis (IDA) (Vamvatsikos and Cornell 2002), often referred as multiple stripe analysis (Lin and Baker 2013), was applied for the structural assessment, in which different ground motion records were selected for each intensity level in order to better match the scenarios that contribute to the expected regional seismic hazard at different intensity levels, as discussed further in the section 5.5.2.

5.5.2 Ground motion record selection

Given the importance of record-to-record variability on the seismic response of structures, careful consideration has been given to the methodology used for selection and scaling of natural ground motion records. The Conditional Spectrum (CS) proposed by Baker and co-workers (Baker 2011, Jayaram *et al.* 2011, Lin *et al.* 2013), incorporating target mean and variance, provides an adequate mechanism to determine structural response variability conditioned to different levels of ground motion intensity. It is based on the empirically verified observation that the set of logarithmic spectral accelerations at various periods follow a random multivariate normal distribution (Jayaram and Baker 2008). Thus, by defining the target spectral acceleration at the first period of vibration, one can obtain its causal earthquake magnitudes, distances and other parameters from disaggregation, in order to compute the conditional mean and variance at the periods of interest.

As described in Sousa *et al* (2014), another fundamental aspect of the addressed method is the selection of ground motion prediction models (GMPM), which is a crucial step to ensure consistency between target spectra and the ground motion properties expected for the site of interest. Thus, Atkinson and Boore (2006) and Akkar and Bommer (2010) models are selected,

following the work of Silva *et al* (2013). In this context, an 'exact' CS is adopted, considering multiple causal earthquake magnitudes, distances and GMPM with corresponding weights as established by Lin *et al* (2013).

For this study, the two structures were assumed to be located in Lisbon. For each spectral acceleration intensity level, the thirty ground motion records that best-fitted the corresponding conditional spectra were selected from the PEER (https://ngawest2.berkeley.edu/site) and ESMD (http://www.isesd.hi.is/ESD_Local/home.htm) databases, as the input for the multiple stripe analyses. A maximum scaling factor of 5 has been considered within the matching algorithm.

5.5.3 Case study structural performance assessment

By combining the damage index for each element (Section 5.3.1) with the fragility parameters in Table 5.1, it is possible to compute, for each element in the building, the probabilities of being in a given damage state, conditioned to the ground shaking level.

Figure 5.5 and Figure 5.6 depicts the average probability of each damage state across the elements, sorted by element type (columns on the left and beams on the right) and floor (where the floor number increases downwards), for both structures. From the evaluation of these results it is possible to observe that the main failure mechanism for both structures was a soft-storey at the ground floor. Thus, it is fair to assume that both structures do not comply with the strong column-weak beam design rule, as expected from gravity-load designed structures. The main difference between them in terms of structural performance is the ground shaking intensity level that leads to structural collapse. It has been observed that the six storey frame (Str2) reaches higher probabilities of column collapse at lower intensity measure levels (IML) than the five storey structure (Str1), which could be expected since Str1 displayed a higher ductility.

The figures also indicate that the structural damage in Str2 is much more concentrated in the columns and the beams do not sustain more than light damage, whereas the beams in Str1 have a small probability of being severely or moderately damaged or even collapsed, despite the overall collapse mechanism of both structures being a ground floor soft-storey.

These differences in the structural behaviour of the case study structures indicate a smoother transition between the elastic response range and the collapse state for Str1, when compared to Str2.

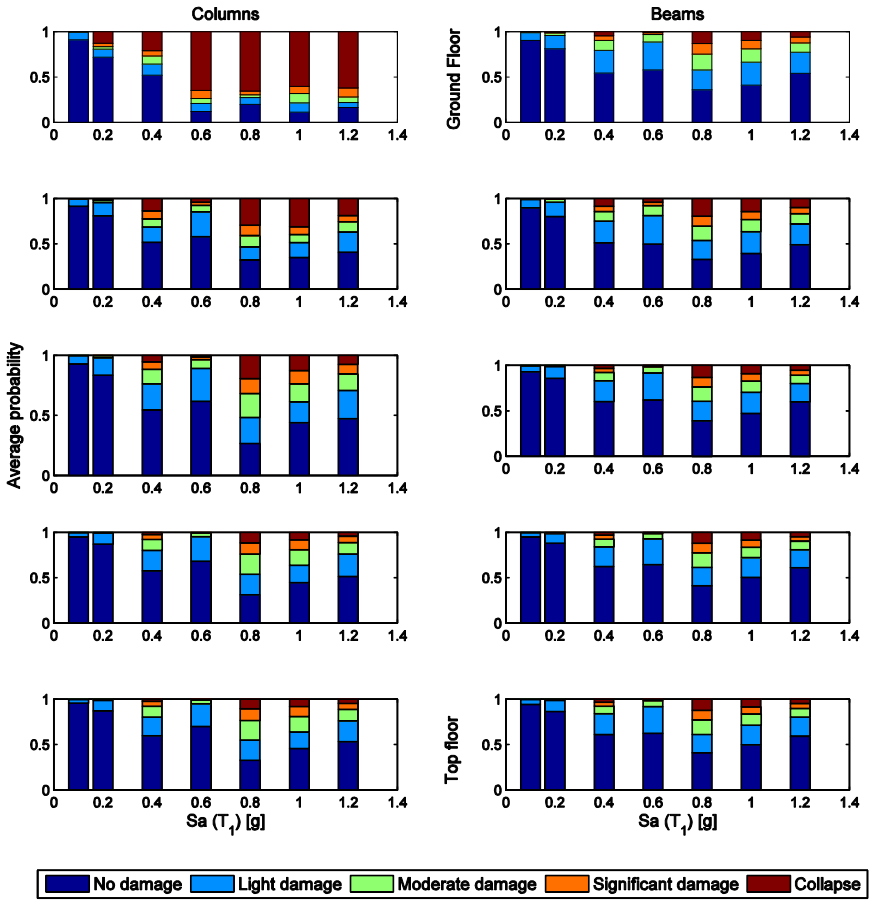

Figure 5.5 - Average probability of element damage (Str1).

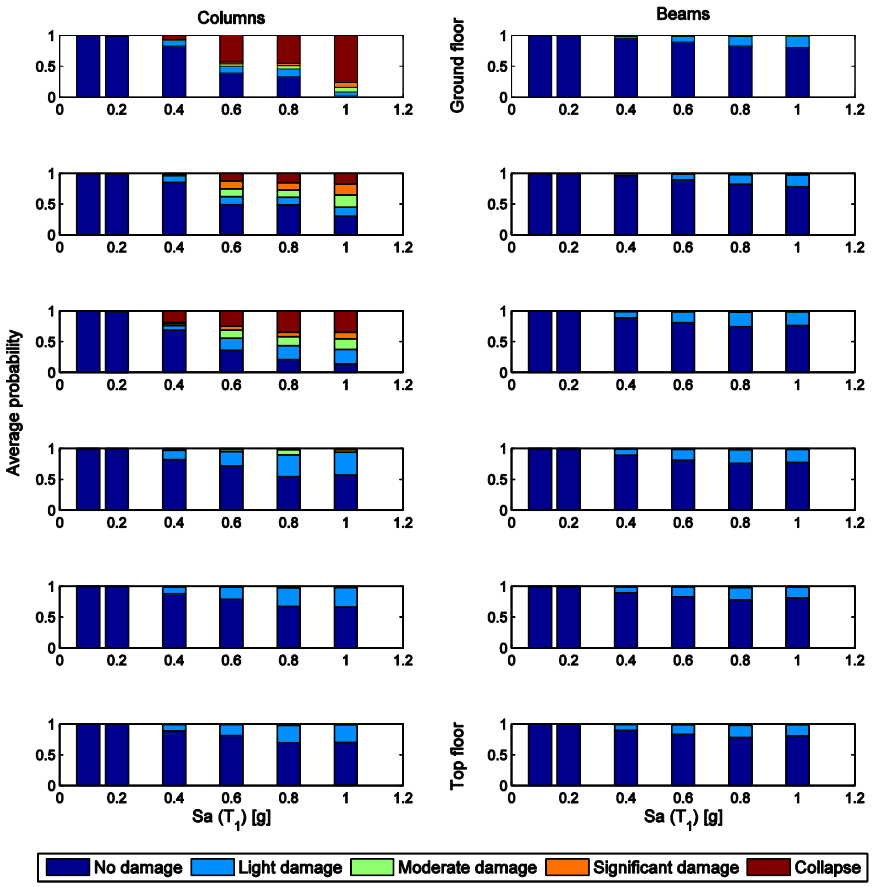

Figure 5.6 - Average probability of element damage (Str2).

5.5.4 Element loss assessment

By applying the methodology described in Section 5.3 to the case study structures, it has been possible to estimate the expected repair costs per technique featured on the current section. Figure 5.7 shows the total repair cost for the epoxy injection technique. In this plot, one can observe not only the effects of the ground shaking intensity but also the effect of the record-to-record variability. The observed dispersion on the plot is a direct result of considering a range of possible repair costs for the epoxy injection and its relationship with the damage index (see Figure 5.2)

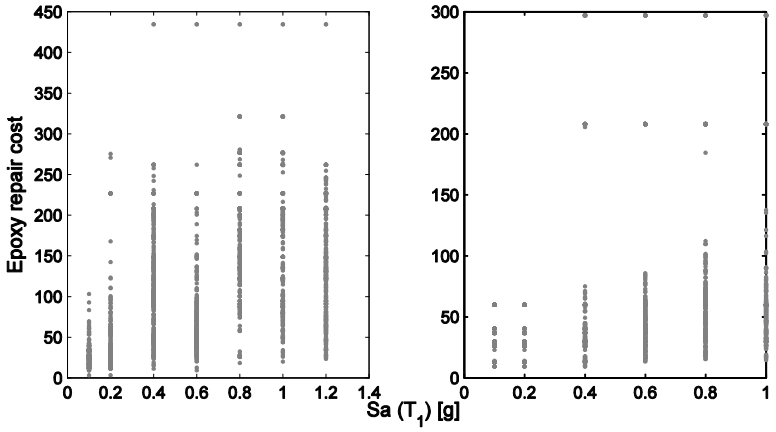

Figure 5.7 - Epoxy injection cost Left: Str1; Right: Str2.

Figure 5.8 represents the distribution of the jacketing repair cost for both structures. It should be noted that the level of damage in a given structural element is correlated with the ground motion. However from the point when an element has sustained enough damage to be repaired with a jacketing, the cost of this operation is constant, since it is solely dependent on the element's geometry (see section 5.3.2.2). It is worth mentioning that the average unit cost for the jacketing operation computed with the methodology suggested in this study is remarkably close to the value proposed by Calvi (2013), in which a unit cost of 200€/m for a jacketing operation is suggested. The average repair cost using the methodology presented here was 202€/m, by considering the data from both frames. It is pertinent to mention that on average, the use of steel jacketing for the beams led to a slightly more expensive unit cost (229€/m) than the RC jacketing considered for the columns (162€/m).

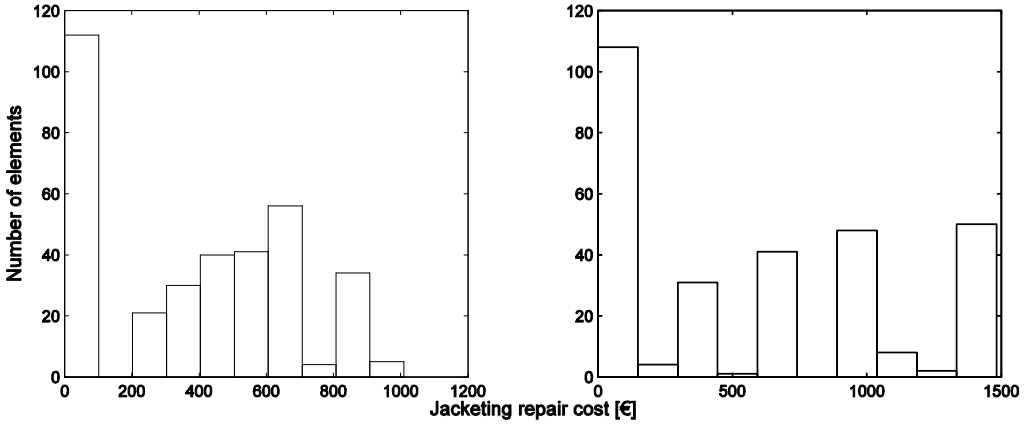

Figure 5.8 - Jacketing cost. Left: Str1; Right: Str2.

The methodology outlined in Section 5.3 requires an estimation of the element replacement cost in order to compute the economic loss for the significant and collapse damage state. In order to understand the replacement cost distribution for the two case studies, Eq. (5.4) has been employed to determine the cost of each structural element, as depicted in the histograms in Figure 5.9.

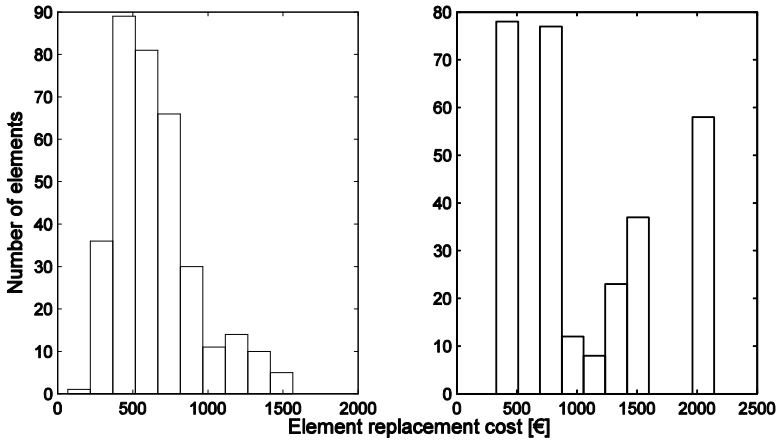

Figure 5.9 - Element replacement cost. Left: Str1; Right: Str2.

Once the expected repair cost for every structural element has been computed with Eq. (5.3), it is divided by the element replacement cost, leading to the expected element loss ratios presented in Figure 5.10. These results indicate negligible structural losses in both structures until $Sa(T_1)=0.4g$. Whilst Str1 exhibits a considerable number of elements with losses exceeding 10% of the replacement cost, the losses in Str2 are separated in clusters with very few elements registering loss ratios above this threshold. This is just another evidence of the more pronounced soft storey collapse mechanism in Str2. The result of this in terms of loss assessment is that the overall economic losses of Str2 are expected to be controlled by the losses due to complete structural collapse.

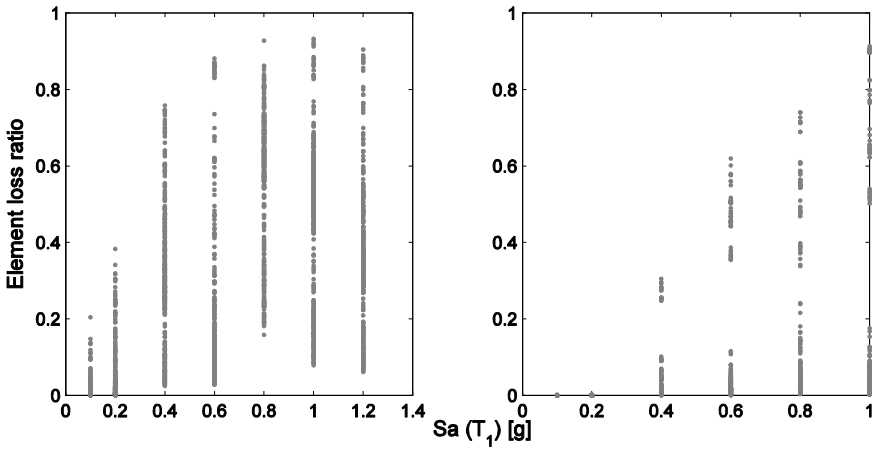

Figure 5.10 - Element loss ratio. Left: Str1; Right: Str2.

5.5.5 Non-structural element loss estimation

From the results of the incremental dynamic analyses the expected losses in non-structural elements have been computed. Figure 5.11 depicts the evolution of the sum of non-structural losses normalized by the total economic value of the non-structural components for each ground motion record. From these results, it can be observed non-negligible losses for lower ground shaking intensities. Most of these are due to damage on the masonry walls, given the limited interstorey drift capacity of these elements.

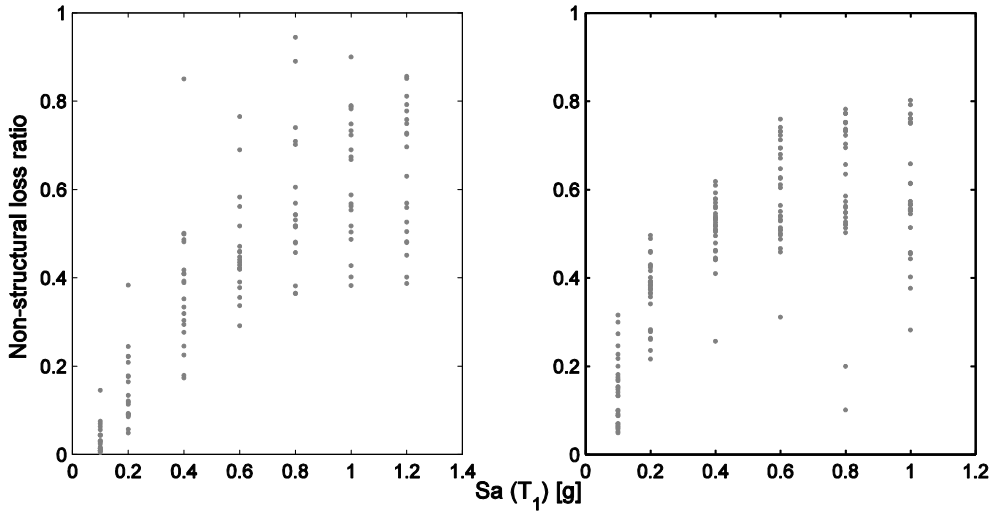

Figure 5.11 - Non-structural loss ratio - Left: Str1; Right: Str2.

5.5.6 Defining a damage scale

Creating a damage-to-loss model often requires the definition of a number of global discrete damage states (DS). As previously discussed, the main observed collapse mechanism for both structures was a soft storey at the ground level, and therefore the selected damage criteria must be able to capture this collapse mechanism.

The damage scale proposed herein makes use of the local element seismic response to define the global structural damage. The criteria for assessing the global structural damage were inspired by the work of Bal *et al* (2010b). This model was based on the nonlinear analysis of numerous structures and correlation of element damage with the structural global performance. The model proposed herein uses most of the thresholds suggested by Bal *et al*; but this original work did not provide a clear separation between slight damage and the undamaged state, and instead merged both into a single DS. In order to keep consistency with the damage scale presented in section 5.3.1, four damage states had to be established herein. A comment on the division between DS2 and DS3 is that it was defined from the point where non-repairable damage starts to be observable on the structure. The global collapse has been correlated with the failure of a storey or with the point where the repair of the structure is no longer cost effective. While few would argue against a collapse criteria defined through the generalized column failure due to the fact that column stability is critical to the stability of the whole structure a comment on the criteria defined by beam failure must be added. Generalized beam failure throughout the building would most likely render the structure as unusable after the earthquake loads have ceased. It should also be taken into consideration that beam repair is often a more complex and costlier operation than repairing columns. It is not uncommon that when facing the decision of repairing a building with generalized beam failure or rebuilding it, the most cost efficient choice is the reconstruction. In this case and from a practical perspective, the structure should be classified as collapsed.

Listed below are the criteria proposed by this study and used in Section 5.5.7 to assess the global structural damage.

- Light damage (DS1) is reached if 5% of the beams exceeded the yield capacity; otherwise the structure is considered to be Undamaged (DS0).
- Moderate damage (DS2) is reached if 10% of the beams or any column has yielded.

- Significant damage (DS3) is reached if 30% of the beams in the direction of loading or more than 80% of the columns at the ground floor have yielded. None of the structural elements must have reached the ultimate capacity.
- Collapse (DS4) is reached if 20% of the beams in the direction of loading or 80% of the columns at ground floor have reached their ultimate capacity. The structure is also considered to be in this damage state if a collapse is verified during the dynamic analyses.

5.5.7 Defining a damage-to-loss model

In order to determine appropriate damage-to-loss models, for each ground motion record and intensity level, the expected loss has been computed and allocated to one of the four previously described damage states. The result of this effort was a vector of loss ratios per damage state from which was Figure 5.12 computed. Information regarding the dispersion in the computed damage-to-loss models is provided in Table 5.4.

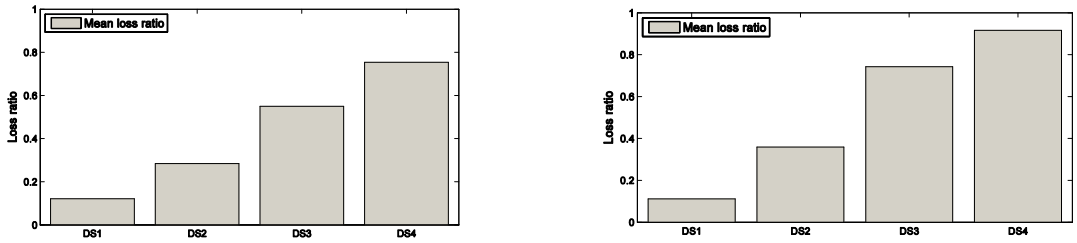

Figure 5.12 - Damage-to-loss models. Left: Str1; Right: Str2.

Table 5.4 - Standard deviation for the damage-to-loss models.

Damage state	Standard deviation	
	Str1	Str2
Light Damage (DS1)	0.049	0.054
Moderate Damage (DS2)	0.070	0.110
Significant Damage (DS3)	0.086	0.118
Collapse (DS4)	0.130	0.094

Since no significant differences between the models in Figure 5.12 have been observed, and both Str1 and Str2 are pre-code mid-rise RC frames, a decision was made to merge information from both case studies into a single damage-to-loss model (see Figure 5.13 and Table 5.5). The

proposed damage-to-loss model was computed using the average of all loss ratios values deemed to be in a given damage state.

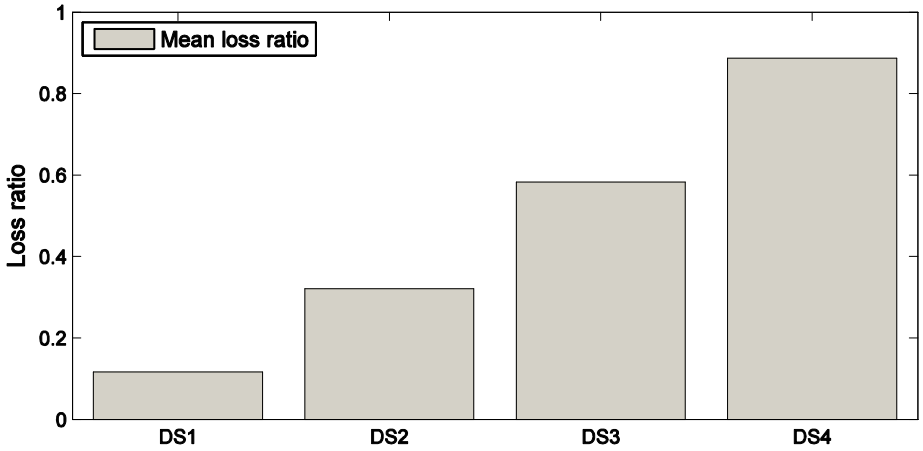

Figure 5.13 - Combined damage-to-loss model.

Table 5.5 - Combined damage-to-loss model.

Damage state	Mean loss ratio	Standard deviation	CoV.
DS1	0.117	0.051	0.430
DS2	0.321	0.099	0.308
DS3	0.583	0.117	0.201
DS4	0.887	0.119	0.134

Comparing the proposed model with some other damage-to-loss models found in the literature for reinforced concrete frames (see Figure 5.14) it can be observed the average loss ratio for the proposed damage-to-loss model for the uppermost damage state is around 89%, which is slightly higher than the central value of the damage-to-loss model proposed for Greece by Kappos *et al* (2006). A loss ratio below 1 for the last DS in the consequence model indicates that the damage scale considered has a conservative approach to assess structural damage, which could signify that a globally defined collapsed state does not actually translate to a total loss of the building. Despite these results, it is important to recognize that repairing a building heavily damaged might not be a practical option, and in reality the structure is likely to be demolished. For example FEMA P-58 (FEMA 2012) mentions that several owners have selected to replace buildings when the expected repair costs exceeded about 40% of the replacement cost. This possibility has been incorporated in the damage-to-loss model derived

by Bal *et al* (2008), which defines a loss ratio for extensive damage equal to 1.04, to account for demolition, removal of debris and re-construction of the structure. Analysing the proposed value for DS1, it should be noted that it is in the same order of magnitude of the one proposed by Bal *et al*, although slightly lower. As previously mentioned, most of the losses for this damage state come from the damage in the infill walls. In fact, it was observed that the 1‰ interstorey drift threshold considered as the onset of damage for the walls was exceeded for low ground shaking intensities, for which the structure has not yet sustained significant structural damage. These results, added to the fact that the masonry walls account for over one third of the building's replacement value, explain the losses computed for in DS1.

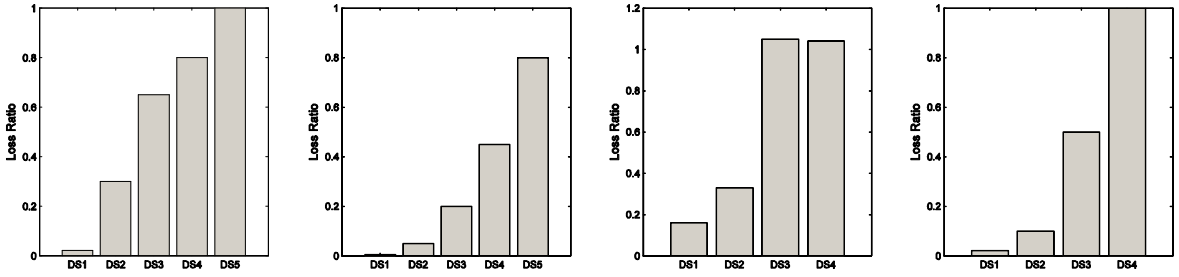

Figure 5.14 - Example of Damage-to-loss models. From left to right: Di Pasquale and Goretti (2001) (Italy); Kappos et al (2006)(Greece); Bal et al (2008)(Turkey) and HAZUS (FEMA 2014) (California).

Having information on the dispersion of the damage to loss model means that in a risk assessment, it is possible to define the consequence model with a random variable, and compute the expected loss and associated uncertainty within a probabilistic framework. To test if any of the most common probability models used in engineering could represent the data for each DS, a one-sample Kolmogorov-Smirnov (K-S) test for a 5% significance level has been performed. Table 5.6 summarizes the results given by the K-S test in which a value of 1 implies a rejection of the null-hypothesis (i.e. there is no sufficient evidence to support the statement that the data can be represented by the selected probability model). In addition, the root mean squared error (RMSE) between the empirical and theoretical cumulative distribution function (CDF) has also been calculated. By analysing the results from Table 5.6, it can be observed that a significant percentage of the probability distributions did not pass the K-S test for the selected significance level and have high RMSE. One of the reasons for this outcome could be that the amount of data is insufficient to ensure a proper fitting of the results,

and thus additional analyses should be performed. Silva *et al* (2014d) refers to the Beta distribution as appropriate to represent consequence models. The results shown in Table 5.6 seem to validate these findings since this probability distribution has passed the K-S test for DS1 and DS4 and exhibits amongst the lowest values for RMSE for DS2 and DS3. It should also be mentioned that the Gamma and Lognormal distributions have also performed reasonably well for the majority of the damage states and could equally be considered as valid options.

An alternative to the representation of the distribution of loss ratio per damage state with a parametric distribution could be the use of a probability mass function. In this approach, a number of loss ratio bins are defined, with an associated probability of occurrence.

Table 5.6 - K-S test results and RMSE for proposed damage-to-loss model.

Probability distribution	DS1		DS2		DS3		DS4	
	K-S test	RMSE	K-S test	RMSE	K-S test	RMSE	K-S test	RMSE
Beta	0	0.3304	1	0.3280	1	0.2646	0	0.0023
Exponential	1	0.3156	1	0.3151	1	0.3223	1	0.4659
Gamma	0	0.3356	0	0.3346	0	0.2661	1	0.0116
Lognormal	0	0.3356	0	0.3346	0	0.2632	1	0.0134
Normal	0	0.3354	1	0.3345	0	0.2705	1	0.0083
Weibull	0	0.3353	1	0.3343	1	0.2830	1	0.0023

K-S - Kolmogorov-Smirnov; RMSE - Root Mean Squared Error

5.6 INVESTIGATION ON THE INFLUENCE OF SELECTING A DAMAGE-TO-LOSS MODEL

5.6.1 Developing a compatible fragility model

Having established a suitable damage scale in Section 5.5.6, compatible fragility functions (Figure 5.15) were developed for the case study structures in order to later compute the expected losses.

For Str1, the median value for the DS1 curve is around 0.14g, which is significantly close to the first spectral acceleration level used for selecting ground motion records, as discussed in Section 5.5.2. It would have been useful to have a better discretization of ground motion intensities around $Sa(T_1)$=0.10g, by adding for example the 0.05g and 0.15g levels; however, due to the computational demand of performing non-linear analysis in 3D models, it was decided to keep the number of intensity levels to a minimum. Furthermore, at this ground

shaking level the structure is expected to respond in the elastic range, which implies a lower response variability. In addition, significant structural damage, which has a higher contribution to the overall loss, only occurs for higher levels of ground motion.

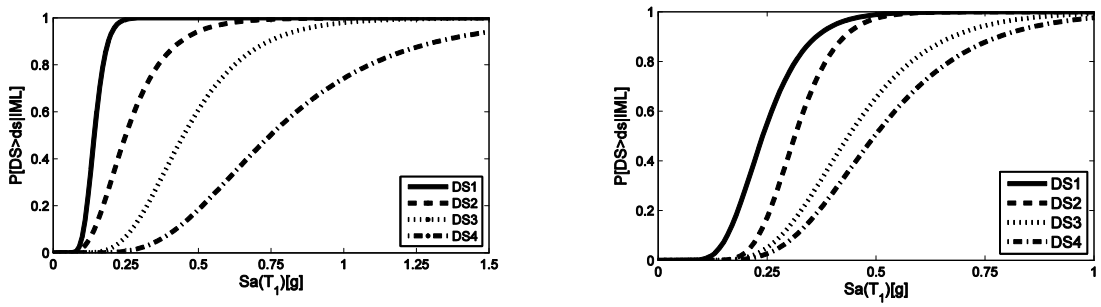

Figure 5.15 - Fragility functions Left: Str1; Right: Str2.

5.6.2 Derivation of vulnerability functions

5.6.2.1 Discrete vulnerability functions

The development of a fragility model is often one of the first steps in a loss estimation exercise (Spence 2007), which can be combined with a consequence model to derive a set of vulnerability functions, and then employed to assess seismic risk (e.g. (Erberik 2008, Costa *et al.* 2010, Silva *et al.* 2014d)). However, this combination can influence greatly the resulting vulnerability functions, and consequently the associated losses, as demonstrated herein.

Section 5.5.7 featured a qualitative comparison between the average model calculated in this study against other damage-to-loss models, e.g. (Di Pasquale and Goretti 2001, Kappos *et al.* 2006, Bal *et al.* 2008, FEMA 2014). This section provides a quantitative analysis on the importance of using compatible fragility and damage-to-loss models. Using the damage-to-loss models derived for each frame (see Figure 5.15)and the models proposed in the literature, mean vulnerability functions have been computed (Figure 5.16) through the convolution of the consequence models with the fragility functions (Eq.(5.6)). In this equation, LR_{ds} refers to the loss ratio provided by the damage-to-loss model for each DS. Both the models from Di Pasquale and Goretti and Kappos *et al* have one more DS than the damage scale considered in this study, and therefore a harmonization was required. For the model proposed by Kappos *et al,* it has been decided to merge the two lowest DS in this model and adopt the average central value. For the second model, given the significant difference between DS1 and DS2, assuming

the average loss ratio of the two damage states would most likely introduce significant bias in the results, and thus this model has not been considered in this comparison.

$$E[LossRatio \mid IM] = \sum_{ds=0}^{nDS} \left(P[DS = ds \mid IM] \cdot LR_{ds} \right) \tag{5.6}$$

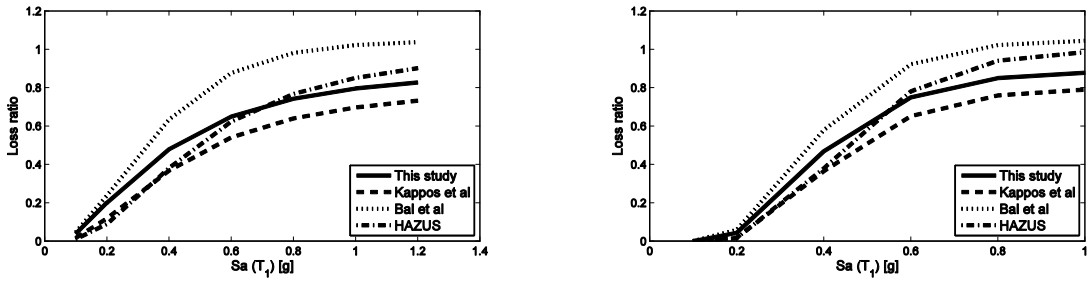

Figure 5.16 - Mean discrete vulnerability functions. Left: Str1, Right: Str2.

5.6.2.2 Continuous vulnerability functions

The proposed methodology to compute losses as presented in Section 5.3 does not require an explicit fragility and consequence model, provided that an estimate of the collapse probability is produced, as discussed previously. This method is recommended for the computation of vulnerability functions since it is not attached to discrete fragility or consequence models, thus avoiding problems of incompatibility between these two components.

Taking the mean value of residual interstorey drift suggested by Ramirez and Miranda (2012) and the number of non-converged analyses as collapse indicators the collapse probability conditional to the ground shaking intensity has been computed. As expected, from the discussion in Section 5.5.3, the collapse curve for Str2 is much steeper than the one for Str1. For the mid to high range intensities the losses computed with Eq. (5.5) for Str2 to be governed by the first half of the equation, while for Str1 the contribution of the losses given by the structural collapse and the element repair and non-structural losses were more evenly distributed. Figure 5.17 depicts the expected mean loss ratios as computed with Eq. (5.5) using the repair costs given by the thirty ground motion records and the respective collapse probabilities.

As previously stated, this approach is the preferred method to compute vulnerability models, and therefore the functions in Figure 5.17 will be used as the reference in the risk comparisons presented in Section 5.6.3.

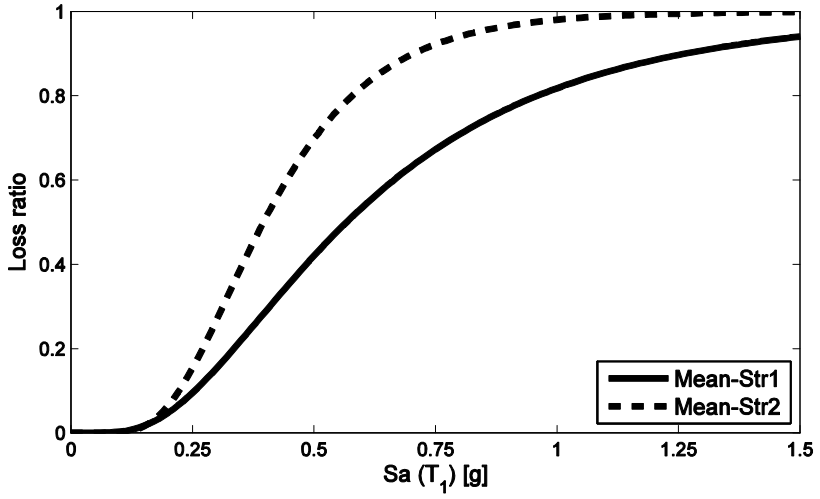

Figure 5.17 - Expected loss ratios given ground shaking intensity.

5.6.3 Impact in seismic loss assessment

In order to determine the influence of the damage-to-loss model on probabilistic loss assessment, the annual expected loss for both case study frames has been calculated. Hazard curves for the same location adopted for the ground motion selection (see Figure 5.18) have been calculated using the results from the FP7 European project SHARE (www.share-eu.org). These curves describe the probability of exceeding a set of ground shaking intensities for a reference time period, and can be combined with vulnerability functions to estimate probabilities of exceeding levels of loss. Further explanations on the numerical procedure to compute the expected losses from the hazard and vulnerability curves are provided in Eads *et al* (2013). Applying this methodology to the vulnerability functions previously computed and the aforementioned hazard curves, leads to the annual expected loss ratios listed in Table 5.7 and Figure 5.19.

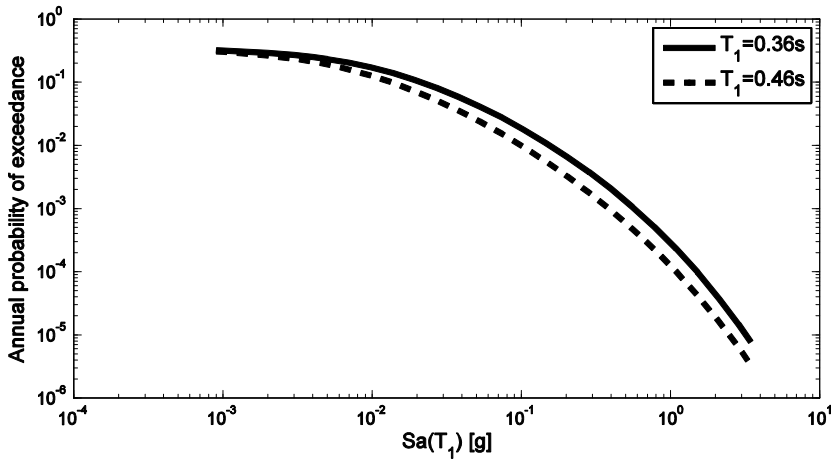

Figure 5.18 - Hazard curves for Lisbon in terms of the spectral acceleration at the fundamental period of each structure.

Table 5.7 - Annual expected loss ratio.

Structure	Annual expected loss ratio (AELR)				
	This study (Damage-to-loss model)	Kappos *et al* (2006) model	Bal *et al* (2008) model	HAZUS	Reference (Continuous vulnerability)
Str1	2.336×10^{-3}	1.953×10^{-3}	4.145×10^{-3}	1.813×10^{-3}	2.148×10^{-3}
Str2	1.232×10^{-3}	9.204×10^{-4}	1.320×10^{-3}	9.983×10^{-4}	1.102×10^{-3}

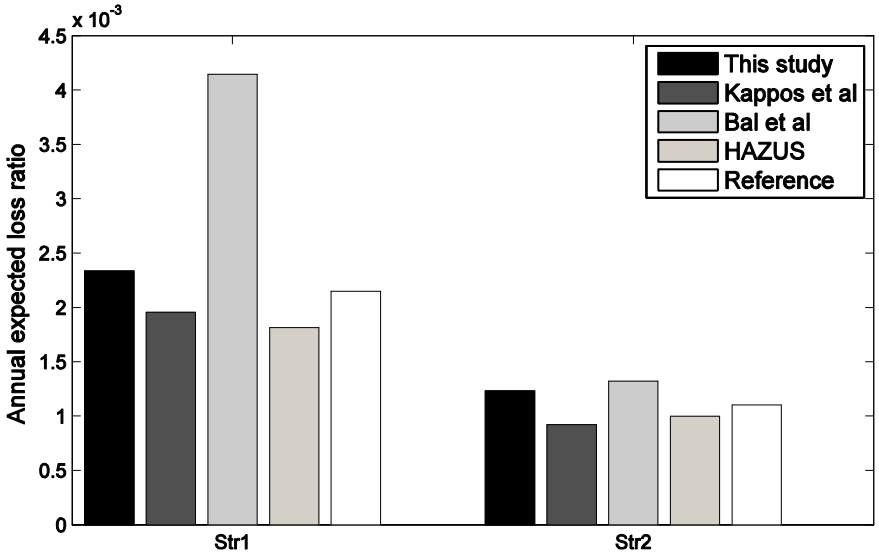

Figure 5.19 - Annual expected loss ratio.

From the results in Figure 5.19, it can be concluded that the consequence model that performed best when compared with the reference AELR was, unsurprisingly, the model proposed in this study. This was expected since the fragility and damage-to-loss models were developed jointly, and therefore compatibility was ensured. Nonetheless, significant differences are still observed when the vulnerability functions derived from the combination of fragility and damage-to-loss models were employed.

This example illustrates one of the main problems with developing a vulnerability function through discrete damage states, in comparison to a model based on continuous damage and loss estimation. The main contribution to the AELR is given by the lowest intensity events. Having failed to have a good discretization of the damage-to-loss model at the lowest damage states (i.e. having a damage scale with less damage states than it would otherwise be recommended) will most likely translate into an erroneous estimate of the expected losses, even in the best-case scenario in which compatibility between fragility and consequence models is guaranteed. From these results, it is fair to state that any loss assessment study that uses the traditional technique to compute losses should be preceded by an investigation of the definition of the minimum number of damage states. Nevertheless, a more accurate alternative is to follow a continuous vulnerability assessment methodology as suggested herein.

5.7 SIMPLIFIED METHODOLOGY FOR COMPUTING STRUCTURAL LOSSES

The previous sections have outlined a generalized methodology to compute structural losses directly from the element damage without the need for an explicit fragility or consequence models that in the authors' opinion has several advantages over the traditional methodology to compute vulnerability functions. The structural damage has been assessed through a modified version of the Park and Ang (1985) index proposed by Beck *et al* (2002), so-called *Deformation Damage Index* (DDI), and defined as a ratio between chord rotations. The proposed technique also requires the explicit computation of the individual repair costs for all structural elements as a function of the probability of exceeding a number of damage states, as proposed by Haselton *et al* (2008). Despite the clear advantages of assessing directly structural losses, as oppose to evaluate damage states and then relate them with a fraction of loss, it is relevant to acknowledge that such methodology requires a significant number of steps, the most

important being correctly assign the element to a damage state, determining the correspondent repair cost and compute the structure's probability of collapse, thus rendering it quite time consuming. In addition, for this methodology is essential to have reliable and up-to-date information on the cost of repairing the elements.

Ideally, one should be able to estimate the expected structural loss directly from the element's performance information as given by the dynamic analyses' outputs. Defining a possible relationship between the expected structural loss and some performance parameter could be described as the main objected of this section. This approach not only has the potential to simplify the overall vulnerability assessment procedure but also to minimize the uncertainty on the final loss computation.

5.7.1 Study on developing simplified relationships for computing structural losses

Using the Matlab algorithm described in section 3.3, three 3-storey and three 5-storey structures designed for increasing levels of ground motion (a_g=0.05g, 0.2g and 0.4g) were analysed. Using the methodology previously described the expected loss ratio, i.e. the quotient between the cost of repair and the cost of replacement, for every structural element has been computed from the results given by the nonlinear dynamic analyses performed on the numerical models.

The expected loss ratio was later plotted against the correspondent damage index value in order to evaluate the potential existence of a significant correlation. Second degree polynomial functions were later fitted to the data (see Figure 5.20). The R^2 coefficient for these functions was found to range from 0.923 to 0.977, which indicates a strong correlation between the variables.

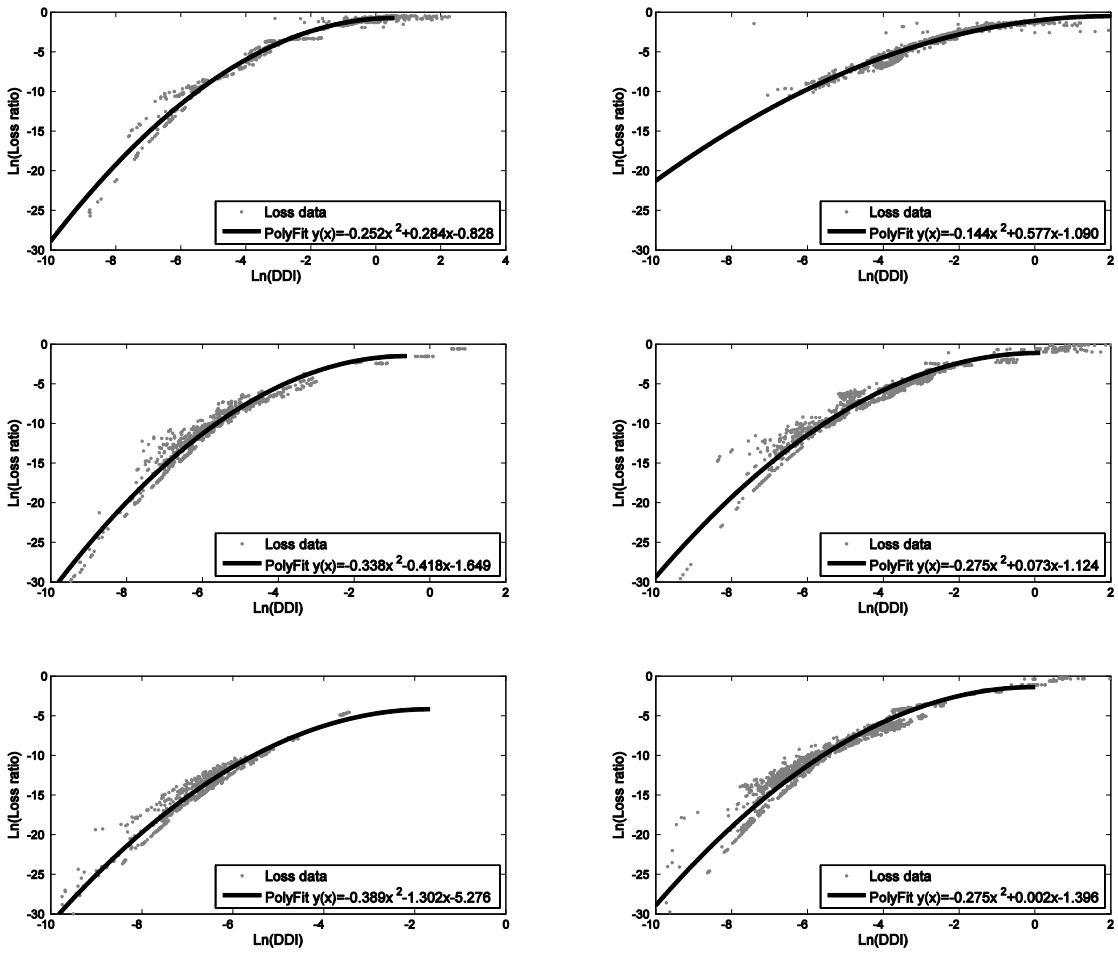

Figure 5.20 - Damage index *vs.* Expected loss ratio. Left: 3 storey frames; Right: 5 storey frames (design acceleration increases downwards).

The findings in Figure 5.20 suggest it is reasonable to assume that a polynomial relationship between the natural logarithm of the damage index and the correspondent loss ratio exists. A comment on the polynomial functions depicted in the figure is that being second degree polynomials, the domain of applicability of fitted functions is limited to the point with a horizontal tangent, at which one starts to observe decreasing loss ratios with increasing damage, which is clearly unreasonable given the physics of the problem.

Having established that a polynomial relationship between the DDI and the expected loss ratio is likely to exist when plotted in a logarithmic space, a global function combining the data from all the structures has been defined (see Figure 5.21). Commenting on the proposed model it must be mentioned that it is only valid for DDI levels lower than 1.06, i.e. an abscissa lower 0.06. It has to be referred that if one was to apply this model to assess the losses of a different

set of structures this would probably not be a limitation because at the corresponding performance level most of the elements are expected to be heavily damaged or even collapsed, meaning that a replacement of the element is likely to be necessary. Thus if a loss estimate beyond the range of applicability is needed, a unit loss ratio should be assumed.

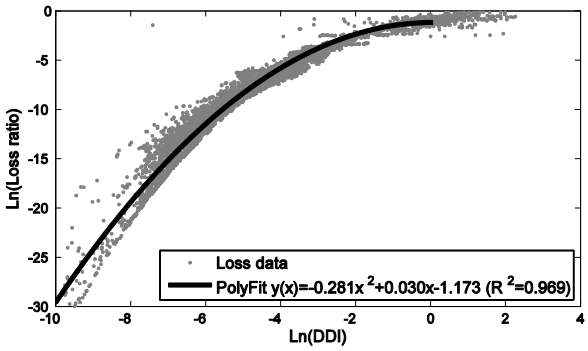

Figure 5.21 - DDI-to-loss model.

5.8 FINAL REMARKS

This section presented an alternative to the commonly applied vulnerability assessment methodologies, with an application to Portuguese RC buildings, through the estimation of element damage and employment of damage-specific repair methods and associated costs. As previously discussed, to the authors' knowledge there were no detailed studies on damage-to-loss models for Portugal, meaning that most of the current loss assessment analyses rely on models developed and calibrated to other regions (e.g. (Costa *et al.* 2010, Silva *et al.* 2014d)).

Through a modified version of the Park and Ang damage index (DDI) and a comprehensive study of the repair costs, it has been possible to estimate element loss ratios, expressed as cost of repair to cost of replacement. The methodology for estimating the repair costs was developed considering the Portuguese building stock, but it can be easily adapted to other realities, provided that a reliable source of information on the required unit costs is available. It is acknowledged that the real repair cost of a damaged element might be different from the one predicted using the methodology presented in this paper if additional tasks (such as demolition and removal of debris) are required prior to the actual repair job. Given that it was

intended to develop a generalised methodology easily modifiable, a decision was made to neglect these additional costs.

The expected losses from the non-structural components have also been considered within this methodology, by using a ratio between structural and non-structural components in the total cost of the building. Only deterministic performance thresholds have been adopted to assess the damage, but the general methodology remains unaltered should a probabilistic approach have been adopted for this purpose.

In addition to presenting the methodology to compute losses, this section also described a case study application considering two existing reinforced concrete structures, through numerical modelling and nonlinear incremental dynamic analysis. Each structure was subjected to a large set of ground motion records, and allocated into a damage state according to the extent of damage in the structural elements. Then, the estimated fraction of loss in each structure per damage state was analysed, in order to derive a loss ratio distribution per damage state. In addition, the portion of structures in each damage state per intensity measure level was also utilised to derive a fragility model for each structure. Both of these models were combined to derive discrete vulnerability functions. In parallel, the distribution of loss ratio per intensity measure level was also used to directly compute a continuous vulnerability function, assumed to be the most accurate approach in the present study. The comparison of the discrete and continuous vulnerability functions revealed significant differences, which consequently affect strongly the associated risk metrics (e.g. average annual loss ratio).

The findings of this study indicate that ideally risk modellers should seek to develop vulnerability models purely based on the distribution of loss ratio per intensity measure levels. In the absence of such possibility (for example, if a comprehensive fragility model is already in place), the selected damage-to-loss model should as much as possible be compatible with the established damage scale and criteria, thus minimising possible bias in the risk analysis.

In addition, evidences for a possible polynomial relationship between the structural losses and the DDI have also been presented. As demonstrated herein, the data can be very well fitted by a polynomial function for the entire range of interest of the damage index when plotted in a logarithmic space. Being second degree polynomial functions, the models provided herein are limited to the maximum abscissa given by the point where the slope of the tangent to the curve

changes sign. It is acknowledged that the expected repair costs per technique necessary for developing the DDI-to-loss functions presented in this study have been calibrated for the Portuguese building stock. Therefore, some of the results and conclusions presented herein may not be directly applicable to other realities.

It is expected that the discovery of a polynomial relationship between the DDI and the correspondent structural loss could stimulate further research in order to develop functions suitable for a larger and more diverse set of structures. This procedure would provide a quick and easy technique to estimate losses without the need to allocate the elements into a discrete damage state and explicitly compute the repair costs. It should also be mentioned that computing structural losses directly from the results given by the nonlinear dynamic analyses has, in the author's opinion, not only the potential to simplify the overall vulnerability assessment procedure but also to minimize the uncertainty on the final loss estimation.

6

AN UPDATED SEISMIC RISK PROFILE FOR MAINLAND PORTUGAL

6.1 SUMMARY

Portugal's history is marked by high intensity seismic events, such as the devastating 1755 Lisbon, believed to have had a moment magnitude above 8.0 (Vilanova *et al.* 2003). More recently, the 1909 and 1969 seismic events were also responsible for great social and economic losses with significant number human fatalities and buildings reported either as heavily damaged or collapsed. Reliable earthquake loss estimates are useful for the development and implementation of mitigation strategies aimed to reduce the expected consequences of future events. Despite the obvious need for reliable vulnerability estimates, more often than not the necessary inputs (i.e. fragility and damage-to-loss models) are either not available or not calibrated for the region of interest and respective building stock.

This study provides an updated seismic risk profile for mainland Portugal considering the latest advances in seismic fragility assessment and the correlation between damage and losses developed specifically for the Portuguese building stock. Fragility models for the most significant building classes identified in the exposure model were developed considering equivalent single degree of freedom systems and nonlinear time history analysis. These were later combined with damage-to-loss models to compute vulnerability curves. For what concerns the seismic hazard analysis (SHA) component, this study considered the hazard model developed for Portuguese mainland proposed by Vilanova and Fonseca (2007).

The earthquake losses were estimated following an event-based approach, in which a large set of stochastic events is generated, representing possible realizations of the seismicity across the region of interest within a given time span. Each generated event is used to calculate an

aggregated economic loss, leading to a set of losses within the same time span. These results can be used to derive annualized average losses, loss exceedance curves and probable maximum losses. This study also advances previous endeavours by following an event-based procedure, as opposed to the classical probabilistic seismic hazard assessment approach.

6.2 SEISMIC HAZARD ASSESSMENT

Located in the vicinity of the southern boundary between the Eurasian and African tectonic plates, mainland Portugal's seismic hazard is primarily characterized by large offshore earthquakes and moderate onshore earthquakes. Seismicity in mainland Portugal is predominantly generated in two distinct tectonic environments: (i) stable continental regions (SCR) and (ii) active continental regions (ACR). SCR comprises the part of continental crust where the main tectonic activity is not directly linked with plate boundary processes, whilst for ACR the tectonic activity is predominantly correlated with plate boundary movements (Vilanova and Fonseca 2007).

Virtually non-existent recorded data for significant earthquakes meant the majority of past seismic hazard studies developed for Portugal have relied on historical and/or macroseismic information (Vilanova and Fonseca 2007). The ground motion fields utilized in this study were computed using the OpenQuake (OQ) engine (Silva et al. 2014b) and the hazard model proposed by Vilanova and Fonseca (2007). The chosen source model comprises two different broad zones (see Figure 6.1) divided in several smaller seismogenic area sources. Zonation SA includes eleven source zones based on the distribution of seismic intensity of past earthquakes, whilst zonation SB is divided in eight distinct source zones and is in essence an adaptation of source model previously proposed by Paláez Montilla and López Casado (2002).

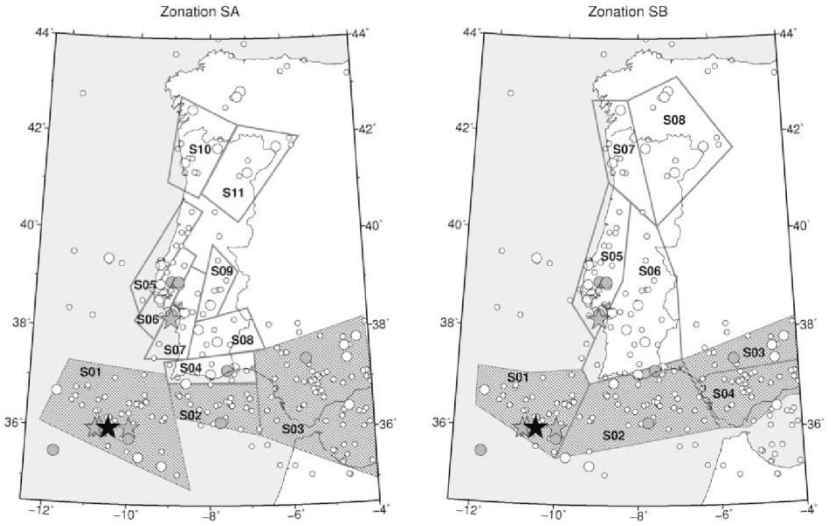

Figure 6.1 - Representation of the source model proposed by Vilanova and Fonseca (2007).

The local soil conditions have been considered by including the average shear wave velocity at the first 30 metres ($V_{s,30}$) into the hazard calculations. Considering $V_{s,30}$ to categorise the local site condition has become a standard in seismic risk analyses with, for example, the OQ engine using ground motion prediction equations that require this value as an input. In order to develop an appropriate distribution of $V_{s,30}$ to be used by the engine, the same topography based approach followed by Silva *et al* (2014b) was used. The resulting map is presented in Figure 6.2 - Left.

The uncertainties on the source model and on the ground motion prediction equations (GPME) were accounted in the hazard calculations with the logic tree suggested by Vilanova and Fonseca (2007). The logic tree was translated into the *nmrl* programming language, and after minor adjustments to account for the GMPE availability in OpenQuake's library, included in the hazard calculations. An example of the hazard maps for a ground shaking with 475 year return period is given in Figure 6.2 - Right.

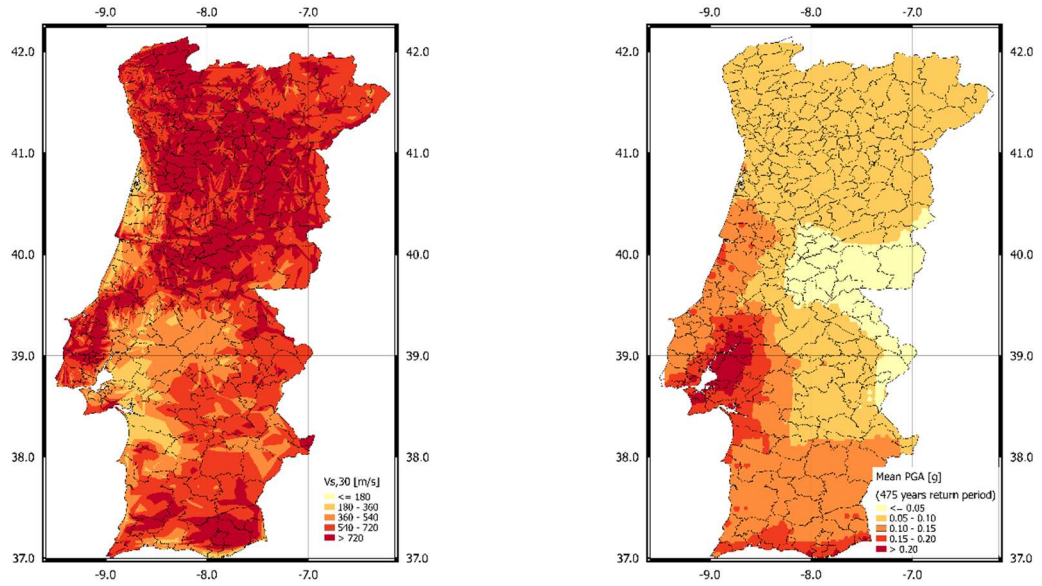

Figure 6.2. - Left) $V_{s,30}$ mapping, Right) Mean ground motion field (IM=PGA, 475 year return period).

6.3 EXPOSURE MODEL

It was not considered within the scope of this study to provide full description on how to develop exposure models, and for that reason the reader is directed to the original work by Silva *et al* (2014c) for detailed information on the exposure model used herein. Despite this, a brief description is provided since it includes important information to justify the building taxonomies considered in section 6.4.

The last national building census held in Portugal in 2011 reported over 3.5 million residential buildings with an estimated replacement cost exceeding 470 billion euros and totalling nearly 5.9 million dwellings (Silva *et al.* 2014c). The survey included information regarding the building material and type of construction, construction year and height. Regarding the building material and type of construction, Silva *et al* (2014c) distributed the Portuguese building stock in five main categories (i) reinforced concrete (RC), (ii) masonry with in concrete floors (M1), (iii) masonry with wooden floors (M2), (iv) weak masonry (e.g. adobe construction, rammed earth or field stone) (M3) and lastly (v) the remaining types of construction (e.g. steel, composite and timber structures) were lumped together in a single category (OT).

Combined, masonry and reinforced concrete make up to 99.2% of the total number of buildings in Portugal. Despite having a slightly inferior representation on the building stock

(48.6%) when comparing with masonry, reinforced concrete structures host the majority (60%) of the Portuguese population due the fact that reinforced concrete structures are often significantly taller than masonry ones (Silva *et al.* 2014c).

The age of a building has a great impact on the seismic performance of structures as it is strongly associated with the minimum requirements for seismic capacity enforced by law at time of construction. Correlating the year of construction with main design codes created for the Portuguese building stock, Silva *et al* (2014c) concluded that only 51% of reinforced concrete buildings were designed according with modern regulations. This means that potentially a very significant number of people are exposed to unacceptable levels of seismic risk. This last observation reinforces the need for a careful analysis on the expected seismic risk of RC structures thus supporting the need for a study like the one presented herein. Adding the building's height to the previous categories, Silva *et al* (2014c) have proposed the disaggregation of the census data represented in Figure 6.3.

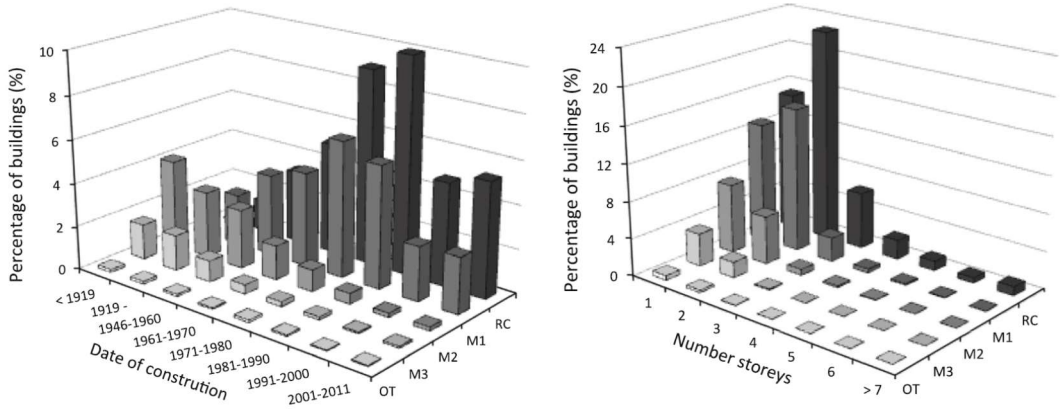

Figure 6.3 - Disaggregation of building census data by typology, year of construction and height proposed Silva *et al* (2014c).

In order to provide an estimate of the economic loss due to ground shaking an approximation of the total value of the Portuguese building stock was necessary. For the purposes of this study a similar approach to the one applied in section 5.3 was followed with the building's replacement cost being assumed to be the product between the total area and the reference cost per square metre given by the Portuguese government. The national Census data provides a spatial distribution of the number of buildings and dwellings at the parish level, however as

denoted by Silva *et al* (2014c) this resolution can result in crude earthquake losses estimation. The authors overcome this limitation by making the spatial distribution of buildings in the national Census data proportional to the population distribution in the LandScan™ database. LandScan allocates the population in a finer grid of 30 arc seconds according an algorithm that reflects several parameters like night lights and proximity to railroads or roads (Silva *et al.* 2014c). Merging the distribution of buildings with the respective replacement cost produced, after some post-processing, the map in Figure 6.4.

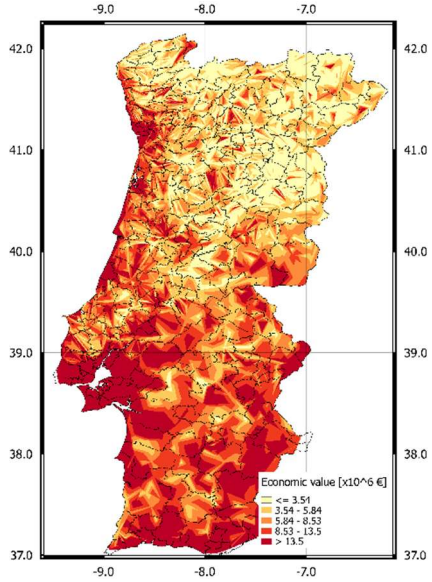

Figure 6.4 - Economic value of Portuguese building stock (interpolated using QGIS™ to a 0.001°x0.001° grid).

Analysing the spatial distribution of economic value of the Portuguese building stock in Figure 6.4 it is firstly possible to observe a concentration of assets along the coast line which is consistent with what is generally perceived for mainland Portugal. Probably more important than this observation is the fact that the areas with highest concentration of economic value and the areas with higher seismic hazard overlap quite remarkably. As a result of that a significant percentage of the assets in Portugal is potentially at risk of unacceptable levels of economic loss in the event of a future earthquake.

6.4 FRAGILITY AND VULNERABILITY ASSESSMENT

For this study updated fragility models have been computed using an analytical framework similar to one by proposed by Silva *et al* (2014d). The framework is based on the analysis of equivalent single degree of freedom (SDOF) systems through nonlinear time history algorithms. Each SDOF is represented by its mean capacity curve (expressed in spectral displacement *vs* spectral acceleration) calculated from the period of vibration, first mode participation factor (Γ) and yield and ultimate displacement capacity. Having estimated the roof displacement on the real structure (e.g. taking the yield/ultimate drift limits in Table 6.1), the spectral displacement (S_d) and spectral acceleration (S_a) of the equivalent SDOF are computed from Eq. (6.1) and (6.2).

$$S_d = \frac{\delta_{roof}}{\Gamma} \tag{6.1}$$

$$S_{a\_y} = S_{d\_y}\left(\frac{2\pi}{T_y}\right)^2 ; S_{a\_ult} = S_{a\_y} \tag{6.2}$$

Similarly to the work of Silva *et al* (2014c), the building classes were allocated in three main categories based on the year of construction and expected seismic design level. The first Portuguese design code to include seismic provisions was introduced in 1961 (*DL 44041 - Regulamento de Solicitações em Edifícios e Pontes*). This first generation of seismic regulations comprised mainly of simplified methodologies to compute the earthquake loads considering the weight of building and seismic coefficients. The next generation of design standards was approved in 1986 (*DL 235/83 - Regulamento de Segurança e Acções para Estruturas de Edifícios e Pontes*) and introduced considerably more restrictive seismic regulations and more advanced design techniques which are still in force to this date. In this study structures built prior to 1961 code were considered as pre-code, consequently with very limited (if any) ductility and energy dissipation capability, whilst buildings designed according with the current design code were considered to have a ductile behaviour. The remaining structures were assumed to

have moderate ductility and their respective capacity parameters were defined considering a balance between a non-ductile and a ductile behaviour.

In addition to the ductility level and height, a distribution of building classes by seismic zonation was also considered. The Portuguese design code (DL 235/83) divides the national territory in four distinct seismic zones (i.e. zone A located in Southwest of Portugal to zone D located in Northeast of Portugal). The prescribed ground shaking for a rock site ranges from 0.08g to 0.23g, with zone A exhibiting the highest seismic demand and zone D the lowest. The seismic zonation included in DL 235/83 is in essence an update on the map proposed in 1961, with the only difference being the addition of zone D generated from the division of zone C in two, and for this reason the same design ground accelerations were considered. To account for the differences in the seismic capacity introduced by the distinct design ground motion in each seismic zone (see example in Figure 6.5 - Left) and also to provide a connection with the work developed in the previous sections, the period-height relationships developed in section 3 were utilized to estimate the expected period of vibration for each reinforced concrete typology designed according to code. For the remaining building classes the expected yield period of vibration was estimated from simplified equations taken from the literature (e.g. (Bal *et al.* 2010b, Crowley and Pinho 2010, Silva *et al.* 2014b)).

When deriving fragility functions the building-to-building variability has also been considered. To this end 150 capacity curves (see Figure 6.5 - Right) were created from a randomly sampled population of S_d-S_a pairs assuming a normal distribution with a 25% coefficient of variation. Silva *et al* (2014d) have concluded that the yield and ultimate displacement capacity are often positively correlated. For this reason, a correlation coefficient of 0.60 was considered when generating capacity curves.

Considering that the main subject of this thesis is the seismic behaviour of reinforced concrete and that these structures host the majority of the population, more detail has been given to this typology when comparing, for example, with masonry buildings. Even so, fragility models for the most represented masonry classes were also developed following the same recommendations of Silva *et al* (2014d). Classes M1 and M2 were merged into a single typology (henceforth labelled simply as M) and no distinction between design levels was considered for M3. The capacity parameters for the masonry classes were defined from (Villar-Vega *et al.*

2017) considering ductile masonry as reinforced masonry, non-ductile masonry as unreinforced masonry and class M3 as unreinforced masonry with adobe blocks. Given the very reduced number of masonry structures with more than 4 storeys (see Figure 6.3) only fragility functions for masonry structures up to 3 storeys have been explicitly developed in this study. A complete list of the building classes considered in this study is provided in Table 6.1. The first pair of letters in the taxonomy code reflects the building material (e.g. RC=reinforced concrete), the second specifies the ductility level (i.e. ND= non ductile, MD=moderate ductile, D=ductile), followed by a reference the height (e.g. 1S=1 storey) and lastly to the seismic zone.

Table 6.1 - Building classes and mean capacity parameters used for fragility assessment.

Building class	**Dsg. PGA [g]**	**T_y [s]**	**Yield global drift [%]**	**Ult. global drift [%]**	**Sd_y [m]**	**Sa_y [g]**	**Sd_ult [m]**	**Sa_y [g]**
RC_ND_1S	N.A.	0.27	0.66	2.61	0.012	0.687	0.048	0.687
RC_ND_2S	N.A.	0.57	0.66	2.61	0.028	0.355	0.112	0.355
RC_ND_3S	N.A.	0.87	0.66	2.61	0.043	0.228	0.169	0.228
RC_ND_4S	N.A.	1.17	0.66	2.61	0.057	0.167	0.225	0.167
RC_ND_5-7S	N.A.	1.77	0.66	2.61	0.085	0.109	0.337	0.109
RC_ND_8-15S	N.A.	2.67	0.66	2.61	0.128	0.072	0.506	0.072
RC_MD_1S_A	0.23	0.16	0.79	3.31	0.013	2.159	0.055	2.159
RC_MD_2S_A	0.23	0.43	0.79	3.31	0.033	0.702	0.136	0.702
RC_MD_3S_A	0.23	0.71	0.79	3.31	0.049	0.393	0.205	0.393
RC_MD_4S_A	0.23	0.98	0.79	3.31	0.065	0.272	0.273	0.272
RC_MD_5-7S_A	0.23	1.54	0.79	3.31	0.098	0.167	0.409	0.167
RC_MD_8-15S_A	0.23	2.36	0.79	3.31	0.147	0.106	0.614	0.106
RC_MD_1S_B	0.16	0.19	0.79	3.31	0.013	1.448	0.055	1.448
RC_MD_2S_B	0.16	0.48	0.79	3.31	0.033	0.577	0.136	0.577
RC_MD_3S_B	0.16	0.76	0.79	3.31	0.049	0.339	0.205	0.339
RC_MD_4S_B	0.16	1.05	0.79	3.31	0.065	0.239	0.273	0.239
RC_MD_5-7S_B	0.16	1.62	0.79	3.31	0.098	0.151	0.409	0.151
RC_MD_8-15S_B	0.16	2.48	0.79	3.31	0.147	0.097	0.614	0.097
RC_MD_1S_C	0.12	0.22	0.79	3.31	0.013	1.142	0.055	1.142
RC_MD_2S_C	0.12	0.51	0.79	3.31	0.033	0.511	0.136	0.511
RC_MD_3S_C	0.12	0.80	0.79	3.31	0.049	0.310	0.205	0.310
RC_MD_4S_C	0.12	1.09	0.79	3.31	0.065	0.222	0.273	0.222
RC_MD_5-7S_C	0.12	1.67	0.79	3.31	0.098	0.141	0.409	0.141
RC_MD_8-15S_C	0.12	2.55	0.79	3.31	0.147	0.091	0.614	0.091
RC_D_1S_A	0.23	0.16	0.91	4.00	0.016	2.585	0.070	2.585
RC_D_2S_A	0.23	0.43	0.91	4.00	0.039	0.840	0.172	0.840
RC_D_3S_A	0.23	0.71	0.91	4.00	0.059	0.471	0.258	0.471
RC_D_4S_A	0.23	0.98	0.91	4.00	0.078	0.325	0.345	0.325
RC_D_5-7S_A	0.23	1.54	0.91	4.00	0.118	0.200	0.517	0.200

RC_D_8-15S_A	0.23	2.36	0.91	4.00	0.176	0.127	0.775	0.127
RC_D_1S_B	0.16	0.19	0.91	4.00	0.016	1.733	0.070	1.733
RC_D_2S_B	0.16	0.48	0.91	4.00	0.039	0.691	0.172	0.691
RC_D_3S_B	0.16	0.76	0.91	4.00	0.059	0.406	0.258	0.406
RC_D_4S_B	0.16	1.05	0.91	4.00	0.078	0.287	0.345	0.287
RC_D_5-7S_B	0.16	1.62	0.91	4.00	0.118	0.180	0.517	0.180
RC_D_8-15S_B	0.16	2.48	0.91	4.00	0.176	0.116	0.775	0.116
RC_D_1S_C	0.12	0.22	0.91	4.00	0.016	1.367	0.070	1.367
RC_D_2S_C	0.12	0.51	0.91	4.00	0.039	0.612	0.172	0.612
RC_D_3S_C	0.12	0.80	0.91	4.00	0.059	0.371	0.258	0.371
RC_D_4S_C	0.12	1.09	0.91	4.00	0.078	0.266	0.345	0.266
RC_D_5-7S_C	0.12	1.67	0.91	4.00	0.118	0.169	0.517	0.169
RC_D_8-15S_C	0.12	2.55	0.91	4.00	0.176	0.110	0.775	0.110
RC_D_1S_D	0.08	0.24	0.91	4.00	0.016	1.078	0.070	1.078
RC_D_2S_D	0.08	0.54	0.91	4.00	0.039	0.540	0.172	0.540
RC_D_3S_D	0.08	0.84	0.91	4.00	0.059	0.337	0.258	0.337
RC_D_4S_D	0.08	1.13	0.91	4.00	0.078	0.245	0.345	0.245
RC_D_5-7S_D	0.08	1.73	0.91	4.00	0.118	0.159	0.517	0.159
RC_D_8-15S_D	0.08	2.62	0.91	4.00	0.176	0.104	0.775	0.104
M_ND_1S	N.A.	0.17	0.14	0.60	0.002	0.317	0.010	0.317
M_ND_2S	N.A.	0.30	0.14	0.60	0.005	0.203	0.020	0.203
M_ND_3S	N.A.	0.45	0.14	0.60	0.007	0.136	0.029	0.136
M_MD_1S	N.A.	0.17	0.37	1.10	0.005	0.733	0.016	0.733
M_MD_2S	N.A.	0.30	0.37	1.10	0.011	0.471	0.033	0.471
M_MD_3S	N.A.	0.45	0.37	1.10	0.016	0.314	0.049	0.314
M_D_1S	N.A.	0.17	0.60	1.60	0.010	1.358	0.026	1.358
M_D_2S	N.A.	0.30	0.60	1.60	0.020	0.872	0.052	0.872
M_D_3S	N.A.	0.45	0.60	1.60	0.029	0.581	0.078	0.581
M3_1S	N.A.	0.17	0.10	0.50	0.002	0.226	0.008	0.226
M3_2S	N.A.	0.30	0.10	0.50	0.003	0.145	0.016	0.145
M3_3S	N.A.	0.45	0.10	0.50	0.005	0.097	0.024	0.097

N.A. - not applicable

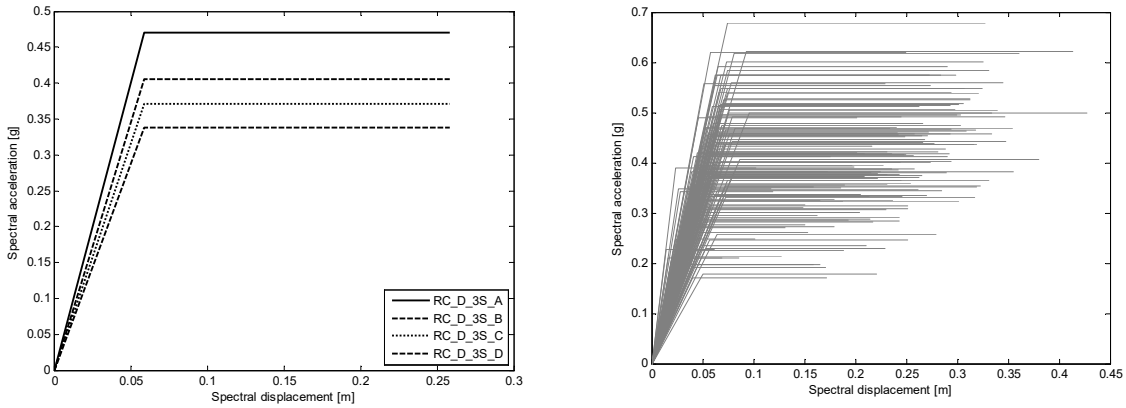

Figure 6.5 - Example of capacity curves used in fragility assessment. Left) Effect of different prescribed design ground motion on the mean capacity; Right) Effect of dispersion on capacity parameters for RC_D_3S_A.

For this study four distinct damage states ranging from light damage (DS1) to collapse (DS4) were considered for deriving fragility functions and the performance thresholds were computed from each capacity curve assuming the limits recommended by Villar-Vega (2017) (see Table 6.2). The equivalent SDOFs were put against ground motion records selected from the European strong motion database (Akkar *et al.* 2014) to be compliant with the main tectonic environment in mainland Portugal and nonlinear time history analyses were conducted. Several intensity measures have been tested and the one that lead to the best fitting was selected. The resulting fragility parameters are listed in Table 6.3.

Table 6.2 - Performance thresholds for fragility assessment.

Damage state	Threshold
Light damage (DS1)	$0.70xS_{d\_y}$
Moderate damage (DS2)	$0.75xS_{d\_y}+0.25xS_{d\_ult}$
Extensive damage (DS3)	$0.50x(S_{d\_y}+S_{d\_ult})$
Collapse (DS4)	S_{d_ult}

S_{d_y} – Spectral displacement at yield; S_{d_ult} – Spectral displacement at ultimate capacity

Table 6.3 - Computed fragility parameters for buildings classes.

Building class	IM	DS1		DS2		DS3		DS4		Mean
		θ [g]	β	θ [g]	β	θ [g]	β	θ [g]	β	R^2
RC_ND_1S	Sa(0.3)	0.24	0.16	0.65	0.51	0.92	0.41	1.39	0.38	0.77
RC_ND_2S	Sa(0.6)	0.16	0.25	0.38	0.28	0.55	0.31	0.96	0.30	0.92
RC_ND_3S	Sa(0.8)	0.09	0.25	0.16	0.44	0.25	0.33	0.42	0.36	0.89
RC_ND_4S	Sa(1.0)	0.09	0.21	0.19	0.30	0.29	0.30	0.46	0.35	0.92
RC_ND_5-7S	Sa(1.8)	0.08	0.29	0.20	0.25	0.29	0.28	0.43	0.38	0.91
RC_ND_8-15S	Sa(2.0)	0.11	0.46	0.27	0.37	0.37	0.39	0.54	0.53	0.77
RC_MD_1S_A	Sa(0.3)	0.76	0.57	1.82	0.49	2.08	0.44	2.40	0.34	0.71
RC_MD_2S_A	Sa(0.6)	0.24	0.48	0.63	0.53	0.93	0.46	1.44	0.34	0.81
RC_MD_3S_A	Sa(0.8)	0.10	0.28	0.23	0.52	0.35	0.41	0.60	0.33	0.86
RC_MD_4S_A	Sa(1.0)	0.10	0.24	0.27	0.29	0.40	0.31	0.63	0.30	0.90
RC_MD_5-7S_A	Sa(1.8)	0.10	0.22	0.25	0.27	0.37	0.29	0.55	0.37	0.91
RC_MD_8-15S_A	Sa(2.0)	0.13	0.39	0.32	0.36	0.45	0.41	0.68	0.62	0.74
RC_MD_1S_B	Sa(0.3)	0.45	0.56	1.23	0.59	1.51	0.55	1.87	0.44	0.69
RC_MD_2S_B	Sa(0.6)	0.22	0.43	0.56	0.42	0.86	0.33	1.38	0.27	0.83
RC_MD_3S_B	Sa(0.8)	0.10	0.27	0.22	0.48	0.39	0.38	0.58	0.33	0.86
RC_MD_4S_B	Sa(1.0)	0.10	0.23	0.26	0.27	0.39	0.31	0.61	0.31	0.90
RC_MD_5-7S_B	Sa(1.8)	0.10	0.22	0.25	0.27	0.36	0.28	0.54	0.40	0.89
RC_MD_8-15S_B	Sa(2.0)	0.14	0.40	0.32	0.36	0.44	0.40	0.68	0.62	0.73
RC_MD_1S_C	Sa(0.3)	0.36	0.59	0.96	0.61	1.22	0.57	1.58	0.49	0.69
RC_MD_2S_C	Sa(0.6)	0.20	0.38	0.50	0.37	0.76	0.37	1.26	0.31	0.88
RC_MD_3S_C	Sa(0.8)	0.10	0.25	0.20	0.48	0.32	0.37	0.54	0.34	0.87
RC_MD_4S_C	Sa(1.0)	0.10	0.24	0.25	0.29	0.38	0.33	0.59	0.33	0.90

RC_MD_5-7S_C	Sa(1.8)	0.10	0.23	0.25	0.26	0.36	0.27	0.54	0.39	0.89
RC_MD_8-15S_C	Sa(2.0)	0.12	0.43	0.31	0.38	0.43	0.41	0.64	0.60	0.75
RC_D_1S_A	Sa(0.3)	0.99	0.51	2.22	0.48	2.51	0.42	2.84	0.32	0.67
RC_D_2S_A	Sa(0.6)	0.32	0.42	0.86	0.57	1.32	0.43	1.91	0.34	0.74
RC_D_3S_A	Sa(0.8)	0.11	0.37	0.28	0.51	0.44	0.38	0.74	0.33	0.85
RC_D_4S_A	Sa(1.0)	0.12	0.27	0.32	0.32	0.49	0.31	0.76	0.30	0.90
RC_D_5-7S_A	Sa(1.8)	0.12	0.20	0.30	0.25	0.44	0.29	0.67	0.39	0.89
RC_D_8-15S_A	Sa(2.0)	0.16	0.40	0.38	0.37	0.53	0.47	0.87	0.70	0.71
RC_D_1S_B	Sa(0.3)	0.53	0.59	1.43	0.57	1.71	0.51	2.14	0.40	0.72
RC_D_2S_B	Sa(0.6)	0.27	0.43	0.73	0.47	1.12	0.35	1.69	0.27	0.80
RC_D_3S_B	Sa(0.8)	0.30	0.23	0.77	0.27	1.16	0.32	1.73	0.45	0.77
RC_D_4S_B	Sa(1.0)	0.12	0.25	0.30	0.27	0.46	0.31	0.71	0.31	0.89
RC_D_5-7S_B	Sa(1.8)	0.12	0.22	0.31	0.26	0.44	0.31	0.67	0.42	0.88
RC_D_8-15S_B	Sa(2.0)	0.16	0.40	0.38	0.38	0.52	0.46	0.87	0.71	0.71
RC_D_1S_C	Sa(0.3)	0.45	0.55	1.24	0.56	1.52	0.49	1.92	0.40	0.70
RC_D_2S_C	Sa(0.6)	0.25	0.42	0.66	0.43	1.03	0.32	1.60	0.29	0.83
RC_D_3S_C	Sa(0.8)	0.10	0.26	0.26	0.43	0.42	0.31	0.68	0.26	0.87
RC_D_4S_C	Sa(1.0)	0.11	0.21	0.31	0.25	0.47	0.31	0.71	0.31	0.90
RC_D_5-7S_C	Sa(1.8)	0.12	0.22	0.30	0.26	0.42	0.32	0.65	0.44	0.86
RC_D_8-15S_C	Sa(2.0)	0.16	0.43	0.36	0.39	0.50	0.46	0.83	0.72	0.71
RC_D_1S_D	Sa(0.3)	0.36	0.69	0.99	0.62	1.27	0.57	1.68	0.51	0.61
RC_D_2S_D	Sa(0.6)	0.22	0.38	0.59	0.36	0.90	0.30	1.46	0.28	0.85
RC_D_3S_D	Sa(0.8)	0.10	0.27	0.26	0.41	0.42	0.30	0.68	0.29	0.87
RC_D_4S_D	Sa(1.0)	0.12	0.22	0.31	0.23	0.47	0.31	0.70	0.31	0.89
RC_D_5-7S_D	Sa(1.8)	0.12	0.27	0.32	0.27	0.45	0.33	0.69	0.49	0.84
RC_D_8-15S_D	Sa(2.0)	0.16	0.42	0.36	0.39	0.49	0.44	0.82	0.74	0.69
M_ND_1S	Sa(0.3)	0.19	0.22	0.28	0.28	0.47	0.27	0.59	0.25	0.95
M_ND_2S	Sa(0.4)	0.11	0.16	0.28	0.26	0.34	0.26	0.50	0.39	0.93
M_ND_3S	Sa(0.6)	0.08	0.17	0.20	0.14	0.24	0.20	0.41	0.31	0.95
M_MD_1S	Sa(0.3)	0.39	0.31	0.79	0.35	0.96	0.34	1.21	0.32	0.83
M_MD_2S	Sa(0.4)	0.24	0.25	0.50	0.24	0.66	0.24	0.91	0.30	0.92
M_MD_3S	Sa(0.6)	0.21	0.11	0.30	0.10	0.51	0.24	0.67	0.27	0.92
M_D_1S	Sa(0.3)	0.77	0.38	1.67	0.36	1.88	0.33	2.23	0.31	0.60
M_D_2S	Sa(0.4)	0.47	0.21	0.98	0.27	1.25	0.22	1.65	0.23	0.89
M_D_3S	Sa(0.6)	0.31	0.30	0.61	0.25	0.76	0.25	1.03	0.29	0.92
M3_1S	Sa(0.3)	0.17	0.14	0.30	0.25	0.36	0.26	0.48	0.30	0.95
M3_2S	Sa(0.4)	0.09	0.23	0.20	0.25	0.28	0.20	0.42	0.41	0.93
M3_3S	Sa(0.6)	0.05	0.30	0.13	0.22	0.18	0.25	0.29	0.33	0.94

θ – Median; β – Logarithmic standard deviation

To estimate the seismic losses firstly it was necessary to convert the fragility models developed in this section into vulnerability models (i.e. distribution of loss given an intensity level). To this end each fragility function was combined with suitable damage-to-loss models. For the masonry building classes the same damage to loss model suggested by Silva *et al* (2014d) was used , whilst for reinforced concrete classes the model developed in section 5.5 was chosen. It is acknowledged that some RC building typologies considered in this section do not belong to

the same class used to develop the consequence model presented in section 5.5. However, to the best of the author's knowledge this is the only consequence model explicitly developed for Portuguese building stock and for this reason this model was selected to compute the expected economic losses. Table 6.4 lists the damage to loss models used in the risk analyses conducted in this section.

Table 6.4 - Damage-to-loss models used in seismic risk study.

Damage state	Mean loss ratio	
	Reinforced concrete	Masonry
DS1	0.117	0.100
DS2	0.321	0.300
DS3	0.583	0.600
DS4	0.887	1.000

6.5 SEISMIC RISK ASSESSMENT

In the current section an event-based approach was followed to the seismic risk for mainland Portugal. Such approach is required when the mean aggregated loss of a spatial distributed portfolio of assets and the respective dispersion are to be estimated. Modelling each seismic event separately allows to model the spatial correlation of ground motion which is known to have a significant impact on the loss predictions. In an event-based seismic risk assessment a Monte Carlo simulation is generally employed to simulate the seismicity over a significant period of time, frequently in the order of hundreds of thousands of years (Crowley 2014). For each rupture the respective losses are computed from the respective ground motion field (see Figure 6.6)

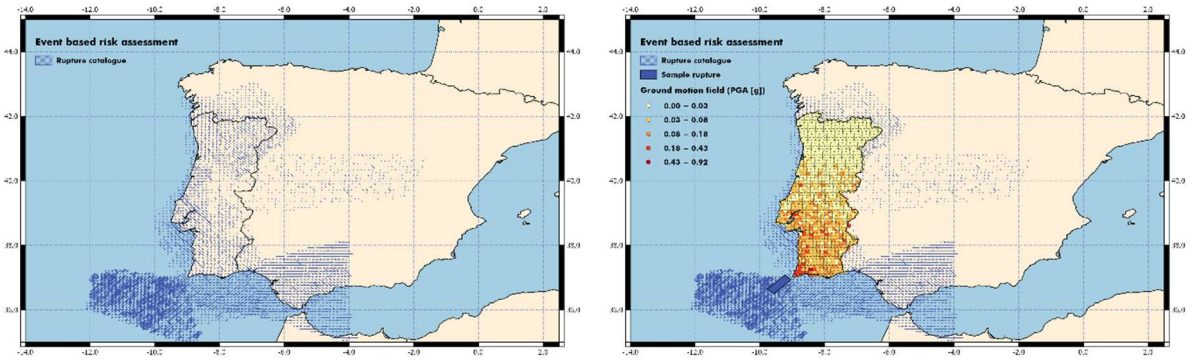

Figure 6.6 - Example of rupture catalogue (Left) and ground motion field (Right).

In the insurance and reinsurance industry the ordinary catalogues used to compute the aggregated average annual loss (AAAL) often contain anything between 10000 to 100000 years of simulated seismicity, with the former being more a more frequent (e.g. http://www.air-worldwide.com/Publications/AIR-Currents/2013/Modeling-Fundamentals--What-Is-AAL-/).

For this study a catalogue of comprising 25000 years of simulated events has been used in computing both the AAAL, loss maps and loss exceedance probability curves (EP curves) shown in this section. The choice for this an event catalogue was a result of an effort to balance the computational power required to simulate an additional 75000 years of seismic activity while still providing meaningful results within the insurance and reinsurance industry standards. The event catalogue yielded an aggregated average annual loss of 262 million euros (standard deviation of 19.2 million euros) and a loss of 27.2 billion euros for the 475 year return period (see Figure 6.7), which translate to loss ratios of 5.42×10^{-4} and 0.058 with respect to the total economic value.

Silva *et al* (2014d) in their study have estimated an annual average loss of 288 million euros, which is about 15% higher than the value computed in this section. Considering the wide spectrum of uncertainties in any seismic risk assessment study, the author believes that the AAAL computed in this section is within reason. Moreover, it was expected the losses to be slightly lower due to the damage-to-loss model used to compute the vulnerability functions for RC structures and the contribution of the design level explicitly incorporated in fragility assessment. Where this study improves on previous attempts to evaluate seismic risk for mainland Portugal is the consideration of spatial correlation of ground motions only possible through an event based seismic risk assessment approach.

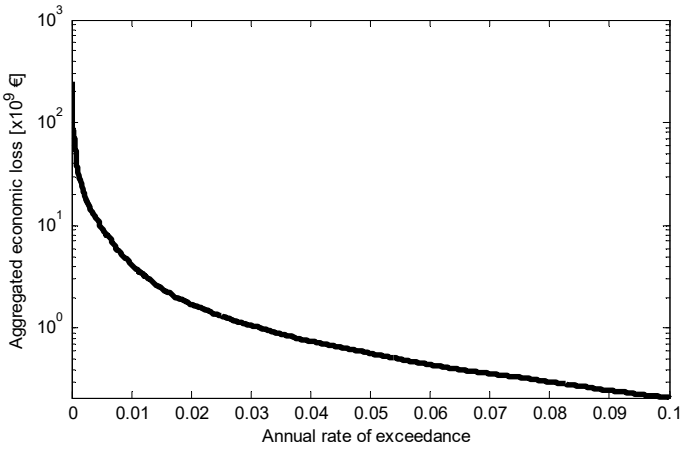

Figure 6.7 - Loss exceedance curve.

In order to understand the spatial distribution of economic loss in the Portuguese territory the average loss map with 475 year return period was plotted (see Figure 6.8). According the results in this section the majority of economic losses in mainland Portugal is mostly concentrated around Lisbon's metropolitan area and the district of Faro, areas with both high concentration of assets and high seismic hazard.

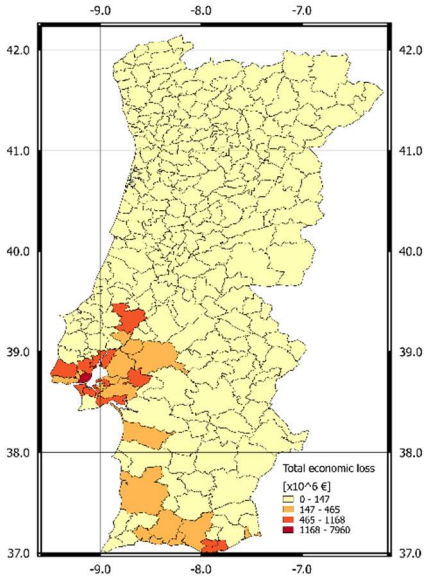

Figure 6.8 - Total economic loss for 475 year return period at municipality level.

6.6 FINAL REMARKS

In this study an updated seismic risk profile of mainland Portugal is presented. New fragility models for the most common building typologies found in Portugal were developed using analytical methodologies based on nonlinear dynamic analyses performed in equivalent single degree of freedom systems. This fragility models were developed explicitly incorporating the effects of the seismic design level through the use of the equations developed in section 3 to estimate the yield period from the height and design acceleration taken from the Portuguese design code. Vulnerability models were computed using the most recent damage-to-loss models developed for Portuguese building stock.

The studies presented in this section are an extension of the work developed by Silva *et al* (2014d) in order to incorporate the most recent developments in loss assessment for Portugal and the spatial correlation between ground motion fields. To this end seismic risk was computed following an event based approach with a catalogue comprising 25000 years of simulated seismicity. The seismic risk assessment study allowed to place the expected average annual loss in about 262 million euros,15% less than previous estimates, and the expected aggregated loss with 10% probability of exceedance in 50 years in 27.2 billion euros. When normalized for the Portuguese GDP these values yielded a loss of 0.1% and 13%. It was observed that seismic risk in mainland Portugal is concentrated in the Lisbon Metropolitan Area and in Algarve. Areas of high seismic risk Figure 6.8 seem to follow closely the areas of high seismic hazard in Figure 6.2 – Left. Therefore an improvement to the studies presented in this section would be the inclusion of an additional seismic source model (e.g. SHARE) and the combination of the seismic risk estimates coming from both models.

7

FINAL REMARKS AND FUTURE DEVELOPMENTS

7.1 FINAL REMARKS

The subjects addressed in this thesis can be divided in two main categories (i) performance and fragility assessment and (ii) damage and loss estimation. Regarding the performance assessment this thesis developed studies on the relationship between the expected period of vibration and height and on the computation of fragility parameters for European structures. On the subject of damage and loss estimation studies on the computing the expected repair costs and the development of damage-to-loss models suitable for Portuguese reinforced concrete.

The period of vibration provides valuable information about a structure and its correct estimation is an essential step of the calculation of the seismic demand in the design process. Nevertheless, correctly estimating this parameter is frequently challenging and more often than not requires time consuming numerical modelling. For large case assessment scenarios this is simply not feasible and simplified relationships are often used. From the discussion in section 3 it was identified that available simplified equations for estimating the period of vibration are more often than not region specific, thus with limited applicability. In addition, it appears to exist an obvious absence of studies on the expected period of vibration for European structures especially those designed according to the new regulations. The work developed herein addressed this lack by developing simplified period *vs.* height relationships for reinforced concrete moment frame structures designed according to the Eurocodes. The structures used in this study shared the same design criteria and basic geometry differing only from each other on the seismic design acceleration level (which ranged from a design PGA of 0.05g up to 0.40g). The results indicated a decrease on the computed periods of vibration (both

elastic and inelastic) with the design ground motion of about 20%. These findings lead to the hypothesis that ideally prior to fitting a mathematical model to predict the period data should be sorted by design acceleration. Having considered also the design ground motion as an input instead of solely the height for the simplified relationships lead to a decrease in standard error of estimate of around 50% when comparing with the models using height as the sole input parameter. The models proposed in this thesis have been compared with some other relationships developed for European structures with equivalent seismic design levels. The models proposed in this thesis yielded good correlation with previous studies with the period estimations being slightly more flexible. The mathematical models proposed in this thesis provide a reliable method to estimate the expected period of vibration for code-compliant reinforced concrete buildings either on the early stages of design or within a performance assessment framework.

Current seismic design codes are based on the assumption that designing for a prescribed ground motion associated with a given return period leads to a uniform distribution of risk. As mentioned in section 4.2 the effects of uncertainties on the shape of seismic hazard and fragility curves have disproven this hypothesis. The studies developed in this thesis aimed to understand the effect of fragility in the expected mapped ground motion within a risk-targeted framework. This goal was achieved through numerical modelling of a significant number of structures designed considering different seismic hazard levels. The results suggest that the average probability of collapse at design ground ($P[a_c<a_{des}]$) should be placed between 10^{-5} to 10^{-3} whilst the average lognormal standard deviation (β) was constrained between 0.5 and 0.8. The findings of this study allow for computing suitable fragility curves for European R.C. moment resisting frames, provided that they have been designed according to the Eurocodes. It should be noted that significantly lower values $P[a_c<a_{des}]$ were found for some structures designed for the lowest design peak ground acceleration level considered. In these cases, the seismic excitation did not determine the final design solution when comparing with other horizontal loads. This behaviour suggests that in regions with low expected seismic hazard the demands imposed by other sources of horizontal excitations may be sufficient to ensure an adequate seismic performance and consequently the design ground motion could be lowered with all the inherent potential reductions in the cost of design and construction.

One of them main sources of uncertainty in a vulnerability assessment study is the correlation between the expected damage and the correspondent loss. Most of available consequence models are region specific thus providing erroneous loss estimates outside the area where they have been calibrated especially when combined with a non-compatible fragility models. The work presented in this thesis highlighted the need to use suitable and compatible fragility and consequence models and their impact on the final loss metrics. With the findings of this study suggesting that in order to minimize bias in the final loss metrics risk modellers should seek to select damage-to-loss model as much compatible as possible with the established damage scale and criteria. Ideally the vulnerability models should be developed purely based on the distribution of loss ratio per intensity measure levels. For this, damage-to-loss models specifically developed for Portuguese reinforced concrete structures have been defined based on a comprehensive analysis on the expected damage and corresponding repair costs. The studies were based on real market value for the materials and labour costs and on the most suitable repair techniques for each damage level. The final loss of each element was obtained as a weighted sum of the different repair costs whist the total loss was considered as a sum of the element's estimated loss. It is acknowledged that considering the total repair cost simply as a sum of the costs of repairing the individual elements, as performed in this thesis, neglects the effect of performing large scale repairs (which lowers the expected total cost) and the preparation works needed prior to the actual repair job (e.g. removing debris). These effects are often difficult to predict since they often require an *in situ* inspection of the damaged buildings and therefore are challenging to implement in a generalized loss assessment methodology as the one developed in this thesis. However, to the extent of the author's knowledge this is the first, and so far only, comprehensive study on the repair cost estimation tailored for the Portuguese building stock.

Summarizing, the findings presented in this thesis provide a better understanding of the seismic performance and damage assessment of reinforced concrete structures.

7.2 FUTURE DEVELOPMENTS

The core of science is to improve on previous works in order to provide a better understanding on the physical world. It is obvious that some subjects addressed in this thesis would benefit from new research endeavours.

On the estimation of the elastic and yield period, the studies presented on this thesis are limited to regular and symmetrical structures both in geometry and in the distribution of mass in plan. It is known that irregularities influence significantly a building's seismic performance, for example an uneven distribution of weights in a floor introduces torsional effects that otherwise would not be present. In addition, it must be noted that the percentage of buildings with irregularities is not negligible. Thus introducing some source of irregularities in the models and comparing the results with the ones presented herein may provide a better understanding on their influence on the dynamic properties of structures. Herein the yield period has been estimated from the bilinear capacity computed by applying the N2 method to the capacity curve given by pushover analysis. Therefore, it is suggested to analyse the differences introduced on the period estimations with the chosen analysis algorithm and the NSP and comparing the subsequent mathematical models with the ones proposed herein.

Running nonlinear time history analyses for a large number of 3D structures and post processing the outputs is obvious very computational intensive. And one of the reasons the studies on the influence of the fragility parameters in a risk-targeted hazard assessment presented herein have only addressed structures from a limited number of building typologies was limitations on the computational runtime. Therefore, future studies should seek to extend the work developed in this thesis to both low-rise and high-rise buildings and register the evolution of the fragility parameters, like the probability of collapse at design ground motion ($P[a_c<a_{des}]$) and the lognormal standard deviation (β), with the building's height. This thesis has provided probability density functions that could be used to model the uncertainty in the fragility parameters within a probabilistic framework. The quality of the fit has been addressed a through a one-sample Kolmogorov-Smirnov (K-S) test. A criticism to the methodology presented in this study is the applicability of the K-S test to a sample size equal to the one used herein, thus in future research the total number of structures should be increased in order to further validate (or refute) the findings presented herein.

On the subject of estimating repair costs and economic losses the studies presented in this thesis have not considered the different dependence relationships between the components. Considering that, for example, plumbing and electric installations are usually imbedded in the infill panels their ultimate capacity should be, in some extent, linked to the performance of the infill panels since a complete loss of the infill should translate into a complete loss of these installations. The approach followed by this study, albeit valid, has only addressed deterministic performance thresholds based on if the elements were drift or acceleration sensitive, thus room for further improvement still exists for example by considering a probabilistic framework. Furthermore, the results presented on section 5 were based on repair costs calculated based on a limited number of repair techniques, however for different cases probably more than one repair techniques may be applicable. Thus the studies presented herein could be improved by creating an inventory of additional alternative suitable repair techniques and analysing the differences on the expected economic losses. Moreover, it is clear that the level of detail when computing repair costs for the RC structure is clearly higher than one for infill walls and other non-structural elements, despite the latter comprising the majority of the building's replacement cost. This is in large due to the many uncertainties associated with masonry infills (e.g. mechanical properties, numerical models). Therefore future studies should seek for a better understanding the physical behaviour of masonry infill in an attempt to define suitable repair techniques in with a similar level of detail to the one currently possible for the RC structure. Finally, the damage-to-loss model developed in this study is limited to pre-code mid-rise R.C moment resisting frames. Additional research on this topic should seek to extend the studies presented herein to other building typologies.

8

REFERENCES

Abrahamson, N.A. and Bommer, J.J. (2005) *Probability and Uncertainty in Seismic Hazard Analysis.* Earthquake Spectra, **21**(2): p. 603-607.

Akkar, S. and Bommer, J.J. (2010) *Empirical Equations for the Prediction of PGA, PGV, and Spectral Accelerations in Europe, the Mediterranean Region, and the Middle East.* Seismological Research Letters, **81**(2): p. 195-206. DOI: 10.1785/gssrl.81.2.195.

Akkar, S., Sandıkkaya, M.A., Şenyurt, M., Azari Sisi, A., Ay, B.Ö., Traversa, P., Douglas, J., Cotton, F., Luzi, L., Hernandez, B. and Godey, S. (2014) *Reference database for seismic ground-motion in Europe (RESORCE).* Bulletin of Earthquake Engineering, **12**(1): p. 311-339. DOI: 10.1007/s10518-013-9506-8.

Antoniou, S. and Pinho, R. (2004) *Development and verification of a displacement-based adaptive pushover procedure.* Journal of Earthquake Engineering, **8**(5): p. 643-661. DOI: 10.1142/s136324690400150x.

ASCE (2005), *Seismic Design Criteria for Structures, Systems, and Components in Nuclear Facilities*, ASCE 43-05,American Society of Civil Engineers, Reston, VA

ATC (1996) *ATC-40 Seismic Evaluation and Retrofit of Concrete Buildings*, Report SSC 96-01, Applied Technology Council

Atkinson, G.M. and Boore, D.M. (2006) *Earthquake ground-motion prediction equations for eastern North America.* Bulletin of the Seismological Society of America, **96**(6): p. 2181-2205.

Baker, J. (2011) *Conditional Mean Spectrum: Tool for Ground-Motion Selection.* Journal of Structural Engineering, **137**(3): p. 322-331. DOI: 10.1061/(ASCE)ST.1943-541X.0000215.

Bal, I.E., Bommer, J.J., Stafford, P.J., Crowley, H. and Pinho, R. (2010a) *The influence of geographical resolution of urban exposure data in an earthquake loss model for Istanbul.* Earthquake Spectra, **26**(3): p. 619-634. DOI: 10.1193/1.3459127.

Bal, İ.E., Crowley, H. and Pinho, R. (2010b) *Displacement-Based Earthquake Loss Assessment: Method Development and Application to Turkish Building stock*, Research Report No. ROSE-2010-02, Instituto Universitario di Studi Superiori di Pavia

Bal, İ.E., Crowley, H., Pinho, R. and Gülay, F.G. (2008) *Detailed assessment of structural characteristics of Turkish RC building stock for loss assessment models.* Soil Dynamics and Earthquake Engineering, **28**(10–11): p. 914-932. DOI: http://dx.doi.org/10.1016/j.soildyn.2007.10.005.

Beck, J.L., Porter, K.A., Shaikhutdinov, R.V., Au, S.K., Mizukoshi, K., Miyamura, M., Ishida, H., Moroi, T., Tsukada, Y. and Masuda, M. (2002) *Impact of seismic risk on lifetime property values*, Report no. EERL2002-04, California Institute of Technology

Benavent-Climent, A. (2011) *A seismic index method for vulnerability assessment of existing frames: application to RC structures with wide beams in Spain.* Bulletin of Earthquake Engineering, **9**(2): p. 491-517. DOI: 10.1007/s10518-010-9200-z.

Bommer, J.J. and Abrahamson, N.A. (2006) *Why do modern probabilistic seismic-hazard analyses often lead to increased hazard estimates?* Bulletin of the Seismological Society of America, **96**(6): p. 1967-1977.

Borzi, B., Pinho, R. and Crowley, H. (2008) *Simplified pushover-based vulnerability analysis for large-scale assessment of RC buildings.* Engineering Structures, **30**(3): p. 804-820. DOI: 10.1016/j.engstruct.2007.05.021.

Bracci, J.M., Kunnath, S.K. and Reinhorn, A.M. (1997) *Seismic performance and retrofit evaluation of reinforced concrete structures.* Journal of Structural Engineering, **123**(1): p. 3-10.

Calabrese, A., Almeida, J.P. and Pinho, R. (2010) *Numerical Issues in Distributed Inelasticity Modeling of RC Frame Elements for Seismic Analysis.* Journal of Earthquake Engineering, **14**(sup1): p. 38-68. DOI: 10.1080/13632461003651869.

Calvi, G.M. (1999) *A displacement-based approach for vulnerability evaluation of classes of buildings.* Journal of Earthquake Engineering, **3**(3): p. 411-438.

Calvi, G.M. (2013) *Choices and Criteria for Seismic Strengthening.* Journal of Earthquake Engineering, **17**(6): p. 769-802. DOI: 10.1080/13632469.2013.781556.

Calvi, G.M., Pinho, R., Magenes, G., Bommer, J.J., Restrepo-Vélez, L.F. and Crowley, H. (2006) *Development of seismic vulnerability assessment methodologies over the past 30 years.* ISET Journal of Earthquake Technology, **43**(3): p. 75-104.

CEN (2005), *Eurocode 8 - Design of structures for earthquake resistance Part 3: Assessment and retrofitting of buildings*, EN1998-3,European Committee for Standardization, Brussels

CEN (2009), *Eurocode 1 - Action on structures Part1-1: General actions Densities, self-weight, imposed loads for buildings*, EN1991-1-1,European Committee for Standardization, Brussels

CEN (2010a), *Eurocode 1 - Action on structures Part1-4: General actions Wind actions*, EN1991-1-4,European Committee for Standardization, Brussels

CEN (2010b), *Eurocode 2 - Design of concrete structures Part1-1: General rules and rules for buildings*, EN1992-1-1,European Committee for Standardization, Brussels

CEN (2010c), *Eurocode 8 - Design of structures for earthquake resistance Part1: General Rules, seismic actions and rules for buildings*, EN1998-1,European Committee for Standardization, Brussels

Chen, W.-F. and Lui, E.M. (2006) *Earthquake engineering for structural design*. Boca Raton: CRC/Taylor & Francis.

Chopra, A.K. (2007) *Dynamics of structures : theory and applications to earthquake engineering*. 3rd ed., Upper Saddle River, N.J.: Pearson/Prentice Hall. xxxiv, 876 p.

Chopra, A.K. and Goel, R.K. (2000) *Evaluation of NSP to estimate seismic deformation: SDF systems.* Journal of structural engineering New York, N.Y., **126**(4): p. 482-490. DOI: 10.1061/(asce)0733-9445(2000)126:4(482).

Chung, Y.S., Meyer, C. and Shinozuka, M. (1987) *Seismic Damage Assessment of Reinforced Concrete*, Technical report NCEER-87-0022, Nacional Center for Earthquake Engineering Research, State University of New York

Cimellaro, G.P., Reinhorn, A.M., D'Ambrisi, A. and De Stefano, M. (2011) *Fragility analysis and seismic record selection.* Journal of Structural Engineering, **137**(3): p. 379-390. DOI: 10.1061/(asce)st.1943-541x.0000115.

Clough, R.W. and Penzien, J. (1993) *Dynamics of structures*. 2nd ed., New York: McGraw Hill. XXII, 738.

Costa, A.C., Sousa, M.L., Carvalho, A. and Coelho, E. (2010) *Evaluation of seismic risk and mitigation strategies for the existing building stock: application of LNECloss to the metropolitan area of Lisbon.* Bulletin of Earthquake Engineering, **8**(1): p. 119-134. DOI: 10.1007/s10518-009-9160-3.

Crisafulli, F.J. (1997) *Seismic behaviour of reinforced concrete structures with masonry infills*, PhD Thesis. University of Cantebury.

Crowley, H. (2014) *Earthquake Risk Assessment: Present Shortcomings and Future Directions*, in *Perspectives on European Earthquake Engineering and Seismology: Volume 1*, A. Ansal, Editor., Springer International Publishing: Cham. p. 515-532.

Crowley, H., Borzi, B., Pinho, R., Colombi, M. and Onida, M. (2008) *Comparison of Two Mechanics-Based Methods for Simplified Structural Analysis in Vulnerability Assessment.* Advances in Civil Engineering, **2008**: p. 19. DOI: 10.1155/2008/438379.

Crowley, H. and Pinho, R. (2004) *Period-Height relationship for existing European reinforced concrete buildings.* Journal of Earthquake Engineering, **8**(sup001): p. 93-119. DOI: 10.1080/13632460409350522.

Crowley, H. and Pinho, R. (2006) *Simplified equations for estimating the period of vibration of existing buildings*. in *Proceedings of the 1st European Conference on Earthquake Engineering and Seismology*

Crowley, H. and Pinho, R. (2010) *Revisiting Eurocode 8 formulae for periods of vibration and their employment in linear seismic analysis.* Earthquake Engineering & Structural Dynamics, **39**(2): p. 223-235. DOI: 10.1002/eqe.949.

Crowley, H., Pinho, R., Bommer, J.J. and Bird, J.F. (2006) *Development of a Displacement-Based Method for Earthquake Loss Assessment*, Research Report No. ROSE-2006-01, Instituto Universitario di Studi Superiori di Pavia

De Biasio, M., Grange, S., Dufour, F., Allain, F. and Petre-Lazar, I. (2014) *A simple and efficient intensity measure to account for nonlinear structural behavior.* Earthquake Spectra, **30**(4): p. 1403-1426. DOI: 10.1193/010614EQS006M.

Deierlein, G., Krawinkler, H. and Cornell, C. (2003) *A framework for performance-based earthquake engineering*. in *Pacific conference on earthquake engineering*. Christchurch, New Zealand

Di Pasquale, G. and Goretti, A. (2001) *Vulnerabilità funzionale ed economica degli edifici residenziali colpiti dai recenti eventi sismici italiani* in *Proceedings of the 10th national conference "L'ingegneria Sismica in Italia"*. Potenza-Matera, Italy.

Di Pasquale, G., Orsini, G. and Romeo, R. (2005) *New Developments in Seismic Risk Assessment in Italy.* Bulletin of Earthquake Engineering, **3**(1): p. 101-128. DOI: 10.1007/s10518-005-0202-1.

Douglas, J., Ulrich, T. and Negulescu, C. (2013) *Risk-targeted seismic design maps for mainland France.* Natural Hazards, **65**(3): p. 1999-2013. DOI: 10.1007/s11069-012-0460-6.

Dunand, F., Bard, P., Chatelain, J., Guéguen, P., Vassail, T. and Farsi, M. (2002) *Damping and frequency from Randomdec method applied to in situ measurements of ambient vibrations. Evidence for effective soil structure interaction*. in *12th European Conference on Earthquake Engineering, London*

Eads, L., Miranda, E., Krawinkler, H. and Lignos, D.G. (2013) *An efficient method for estimating the collapse risk of structures in seismic regions.* Earthquake Engineering and Structural Dynamics, **42**(1): p. 25-41.

Elnashai, A.S. and Di Sarno, L. (2008) *Fundamentals of earthquake engineering*. Chichester, U.K.: Wiley. 347 p.

Erberik, M.A. (2008) *Fragility-based assessment of typical mid-rise and low-rise RC buildings in Turkey.* Engineering Structures, **30**(5): p. 1360-1374. DOI: http://dx.doi.org/10.1016/j.engstruct.2007.07.016.

Fajfar, P. (1999) *Capacity spectrum method based on inelastic demand spectra.* Earthquake Engineering and Structural Dynamics, **28**(9): p. 979-993. DOI: 10.1002/(sici)1096-9845(199909)28:9<979::aid-eqe850>3.0.co;2-1.

Fajfar, P. and Gašperšič, P. (1996) *The N2 method for the seismic damage analysis of RC buildings.* Earthquake Engineering and Structural Dynamics, **25**(1): p. 31-46.

Fardis, M.N. (2009) *Seismic design, assessment and retrofitting of concrete buildings : based on EN-Eurocode 8*. Geotechnical, geological, and earthquake engineering. Dordrecht ; New York: Springer. xxiii, 743 p.

Fardis, M.N., Papailia, A. and Tsionis, G. (2012) *Seismic fragility of RC framed and wall-frame buildings designed to the EN-Eurocodes.* Bulletin of Earthquake Engineering, **10**(6): p. 1767-1793. DOI: 10.1007/s10518-012-9379-2.

FEMA (1997), *FEMA 273 - NEHRP Guidelines for the seismic rehabilitation of buildings*, FEMA 273,Department of Homeland Security - Federal Emergency Management Agency, Washington, D.C.

FEMA (2005), *FEMA 440 - Improvement of nonlinear static seismic analysis procedures*, FEMA 440,Department of Homeland Security - Federal Emergency Management Agency, Washington, D.C.

FEMA (2009) *Quantification of building seismic performance factors*, Technical report FEMA P695, Applied Technology Council, Redwood City, California

FEMA (2012), *Seismic Performance Assessment of Buildings*, FEMA P-58-1,Department of Homeland Security - Federal Emergency Management Agency, Washington, D.C.

FEMA (2014) *HAZUS-MH MR5, Technical Manual*, Department of Homeland Security - Federal Emergency Management Agency

M.d. Finanças (2003), *Código do imposto municipal sobre imóveis* Decreto-lei 287/2003, published in Diário da República 1.ª série - N.º 262 (in Portuguese)

M.d. Finanças (2013), Portaria 370/2013, published in Diário da República 1.ª série - N.º 251 (in Portuguese)

Freeman, S.A., Nicoletti, J.P. and Tyrrell, J.B. (1975) *Evaluation of existing buildings for seismic risk - A case study of the Puget Sound Naval Shipyard, Bremerton, Washington*, in *Proceddings of US National Conference on Earthquake Engineering*: Berkley, USA. p. 113-122.

Gallipoli, M.R., Mucciarelli, M. and Vona, M. (2009) *Empirical estimate of fundamental frequencies and damping for Italian buildings.* Earthquake Engineering & Structural Dynamics, **38**(8): p. 973-988.

Ghobarah, A. (2004) *On drift limits with different damage levels*, in *Proceedings of International Workshop on Performance-based seismic design concepts and implementation*: Bled, Slovenia.

Goulet, C.A., Haselton, C.B., Mitrani-Reiser, J., Beck, J.L., Deierlein, G.G., Porter, K.A. and Stewart, J.P. (2007) *Evaluation of the seismic performance of a code-conforming reinforced-concrete frame building - From seismic hazard to collapse safety and economic losses.* Earthquake Engineering and Structural Dynamics, **36**(13): p. 1973-1997. DOI: 10.1002/eqe.694.

Gulkan, P. and Sozen, M.A. (1974) *Inelastic Responses of Reinforced Concrete Structures to Earthquake Motions.* J Am Concr Inst, **71**(12): p. 604-610.

Gunturi, S.K.V. (1993) *Building-specific earthquake damage estimation*, PhD. Thesis. Stanford University: California, U.S.A. p. 370 p.

Haselton, C.B., Goulet, C.A., Mitrani-Reiser, J., Beck, J.L., Dierlein, G.G., Porter, K.A., Stewart, J.P. and Taciroglu, E. (2008) *An assessment to benchmark the seismic performance of a code-confirming reinforced concrete moment-frame building*, PEER Report 2007/12, PEER - Pacific Earthquake Engineering Research Center

Haselton, C.B., Liel, A.B., Deierlein, G.G., Dean, B.S. and Chou, J.H. (2011) *Seismic Collapse Safety of Reinforced Concrete Buildings. I: Assessment of Ductile Moment Frames.* Journal of Structural Engineering, **137**(4): p. 481-491. DOI: doi:10.1061/(ASCE)ST.1943-541X.0000318.

Ibarra, L.F. and Krawinkler, H. (2005) *Global collapse of frame structures under seismic excitations*, Report no. 152, The BlumeEarthquake Engineering Center, Department of Civil and Environmental Engineering, Stanford University

INE (2011) *Censos 2011 – Resultados definitivos – Portugal: XV recenseamento geral da população; V recenseamento geral da habitação*, Instituto Nacional de Estatistica

Jaiswal, K. and Wald, J. (2008) *Creating a Global Building Inventory for Earthquake Loss Assessment and Risk Management*, USGS

Jayaram, N. and Baker, J.W. (2008) *Statistical tests of the joint distribution of spectral acceleration values.* Bulletin of the Seismological Society of America, **98**(5): p. 2231-2243.

Jayaram, N., Lin, T. and Baker, J.W. (2011) *A Computationally Efficient Ground-Motion Selection Algorithm for Matching a Target Response Spectrum Mean and Variance.* Earthquake Spectra, **27**(3): p. 797-815. DOI: 10.1193/1.3608002.

Julio, E., Branco, F. and Silva, V. (2003) *Structural rehabilitation of columns with reinforced concrete jacketing.* Progress in Structural Engineering and Materials, **5**(1): p. 29-37.

Kappos, A., Panagopoulos, G., Panagiotopoulos, C. and Penelis, G. (2006) *A hybrid method for the vulnerability assessment of R/C and URM buildings.* Bulletin of Earthquake Engineering, **4**(4): p. 391-413. DOI: 10.1007/s10518-006-9023-0.

Kappos, A., Stylianidis, K. and Penelis, G. (1991) *Analytical prediction of the response of structures to future earthquakes.* European Earthquake Engineering, **1**: p. 10-21.

Kappos, A.J. (1991) *Analytical prediction of the collapse earthquake for R/C buildings: suggested methodology.* Earthquake Engineering and Structural Dynamics, **20**(2): p. 167-176.

Kappos, A.J. (1997) *Seismic damage indices for RC buildings: evaluation of concepts and procedures.* Progress in Structural Engineering and Materials, **1**(1): p. 78-87. DOI: 10.1002/pse.2260010113.

Kappos, A.J., Stylianidis, K.C. and Pitilakis, K. (1998) *Development of Seismic Risk Scenarios Based on a Hybrid Method of Vulnerability Assessment.* Natural Hazards, **17**(2): p. 177-192. DOI: 10.1023/a:1008083021022.

Kobayashi, H., Vidal, F., Feriche, D., Samano, T. and Alguacil, G. (1996) *Evaluation of dynamic behaviour of building structures with microtremors for seismic microzonation mapping*. in *11th WCEE*. Acapulco, México

Kramer, S.L. (1996) *Geotechnical earthquake engineering*. Prentice-Hall international series in civil engineering and engineering mechanics. Upper Saddle River, N.J.: Prentice Hall. xviii, 653 p.

Krawinkler, H. and Seneviratna, G.D.P.K. (1998) *Pros and cons of a pushover analysis of seismic performance evaluation.* Engineering Structures, **20**(4-6): p. 452-464. DOI: 10.1016/s0141-0296(97)00092-8.

Lazar, N. and Dolšek, M. (2014) *Incorporating intensity bounds for assessing the seismic safety of structures: Does it matter?* Earthquake Engineering & Structural Dynamics, **43**(5): p. 717-738. DOI: 10.1002/eqe.2368.

Lin, T. and Baker, J.W. (2013) *Introducing adaptive incremental dynamic analysis: A new tool for linking ground motion selection and structural response assessment*. in *Safety, Reliability, Risk and Life-Cycle Performance of Structures and Infrastructures - Proceedings of the 11th International Conference on Structural Safety and Reliability, ICOSSAR 2013*

Lin, T., Harmsen, S.C., Baker, J.W. and Luco, N. (2013) *Conditional spectrum computation incorporating multiple causal earthquakes and ground-motion prediction models.* Bulletin of the Seismological Society of America, **103**(2 A): p. 1103-1116. DOI: 10.1785/0120110293.

Luco, N., Ellingwood, B.R., Hamburger, R.O., Hooper, J.D., Kimball, J.K. and Kircher, C.A. (2007) *Risk-target versus current seismic design maps for the conterminous United States*, in *Proceedings of SEAOC2007 Convention*

Mander, J.B., Priestley, M.J.N. and Park, R. (1988) *Theoretical Stress-Strain Model for confined concrete.* Journal of structural engineering New York, N.Y., **114**(8): p. 1804-1826.

Martins, L., Silva, V., Bazzurro, P., Crowley, H. and Marques, M. (2015) *Investigation of Structural Fragility for Risk-targeted Hazard Assessment*, in *ICASP12 - 12th International Conference on Applications of Statistics and Probability in Civil Engineering*: Vancouver, Canada.

Martins, L., Silva, V., Marques, M., Crowley, H. and Delgado, R. (2014) *Evaluation of Analytical Fragility and Damage-to-loss Models for Reinforced Concrete Buildings*, in *2nd European Conference on Earthquake Engineering and Seismology*: Istanbul, Turkey.

Martins, L., Silva, V., Marques, M., Crowley, H. and Delgado, R. (2016) *Development and assessment of damage-to-loss models for moment-frame reinforced concrete buildings.* Earthquake Engineering & Structural Dynamics, **45**(5): p. 797-817. DOI: 10.1002/eqe.2687.

MathWorks (2013) *Matlab - Version 8.2.0.701 (R2013b)*. The MathWorks, Inc.: Natick, Massachusetts.

McKenna, F., Fenves, G., Scott, M. and Jeremic, B. (2000) *Open System for Earthquake Engineering Simulation (OpenSees). Pacific Earthquake Engineering Research Center.* University of California, Berkeley, CA.

Mêda, P. (2014) *Integrated Construction Organization*, Msc Thesis. Universtity of Porto - Faculty of Engineering.

Mendes, N. (2011) *Estrutura de Custos de Edifícios de Habitação*, MSc. Thesis. ISEL.

Menegotto, M. and Pinto, P.E. (1973) *Method of analysis for cyclically loaded R.C. plane frames including changes in geometry and non-elastic behaviour of elements under combined normal force and bending*, in *Symposium on the Resistance and Ultimate Deformability of Structures Acted on by Well Defined Repeated Loads, International Association for Bridge and Structural Engineering*: Zurich, Switzerland p. 15-22.

Miranda, E., Mosqueda, G., Retamales, R. and Pekcan, G. (2012) *Performance of Nonstructural Components during the 27 February 2010 Chile Earthquake.* Earthquake Spectra, **28**(S1): p. S453-S471. DOI: doi:10.1193/1.4000032.

MunichRe (2012) *Topics Geo: Natural catastrophes 2011 Analyses, assessments, positions.*,

Navarro, M., Sánchez, F., Feriche, M., Vidal, F., Enomoto, T., Iwatate, T., Matsuda, I. and Maeda, T. (2002) *Statistical estimation for dynamic characteristics of existing buildings in Granada, Spain, using microtremors*. in *Eurodyn*. Munich, Germany

Oliveira, C.S. and Navarro, M. (2010) *Fundamental periods of vibration of RC buildings in Portugal from in-situ experimental and numerical techniques.* Bulletin of Earthquake Engineering, **8**(3): p. 609-642. DOI: 10.1007/s10518-009-9162-1.

Park, Y.-J. and Ang, A.H.S. (1985) *Mechanistic Seismic Damage Model for Reinforced Concrete.* Journal of Structural Engineering, **111**(4): p. 722-739.

Park, Y.J., Ang, A.H.S. and Wen, Y.K. (1987) *Damage-limiting aseismic design of buildings.* Earthquake Spectra, **3**(1): p. 1-26.

Peláez Montilla, J.A. and López Casado, C. (2002) *Seismic Hazard Estimate at the Iberian Peninsula.* Pure and Applied Geophysics, **159**(11): p. 2699-2713. DOI: 10.1007/s00024-002-8754-3.

Pinto, L. (2007) *Observatório da Construção de TMAD – Estrutura de Custos de Edifícios de Habitação*, MSc. Thesis. UTAD.

Priestley, M.J.N., Calvi, G.M. and Kowalsky, M.J. (2007) *Displacement-based seismic design of structures*. Pavia, Italy: IUSS Press : Distributed by Fondazione EUCENTRE.

Priestley, M.J.N. and Park, R. (1987) *Strength of Ductility of Concrete Bridge Columns Under Seismic Loading.* ACI Structural Journal, **84**(1): p. 61-76.

Ramirez, C.M., Liel, A.B., Mitrani-Reiser, J., Haselton, C.B., Spear, A.D., Steiner, J., Deierlein, G.G. and Miranda, E. (2012) *Expected earthquake damage and repair costs in reinforced concrete frame buildings.* Earthquake Engineering & Structural Dynamics, **41**(11): p. 1455-1475. DOI: 10.1002/eqe.2216.

Ramirez, C.M. and Miranda, E. (2012) *Significance of residual drifts in building earthquake loss estimation.* Earthquake Engineering & Structural Dynamics, **41**(11): p. 1477-1493. DOI: 10.1002/eqe.2217.

Ricci, P., Verderame, G.M. and Manfredi, G. (2011) *Analytical investigation of elastic period of infilled RC MRF buildings.* Engineering Structures, **33**(2): p. 308-319. DOI: https://doi.org/10.1016/j.engstruct.2010.10.009.

Rossetto, T. and Elnashai, A. (2003) *Derivation of vulnerability functions for European-type RC structures based on observational data.* Engineering Structures, **25**(10): p. 1241-1263. DOI: 10.1016/s0141-0296(03)00060-9.

Sen, T.K. (2009) *Fundamentals of seismic loading on structures*. Chichester: Wiley-Blackwell. xviii, 384 p.

Shinozuka, M., Feng, M.Q., Lee, J. and Naganuma, T. (2000) *Statistical analysis of fragility curves.* Journal of Engineering Mechanics, **126**(12): p. 1224-1231. DOI: 10.1061/(asce)0733-9399(2000)126:12(1224).

Shome, N. and Cornell, C.A. (1999) *Probabilistic seismic demand analysis of nonlinear structures*, Technical Report RMS-35, Stanford University

Silva, V. (2013) *Development of open models and tools for seismic risk assessment: Application to Portugal*, Ph.D. Thesis. Universidade de Aveiro.

Silva, V., Crowley, H. and Bazzurro, P. (2014a) *Risk-targeted hazard maps for Europe*, in *2nd European Conference on Earthquake Engineering and Seismology*: Istanbul, Turkey.

Silva, V., Crowley, H. and Bazzurro, P. (2016) *Exploring risk-targeted hazard maps for Europe.* Earthquake Spectra, **32**(2): p. 1165-1186. DOI: 10.1193/112514EQS198M.

Silva, V., Crowley, H., Pagani, M., Monelli, D. and Pinho, R. (2014b) *Development of the OpenQuake engine, the Global Earthquake Model's open-source software for seismic risk assessment.* Natural Hazards, **72**(3): p. 1409-1427. DOI: 10.1007/s11069-013-0618-x.

Silva, V., Crowley, H., Pinho, R. and Varum, H. (2013) *Extending displacement-based earthquake loss assessment (DBELA) for the computation of fragility curves.* Engineering Structures, **56**: p. 343-356. DOI: 10.1016/j.engstruct.2013.04.023.

Silva, V., Crowley, H., Varum, H. and Pinho, R. (2014c) *Seismic risk assessment for mainland Portugal.* Bulletin of Earthquake Engineering: p. 1-29. DOI: 10.1007/s10518-014-9630-0.

Silva, V., Crowley, H., Varum, H., Pinho, R. and Sousa, L. (2014d) *Investigation of the characteristics of Portuguese regular moment-frame RC buildings and development of a vulnerability model.* Bulletin of Earthquake Engineering: p. 1-36. DOI: 10.1007/s10518-014-9669-y.

Sinković, N.L., Brozovič, M. and Dolšek, M. (2016) *Risk-based seismic design for collapse safety.* Earthquake Engineering & Structural Dynamics: p. n/a-n/a. DOI: 10.1002/eqe.2717.

Smyrou, E. (2006) *Implementation and verification of a mansonry panel model for nonlinear dynamic analysis of infilled RC frames*, MSc Thesis. Universitá degli Studi di Pavia.

Smyrou, E., Blandon, C., Antoniou, S., Pinho, R. and Crisafulli, F. (2011) *Implementation and verification of a masonry panel model for nonlinear dynamic analysis of infilled RC frames.* Bulletin of Earthquake Engineering, **9**(5): p. 1519-1534. DOI: 10.1007/s10518-011-9262-6.

Sousa, L. (2006) *Seismic risk in portuguese mainland*, PhD Thesis. Instituto Superior Técnico.

Sousa, L., Silva, V., Marques, M., Crowley, H. and Pinho, R. (2014) *Including multiple IMTs in the development of fragility functions for earthquake loss estimation*, in *ASCE-ICVRAM-ISUMA Conference*: Liverpool, U.K.

Spence, R. (2007) *Earthquake disaster scenario prediction and loss modelling for urban areas.*, Instituto Universitario di Studi Superiori di Pavia

Sullivan, T.J. and Calvi, G.M. (2012) *A Model Code for the Displacement-Based Seismic Design of Structures DBD12*, Instituto Universitario di Studi Superiori di Pavia

Taghavi, S. and Miranda, E. (2003) *Response assessment of nonstructural building elements*, PEER Report 2003/05, Pacific Earthquake Engineering Research Center

Ulrich, T., Negulescu, C. and Douglas, J. (2014) *Fragility curves for risk-targeted seismic design maps.* Bulletin of Earthquake Engineering, **12**(4): p. 1479-1491. DOI: 10.1007/s10518-013-9572-y.

Vamvatsikos, D. and Cornell, C.A. (2002) *Incremental dynamic analysis.* Earthquake Engineering and Structural Dynamics, **31**(3): p. 491-514. DOI: 10.1002/eqe.141.

Vilanova, S.P. and Fonseca, J.F.B.D. (2007) *Probabilistic seismic-hazard assessment for Portugal.* Bulletin of the Seismological Society of America, **97**(5): p. 1702.

Vilanova, S.P., Nunes, C.F. and Fonseca, J.F.B.D. (2003) *Lisbon 1755: A case of triggered onshore rupture?* Bulletin of the Seismological Society of America, **93**(5): p. 2056-2068.

Villar-Vega, M., Silva, V., Crowley, H., Yepes, C., Tarque, N., Acevedo, A.B., Hube, M.A., Gustavo, C.D. and María, H.S. (2017) *Development of a Fragility Model for the Residential Building Stock in South America.* Earthquake Spectra, **33**(2): p. 581-604. DOI: 10.1193/010716eqs005m.

Waghmare, S.P.B. (2011) *Materials and Jacketing Technique for Retrofitting of Structures.* International Journal of Advanced Engineering Research and Studies, **1**(1): p. 15-19.

Williams, M.S. and Sexsmith, R.G. (1995) *Seismic Damage Indices for Concrete Structures: A State-of-the-Art Review.* Earthquake Spectra, **11**(2): p. 319-349.

Woessner, J., Laurentiu, D., Giardini, D., Crowley, H., Cotton, F., Grünthal, G., Valensise, G., Arvidsson, R., Basili, R., Demircioglu, M.B., Hiemer, S., Meletti, C., Musson, R.W., Rovida, A.N., Sesetyan, K. and Stucchi, M. (2015) *The 2013 European Seismic Hazard Model: key components and results.* Bulletin of Earthquake Engineering, **13**(12): p. 3553-3596. DOI: 10.1007/s10518-015-9795-1.